Silvan Poschenrieder, BSc

Biocatalytic Reaction Systems for photosynthetic NADPH Regeneration

MASTERARBEIT

zur Erlangung des akademischen Grades

Master of Science

Masterstudium Chemie

eingereicht an der

Technischen Universität Graz

Betreuer

Univ.-Prof. Dipl.-Ing. Dr.techn. Wolfgang Kroutil

Institut für Chemie

Zweitbetreuer
Dr. Christoph Winkler

Graz, Febuary

EIDESSTATTLICHE ERKLÄRUNG

Ich erkläre an Eides statt, dass ich die vorliegende Arbeit selbstständig verfasst, andere als die angegebenen Quellen/Hilfsmittel nicht benutzt, und die den benutzten Quellen wörtlich und inhaltlich entnommenen Stellen als solche kenntlich gemacht habe. Das in TUGRAZonline hochgeladene Textdokument ist mit der vorliegenden Masterarbeit identisch.

Datum

Unterschrift

Danksagung

An dieser Stelle möchte ich mich bei allen bedanken, die mich bei der Ausarbeitung und Anfertigung meiner Masterarbeit unterstützt haben.

Besonderer Dank gebührt Professor Wolfgang Kroutil, für die Möglichkeit, meine Masterarbeit auf dem Gebiet der Biokatalyse und organischen Synthese verfassen zu können und für seine Unterstützung während dieser Zeit.

Bei Dr. Christoph Winkler möchte ich mich recht herzlich für die engagierte Betreuung meiner Masterarbeit und für die tolle Zusammenarbeit bedanken. Vielen Dank für deinen Einsatz, der es mir ermöglicht hat, sehr viel Neues zu lernen und mich weiterzuentwickeln.

Dr. Gábor Tasnádi möchte ich für seine Expertise und Unterstützung bei der Handhabung der Instrumente zur Chromatographie danken.

Dr. Michael Fuchs danke ich für die Bereitstellung der Transaminasen.

Tamara Reiter danke ich dafür, dass sie sich immer Zeit genommen hat, wenn ich Fragen hatte oder eine Chemikalie bestellen wollte.

Natürlich gilt mein Dank auch der gesamten Elk Crew für das freundliche Arbeitsklima, die Unterstützung und den netten Umgang.

Msc. Thomas Flecker danke ich für die Bereitstellung seiner Expertise auf dem Gebiet der HPLC.

Pascal Poschenrieder, der Firma Armesca ProCon GmbH und den Mitarbeitern der Universitätswerkstatt danke ich für die Unterstützung beim Bau der LED marbles.

Meinen Eltern meinem Bruder Pascal und meiner Freundin Johanna danke ich für die fortwährende moralische Unterstützung und den Rückhalt, nicht nur während der Masterarbeit, sondern während meiner gesamten Studienzeit.

Abstract

Biocatalytic synthesis strategies become increasingly popular in industry, because they are more selective and greener than conventional chemical methods. Additionally, increasing amounts of biocatalysts and biocatalytic methodologies are available every year.

Biocatalytic reduction reactions driven by nicotine amide dinucleotides either need the expensive cofactor in stoichiometric amounts or a cofactor regeneration system. *Synechocystis* bacteria use photosynthesis to regenerate NADPH and have been shown to be an effective host for recombinant reductive enzymes.

Biocatalytic model reactions were established, to broaden the field of application of the photosynthetic NADPH regeneration in cyanobacteria.

Five model reactions were established, using the transaminase from *Paracoccus denitrificans* in the NADPH dependent amination of acetophenone derivates.

Eight artificial enzymatic linear cascades were established. Four for the deracemisation of phenylalanine and leucine, four for the enantioselective production of 2-hydroxyisocaproic acid and 2-phenyllactic acid. Most cascades exhibited excellent conversion (>90%) and excellent enantioselectivity (>99%).

Finally, a new method to introduce light into chemical reaction systems is introduced: the LED-marble.

Kurzfassung

Biokatalytische Synthesestrategien werden in der Industrie immer beliebter, weil sie selektiver und grüner sind als konventionelle Methoden der Synthese. Außerdem werden jedes Jahr mehr Biokatalysatoren und biokatalytische Methoden verfügbar.

Von Nikotinamiddinucleotiden angetriebene biokatalytische Reduktionen benötigen entweder einen teuren Kofaktor in stöchiometrischer Menge, oder ein Kofaktor Regenerationssystem. *Synechocystis* Bacterien nutzen Photosynthese, um NADPH zu regenerieren und es wurde gezeigt, dass sie ein effizienter Wirt für rekombinante reduktive Enzyme sind.

Um das Feld der, durch photosynthetische NADPH Regeneration angetriebenen, Reduktionen in Cyanobakterien zu erweitern, wurden in dieser Arbeit mehrere biokatalytische Modellreaktionen etabliert.

Dabei nutzen fünf der etablierten Modellreaktionen die Transaminase von *Paracoccus denitrificans* zur NADPH abhängigen Aminierung von Acetophenonderivaten.

Acht künstliche, enzymatische, lineare Kaskadenreaktionen wurden etabliert. Die Hälfte wird zur Deracemisierung von Phenylalanin und Leucin und die anderen werden zur enantioselektiven Darstellung von 2-Hydroxyisocapronsäure und 2-Hydroxyphenylmilchsäure verwendet. Die meisten der Kaskadenreaktionen zeigten exzellenten Umsatz (>90%) und herausragenden Enantiomerenüberschuss (>99%).

Darüber hinaus wurde eine neue Methode entwickelt, um Licht in chemische Reaktionssysteme einzubringen.

Inhalt

1 Introduction

The goal of this master's thesis is to identify reductive biocatalytic reactions, feasible for coupling with a photobiocatalytic cofactor regeneration system (fig. 1).

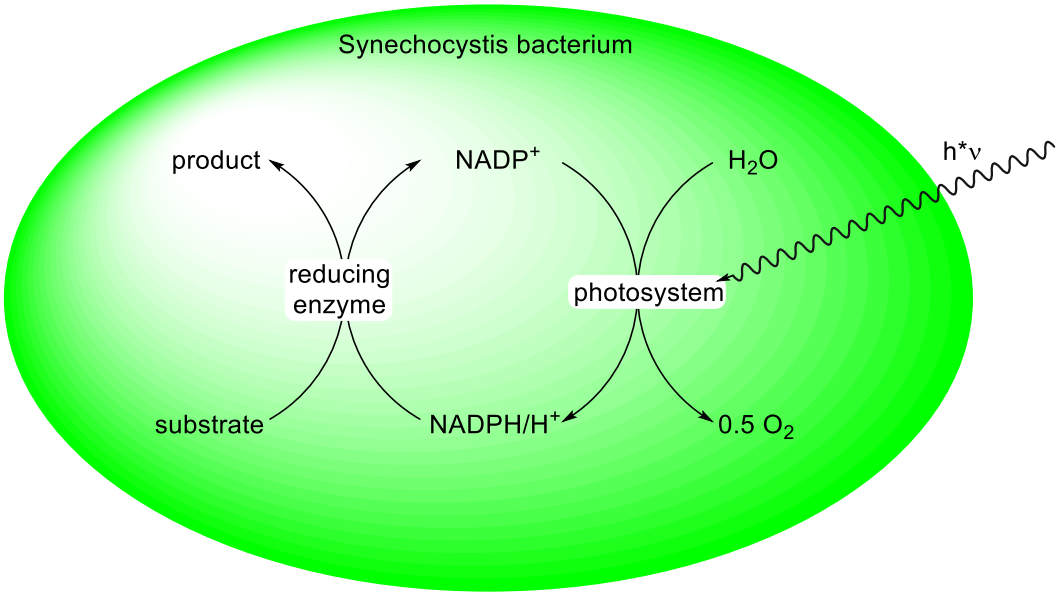

Figure 1: General scheme for the coupling of enzymatic reductions to the photosystem of *Synechocystis* bacteria *in vivo* heterologous expression.

The photobiocatalytic cofactor regeneration is facilitated by the photosystem of *Synechocystis* sp. PCC 6803 bacteria. This photosystem is capable of transferring electrons from water to $NADP^+$ in a light-dependent reaction, thereby regenerating NADPH. The use of water as the electron source leaves nothing but oxygen as a by-product. NADH regeneration would require an additional transnucleotidase and is thereby expected to be less effective. Thus, already established exclusively NADH-dependent enzymatic reductions and cascades containing a reductive step, need to be trimmed towards the use of NADPH as cofactor, primarily by selection of feasible enzymes.

Three types of reactions were chosen to demonstrate the viability of the concept: the reductive amination of benzaldehyde derivates using a transaminase, combined with a NADPH-dependent alanine dehydrogenase for cosubstrate recycling and the reduction of α-keto acids to either α-amino acids using a NADPH-dependent amino acid dehydrogenases or α-hydroxy acids using NADPH-dependent keto acid dehydrogenases. The latter two are designed to be part of an enzymatic cascade for

production of enantiomerically pure α-amino acids or α-hydroxy acids, starting from racemic or L-amino acids.

The identified reduction systems then shall be cloned into *Synechocystis* sp. PCC 6803 to perform the reductions under light driven cofactor regeneration, similar to the work of Prof. Dr. Kourist *et al.* who demonstrated the light-dependent reduction of activated alkenes using a heterologously expressed ene-reductase in *Synechocystis* sp. PCC 6803 cells.[1]

The major challenge for establishing cascades that will be the focus in this work, is the selection of appropriate enzymes. These combined enzymes not only need to be all stable and productive under the reaction conditions, but the reductive enzymes also need to be able to utilise NADPH as electron source.

2 Theory

2.1 Cascades

According to Kroutil et al., a cascade is defined as combination of at least two chemical steps in a single reaction vessel without isolation of intermediates.[2] This definition is very broad and can be applied on various reaction sequences of which most are everything else but new. For example, hazardous diazonium salts can be generated from amines, using *tert*-butylnitrite for subsequent reactions.[3] This can easily be achieved in one vessel and is simply called in-situ generation of intermediates. Nonetheless, such systems are highly advantageous as avoidance of intermediate isolation leads to higher yields, increased synthetic efficiency, reduced waste and cost, and easier handling of hazardous or instable substrates or intermediates. All these advantages are especially valuable since there is an increasing effort to reach greener methodology in chemistry.

The main reason for the increasing importance of this concept in biocatalysis is that combining enzymes is much more convenient than combining other chemical steps due to high compatibility of enzymes' reaction conditions. The high compatibility leads to a modularity of reaction steps. This way, vast numbers of results can be generated in short amounts of time by combinatory means.

An ever-increasing access to enzymes and novel reactivities drives the development of new biocatalytic cascades. Not only does the pool of different enzymes offered by nature seem inexhaustible but the handling and engineering of enzymes is also becoming more convenient due to improvements in DNA synthesis, high throughput strategies and ever growing experience in general.[4,5,6]

When it comes to the classification of cascades in general and biocatalytic cascades in particular, it is not possible to pass by the encyclopedic review of Dr. Schrittwieser *et al.*,[4] who summarized cascade attributes and introduced a useful hierarchy for these attributes whose application leads to a conclusive classification of biocatalytic cascades. Herein, only a few attributes that are important for this work are discussed.[4]

A cascade is considered biocatalytic, if there is at least one reaction step enabled by a biocatalyst.

There are several possible ways to interconnect reaction steps, whose entirety is called cascade. Two of them are important herein: linear and parallel cascades (Figure 2 and Figure 3).

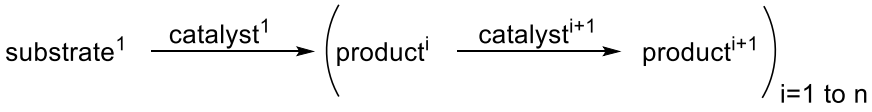

Figure 2: Linear cascades. In the case of domino cascades: catalyst^{i+1} = catalyst^{1}.[4]

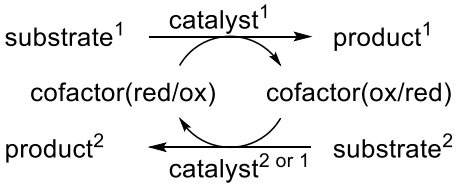

Figure 3: Parallel interconnected reactions at the example of a parallel cascade utilizing cofactor dependent redox enzymes.[4]

Cascades are classified to be linear if a single substrate is modified more than once in subsequent reaction steps, or parallel if different substrates are modified simultaneously. If a biocatalytic cascade is carried out with recycling of a cosubstrate in one pot, the two reactions, responsible for production and consumption of the cofactor are defined to be a parallel cascade. Nonetheless, cofactor recycling is such a frequent concept that it is barely emphasized as a parallel cascade.

Biocatalytic cascades are considered artificial if enzymes of more than one organism are employed, meaning that there is no known natural organism carrying out a similar reaction scheme.

Even though part of literature, defines cascades to be *in vivo* if freeze dried whole cells are employed, in this work these cascades are defined *in vitro*, since no living cells are present and because an external cofactor regeneration system is used. This definition of *in vivo* follows the one from Schrittwieser *et al.*.[4]

Cascades are defined as redox cascades if there is at least one reaction step, modifying the redox state of the substrate. If a substrate's redox state is modified in the cascade but the product has the same redox state as the substrate, the cascade is defined to be redox-neutral. Hydrogen-borrowing cascades are a special case of redox-neutral cascades in which the sum of transferred redox-equivalents equals a hydrogen molecule.[4]

Four artificial, linear cascades were established in this work (Figure 27). In the first step of the linear cascades, cheap and abundant L- or racemic amino acids are converted to the respective α-oxo-acids. In the second step, these oxo-acids are then converted either to enantioenriched L- or D-amino acids or the respective chiral hydroxy acids. Such reaction schemes represent either deracemisation processes or production of enantioenriched hydroxy acids from amino acids. Since the substrates of the cascades have the same redox state as the products, these cascades are all overall redox-neutral. They cannot be considered hydrogen borrowing, since the cofactor NADPH is not recycled within the linear reaction sequence. Cascades, leading to amino acids as final products may be considered ammonia borrowing.

When cloned into *Synechocystis* bacteria, the cascades may be considered water borrowing (Figure 47).

2.2 Studied enzymes

In the course of this study many different enzymes were employed. They belong to the following enzyme classes: dehydrogenases, oxidases, deaminases, and transaminases. This differentiation is based on the cofactor/coenzyme specificity.

Dehydrogenases catalyse the reversible dehydrogenation of amines and alcohols and use nicotinamide adenine dinucleotide (DAD(P)(H)).

Oxidases catalyse the irreversible dehydrogenation of alcohols or amines and directly transfer the liberated electrons to dioxygen, yielding hydrogen peroxide. When imines are formed, they are transformed to ketones *via* hydrolysis, as soon as they come into contact with the aqueous medium.

Deaminases also catalyse the irreversible dehydrogenation of amines but do not transfer the electrons to dioxygen directly. Instead, the electrons are transferred to the respiratory chain *via* shuttle proteins.

Transaminases transfer amine groups to ketones and vice versa. The equilibrium is generally defined by the concentration of the different substrates.

2.2.1 L-Amino acid dehydrogenases

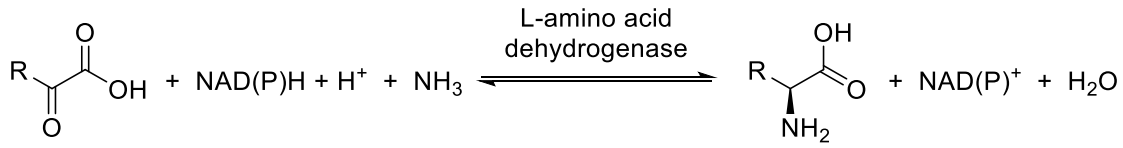

Figure 4: General reaction catalysed by L-amino acid dehydrogenases.

2.2.1.1 L-Glutamate dehydrogenase

Glutamate dehydrogenase (GluDH, EC: 1.2.1.2-4) is a fundamental enzyme at the interface of the carbohydrate and amino acid metabolic pathways and an integral part of every organism.[7,8,9] It catalyses the reversible reduction of α-keto acids to α-amino acids, facilitated either by NADH or NADPH and ammonium ions. However, *in vivo* microbial NADPH dependent GluDH reactions are not reversible.[10]

Consequently, the enzyme family is very large and subdivided into groups, based on the cofactor specificity or the number of subunits in the oligomeric enzymes. There are tetrameric and hexameric versions of the enzyme in microorganisms, but based on sequence homology, the evolutionary distance between GluDHs of different cofactor specificity seems to be greater. NAD(H) exclusive GluDHs are found in microorganisms and may be tetrameric or hexameric. All other GluDHs are preferably hexameric in solution. NADP(H) dependent GluDHs are also found in microorganisms. Mammalian GluDHs are dual-specific hexameric proteins and classified into the latter group.[8]

Based on the comparison of intracellular NAD(P)H/NAD(P)-proportion under aerobic conditions and initial rates of the individual enzymes, NADPH dependent GluDHs are believed to be anabolic enzymes, catalysing the synthesis of L-glutamate, while NAD^+ dependent GluDHs are catabolic enzymes.[8,10] An additional function of a human brain tissue GluDH has recently been found: it controls aspartate levels in astrocytes.[11]

Structure

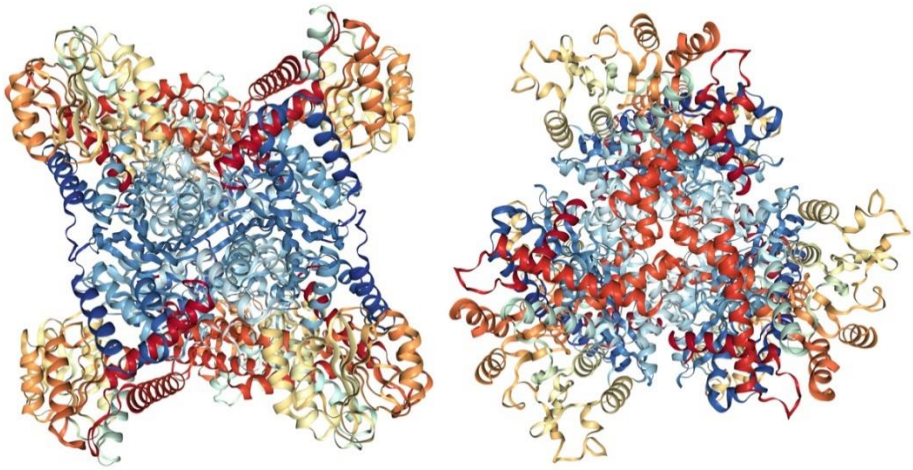

Figure 5: Glutamate dehydrogenase from *Aspergillus niger* in super-closed conformation (pdbid: 5XVX).[9]

The structural discussion is mainly based on a very recent article because, despite the enzyme having been extensively researched in the last 40 years, it is the first publication of the super closed conformation.[9] Since the enzyme's reaction mechanism is governed by interdomain movement, the super closed conformation represents an important missing piece in the description of the mechanism. Another missing piece is the identification of reaction intermediates, also achieved in this study. The authors also have emphasized allosteric substrate cooperativity and cofactor recognition.

The article is based on five new X-ray structures of GluDH from *Aspergillus niger* (*A.n.* GluDH) in complex with different ligands.[9] The *A.n.* GluDH structures are stated to be similar to *E.coli* GluDH structures and therefore serve as a structural model for the structure of microbial NADPH dependent hexameric GluDHs.[9] Sequence alignment reveals 55% identity and 69% similarity.

The super-closed conformation has been found in all six subunits of the structure of the enzyme in complex with α-ketoglutarate (AKG) and NADPH (pdbid: 5XVX). Reaction intermediates were identified after soaking the crystals of the apo-structure in a solution of AKG, ammonia, and $NADP^+$ (pdbid: 5XWC). In this structure, the ligands bind to the enzyme and ammonia is added but no reduction can occur, since the cosubstrate is in the oxidized state. In other parts of this work, such complexes are called abortive. Two of the five crystal structures, namely the apo-structure and the structure of the forward inhibited, covalently modified enzyme with only AKG as ligand (pdbid: 5XVI, 5XVV), exhibit special characteristics. Contrary to the other structures,

their subunits do not all have the same conformation: three subunits on one side of the barrel-shaped enzymes are in the closed conformation and the other three in the open conformation. In the structure with AKG as a ligand, this ligand is only bound to closed-conformation subunits.

In this publication,[9] the openness of a subunit is measured as the distance between the αCs of K122 and R280, two residues at opposite sides of the domain interface. Open conformations are characterized by distances larger than 10 Å, closed conformations by distances between 10 and 7 Å, and in the super closed conformation, the two amino acids have a distance of only 6 Å.

The enzyme consists of a hexameric cylindrically shaped protein oligomer that can be seen as a concentric dimer of trimers.

The subunits are built from 436 amino acids and can be further subdivided in two domains, both derived from the Rossmann-fold and separated by a deep cleft (domain I: substrate binding domain, domain II: nicotinamide dinucleotide binding domain). A similar subunit structure can be observed in tetrameric microbial D-LDHs (*vide infra*). The hexamer assembly is highly symmetrical (32-fold) with the subunits' interactions mainly mediated by domain II. The substrate binding domains (domain I) point away from the centre of the barrel like turbine blades. The hinge, separating the two domains lies at the bottom of the deep cleft and is kinked, depending on the state of catalysis and the availability of ligands.

The dimer interactions are mainly mediated by the β_1, β_2 sheets and the α_1, and α_{16} helices. The trimers mainly interact *via* α_{15}. These crystal structures with subunits in different conformations imply subunit cooperativity and communication that would have to be mediated by the dimer interactions. The cooperativity is stated to follow the Monod-Wyman-Changeux model.

The Rossmann-fold, constructed of seven α-helices and seven β-strands is found in the coenzyme binding domain (domain II, amino acid 191-436). It is slightly modified from the classical version by reversal of the direction of one of the β-strands and the occurrence of an additional α-helix.[12] The cofactor specificity for NADPH is mainly mediated by H82, K122, S253, K277 and Q282 as proved in mutational studies. While S253, Q282 of the coenzyme binding domain and K122 from the substrate binding domain make direct hydrogen bonds to the phosphate group, H84 and K277 make

hydrogen contacts, mediated by a conserved active site water. S253 is provided by the $\beta_{8\text{-}9}$ loop. Q282 and K277 are close to the negatively charged D252 which, together with S253, is highly conserved and thus may play a crucial role in positioning catalytically essential residues rather than its previously proposed role in destabilizing the NADPH binding.[9] Q282 is not conserved in *E. coli* GluDH. Instead, R285 (as in the PDB-structure 4FCC) may have a similar role.

The other domain (domain I, amino acid 1 – 190) functions in subunit assembly and substrate recognition. Polar interactions of the protein with the substrate in the super-closed conformation are mediated by K78, Q99, K102, K114, D154, R193, and N346. In this conformation, the C(4) of NADPH is 2.8 Å away from the αC of the substrate with the NADHs *Si*-H pointing towards the αC. This distance is ideal for hydrogen transfer.[13] The greater distance in the closed conformation is also why the super closed conformation has been predicted before.[8] The protein-substrate interaction pattern changes upon transition from the closed to the super-closed conformation. In the closed, also called semi-closed conformation, the substrate's α-carbonyl group makes contacts to K114 and main chain atoms of G80 while in the super-closed conformation, it binds to D154 and main chain atoms of G153. In the super closed conformation, the D154's ionization state is maintained by a highly conserved R82. The differences between the closed and the super-closed conformations stress the importance of the discovery of the super-closed conformation. The α-carboxy group is hydrogen-bound by K114, N346, Q99, and K102 in the super closed conformation, while the γ-carboxy group is bound by K78, R193, and S386. These three residues thus represent targets for mutation to alter the substrate specificity.

Three of the four L-amino-acid dehydrogenases were derived from the *E. coli* GluDH (pdbid: 4FCC): the mutants F11, F18, and F18-T195A.[10] The mutant F18 was constructed in a stepwise substrate walking approach with the goal of making it feasible for L-homophenylpyruvate reduction. Phenylpyruvate was chosen as the intermediate substrate. In the first round of mutagenesis, directed evolution targeted K92, A166, V377, and S380, chosen from sequence alignment with the GluDH from *Clostridium symbiosum*. The new structural model (*vide infra*) was not yet available but proves that the selected K92 equals K78 in *A.n.* GluDH and S280 equals S386. Both residues make hydrogen bonds with the γ-carboxylate in the wild type enzyme. If a new selection would be made, R210 (as in the PDB-structure 4FCC, R193 in 5XW0) could

be selected for a rational approach, since it is the third residue participating in γ-carboxylate binding. The two quadruple mutants F11 (K92C-A166G-V377A-S380A) and F18 (K92A-A166G-V377A-S380A) rescued growth on phenylalanine as the sole carbon source. F18 exhibited 43-fold increased catalytic efficiency for phenylpyruvate. F18 was chosen for an additional round of rational mutagenesis, choosing T195A as mutation, selected by sequence comparison with leucine and phenylalanine dehydrogenases. Sequence alignment with *A.n.* GluDH shows T181 to be equivalent. The tryptophane's residue is not reported to be involved in substrate binding but may contribute to steric hinderance of larger substrates.

Mechanism

The ammonium ion is hydrogen bound to main-chain atoms of G153 and by the negatively charged D154 residue. This aspartate takes the role of a catalytic base, deprotonating the ammonium ion and activating it for the nucleophilic attack on the αC-atom.[9] In an D165S variant GluDH from *E. coli*, a weaker affinity for ammonia was observed, indicating that D165 in *E. coli* GluDH has the same role as D154 in *A.n.* GluDH. Sequence alignment revealed that there is a sequence absolutely conserved between the enzymes from amino acid 145 to 162 (as in the PDB-structure 5XWO) between the two enzymes with D171 from *E. coli* GDH taking the place of D154 in *A.n.* GluDH.

Even though first believed to proceed *via* a Schiff-base,[7] the structure with the caught intermediates demonstrates that the reaction proceeds *via* an α-iminoglutarate intermediate. First step after polarization of the substrates carbonyl functionality is therefore the attack of the properly positioned and deprotonated (D154) ammonia molecule on the α-carbon. Protonation of the α-oxygen then leads to the carbinolamine intermediate, which has also been detected. This proton is provided by K114, shuttled *via* a conserved active site water. Subsequent water elimination leads to the iminoglutarate intermediate that has previously been detected in bovine GluDH. Proton transfer for facilitation of the water elimination is mediated by D165. The final hydrogen transfer from the NADPH's C(4) then leads to product formation. The rate determining step has, to my knowledge, not yet been identified.[8,14,9]

Application

There are many effectors influencing the activity of GluDHs from different sources. In general, substances mimicking glutamate or α-ketoglutarate, reportedly D-glutamete, *m*-dihalo arenes, and *m*-nitrobenzoates can competitively inhibit GluDH activity.[7] The competitive inhibitor isophthalate[7,9] deserves special mentioning because it can serve as good example pointing out, what requirements are posed upon a molecule, to be an effective glutamate mimic in this case. The rigid phenyl ring strictly defines the positions of the hydrogen bound carboxy groups that mimic the glutamate's carboxy groups. The small degree of conformational freedom facilitates binding in a cooperative way. The hydrophobic phenyl ring effectively mimics the hydrophobic methylene groups of the glutamate and the small size of the isophthalate removes any steric hinderance which may impede binding. For more insight into mimic design, see the literature.[15]

Also, allosteric inhibitors are reported for mammalian GluDHs, functioning for example in facilitation of GluDH-hexamer polymerization, like steroid hormones or chlorpromazine.[7]

The complex control of mammalian GluDHs is also facilitated by small activator molecules like D-leucine.[7]

For the GluDH wild type, the F18 mutant, and the F18-T195A mutant, the catalytic efficiencies towards α-ketoglutarate are 206, 0.037, and 0.06 s^{-1} mM^{-1} respectively, and for phenylpyruvate 0.061, 2.16, and 0.53 s^{-1} mM^{-1} respectively. For homophenylpyruvate the highest catalytic efficiency (28.9 s^{-1} mM^{-1}) is obtained in the F18-T195A mutant. The F11 mutant is yet to be characterized.

2.2.1.2 L-Leucine dehydrogenase

Enzymes of the L-leucine dehydrogenase family (L-LeuDH, EC: 1.2.1.9) are closely related to glutamate dehydrogenase (L-GluDH) in terms of their monomeric tertiary structure and belong to the same enzyme-superfamily, related by divergent evolution. Further superfamily-members are valine dehydrogenase (EC: 1.4.1.8) and phenylalanine dehydrogenase (1.2.1.20).

Like L-GluDH, the enzyme catalyses the reversible reductive amination of the corresponding α-keto acid to the L-amino acid. The coenzyme providing the redox equivalent is NAD(H). In the reductive direction, ammonium ions must also be

provided. The oxidative direction prevails in living organisms due to the low NADH/NAD ratio[16,17] in cells under aerobic conditions. Consequently, the enzyme functions as catabolic enzyme in the aliphatic branched side chain amino acid metabolism.[18]

Structure

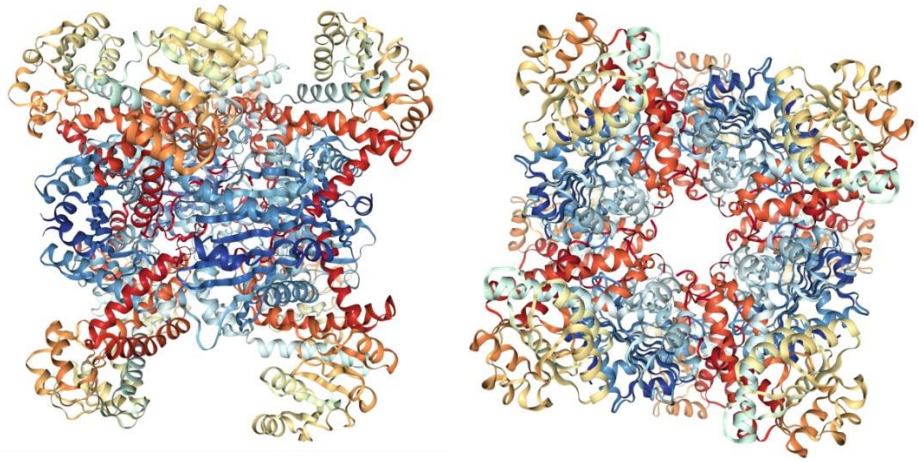

Figure 6: Leucine dehydrogenase from *Bacillus sphaericus* (pdbid: 1LEH).

The crystal structure has been elucidated by Baker *et al.* for the LeuDH from *Bacillus stearothermophilus* (*B.s.*).[14] This enzyme is structurally similar to the LeuDH from *Thermoactinomyces intermedius* (*T.i.*) and blast sequence alignment reveals very high sequence identity of 78% and similarity of 86%. The two enzymes differ mainly in a *C*-terminal extension present in the enzyme from *Bacillus sphaericus*, forming an additional α-helix with a *C*-terminal 15 amino acid loop, involved in subunit interweaving. The numbers given for amino acids and secondary structural elements in the protein chain, are derived from the amino acid sequence of *B.s.* LeuDH (pdbid: 1LEH). Sequence alignment also revealed that the numbering for the first 361 amino acids of *T.i.* LeuDH is identical to *B.s.* LeuDH. The *T.i.* LeuDH sequence was elucidated by Ohshima *et al.*.[19]

In contrast to the discussed GluDH, LeuDH has an overall octameric structure,[20] (42 × symmetry) even though the subunits and their assembly are very similar (turbine, barrel, *vide supra*). The solvent channel, running through the middle of the barrel in direction of the fourfold symmetry axis, is larger than in GluDHs, due to the octameric assembly.

The subunit assembly has been studied in detail based on the apo crystal structure (pdbid: 1LEH).[14] In the dimer interface, six β-sheets from each subunit assemble to a

12-sheet, expanding from one subunit into the other. This sheet is flanked on both sides by α-helices from both subunits. Subunit interactions are probably governed by α3 which packs with its *C*-terminus against the complementary *C*-terminus of α3' from the other subunit. The tetramer interface is mainly hydrophobic, with 18 additional hydrogen bonds of which 11 are conserved in *T.i.* LeuDH. The additional *C*-terminal α-helix in *B.s.* LeuDH together with its terminal loop, forms an arm reaching into a U-shaped pocket of the other subunit. Extensive subunit interactions, mediated by this arm, are described as handshake. These additional subunit interactions are probably the main differences between *T.i.* and *B.s.* LeuDH. As a consequence of these extensive interactions, about 20% of the overall monomer surface, (~16000 $Å^2$) is buried upon octamer formation of which 7.9% is buried upon dimer formation.

The eight subunits in the *B.s.* LeuDH crystal structures can be divided into two groups based on their conformation. Group A subunits, located at one barrel-lid, have a closed conformation in between the open and the super-closed conformation, with no cosubstrate or substrate bound to them. Group B subunits, at the other lid, have an open conformation (*vide supra*). Interdomain closing probably follows the Monod-Wyman-Changeux model (*vide supra*). The attempt to switch the open conformation subunits into closed ones by soaking the crystals in solutions of higher NAD^+ concentrations lead to crystal cracking. This behaviour of the enzyme, with subunits adopting distinct conformations depending on ligand binding, has been also observed in other dehydrogenases and is an indication for cooperative subunit behaviour (*vide supra*).

As in GluDH, the subunits can be divided into two domains. Domain I consists of amino acids 1-136 and 332-364 and is composed of a mixed parallel/antiparallel β-sheet, flanked on each side by two α-helices. Domain II, built from amino acids 136-331, folds into the classical Rossmann fold, in contrast to GluDH (*vide supra*).

Due to the close relation to L-GluDH it is sufficient to discuss the main differences and key catalytic residues. Overall domain movement and function will not be discussed.

Mechanism

The interdomain movement, interconverting open and closed conformations, is facilitated by two hinges in α6 and α13 (residues 141-146, 166-175). This movement is described as a rigid body screw rotation of 5.4° around an axis at the connection of

the two domains with a translational motion of 0.1 Å along this axis. To facilitate direct hydrogen transfer, the α-C atom of the substrate has to be about as close as 3 Å to the nicotinamides C(4) atom,[21] instead of about 7 Å, that are found when the substrate is modelled into the closed conformation's active site. This clearly indicates the existence of the super-closed conformation.

The active site is located at the bottom of the deep cleft, close to the hinge between the two domains. Key catalytic residues are provided from both domains. Since the mechanism of catalysis is believed to be similar between LeuDHs and GluDHs similar catalytic residues should be expected. In fact, as in GluDH, the shape of the active site is governed by five conserved glycine residues and the three key catalytic residues K102, K114, and D165 of GluDH (*vide supra*) correspond to K68, K80, and D115 in the two LeuDHs. Main alterations apply to the amino acid side-chain binding. The hydrophobic side chain binding in LeuDH is mediated by G41, A113, and Vl291 in the LeuDHs. The γ-carboxylate binding residues in GluDH (K78, S386, R210) correspond to L40, P146, and V294, thus cationic residues for carboxylate binding are replaced by neutral residues for hydrophobic binding. In contrast to this simple finding, a mutational study revealed the double mutant K78L-S386V to be catalytically incompetent.[22] A closer look at the structure revealed the simple substitution to cause a steric clash leading to subtle rearrangement of secondary structural elements, rendering the enzyme inactive. Thus, alteration of substrate specificity is not that trivial. As there is no available crystal structure of the super-closed conformation, these specifications should be regarded as preliminary.

Alteration of the cofactor specificity was achieved in the triple mutant variant *T.i.* LeuDH D203A-I204R-D210R. The residues were chosen based on previous studies on coenzyme specificity (e.g. Feeney *et al.*)[23] in dehydrogenases and on sequence alignment with NADP(H) dependent oxidoreductases. To facilitate NADP(H) binding, two negatively charged residues in proximity to the 2'-phoshate of the adenine ribose of NADP(H) were removed and two positively charged residues were introduced instead. These positively charged residues are believed to bind the negatively charged phosphate group. However, this mutational study has been done prior to elucidation of the crystal structure, thus improving the mutant dehydrogenase's NADP(H) specificity might be close at hand now.[24]

Application

Compared to the wild type *T.i.* LeuDH, the triple mutant's catalytic efficiency with NAD^+ decreases to only 0.03% as compared to the wild type's. On the other hand, the catalytic efficiency with $NADP^+$ is increased from 0.24 s^{-1} mM^{-1} to 5.20 s^{-1} mM^{-1}, representing about 2% rescued activity compared to the wild type enzyme in reaction with NAD^+. The specific activity of the mutant with $NADP^+$ is 19 µmol mg^{-1} min^{-1}.[24]

Thiol reagents like pyridoxal-5-phosphate are reported to be inhibitors for leucine dehydrogenases.[18]

2.2.2 D-Amino acid dehydrogenases

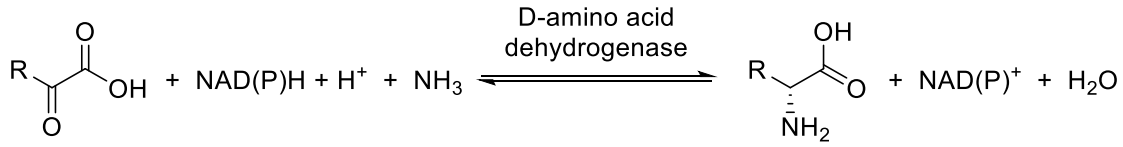

Figure 7: General reaction catalysed by D-amino acid dehydrogenases.

2.2.2.1 *meso*-Diaminopimelate dehydrogenases

Compared to L-amino acid dehydrogenases, D-amino acid dehydrogenases are much less abundant in nature and a lot less explored. Consequently, the range of possible enzymes for this research was restricted. On the other hand, the scarcity has increased pressure to develop industrially applicable enzymes of this kind. The discovery[25] of the family of *meso*-diaminopimelate dehydrogenases acting on the D-amino acid centre of the substrate has thus led to an increased effort to widen the substrate scope of these enzymes. The ultimate goal is to create a broad-spectrum D-amino acid dehydrogenase through mutation.[26,27]

In this research, four highly engineered D-amino acid dehydrogenase variants from different sources were used. They were all derived from *meso*-diaminopimelate dehydrogenases (*m*-DAPDH, EC 1.4.1.16). In nature, they are key enzymes in D-lysine synthesis, abundant in plants and microorganisms. The following mutants were used in this research: the quintuple variant *C.g.* DAPDH (Q151L-D155G-R196M-T170I-H245N), derived from *m*-DAPDH from *Corynebacterium glutamonicum* (*C.g.*);[27] the quintuple variant A (Q154L-D158G-T173I-R199M-H249N), derived from *m*-DAPDH from *Ureibacillus thermosphaericus* (*U.t.*);[28] an additional variant B (D94A-Q154L-D158G-T173I-R199M-H249N), also derived from *U.t.*;[29] and a variant (H227V), derived from *m*-DAPDH *Symbiobacterium thermophilum* (*S.t.*).[30]

The parental *m*-DAPDHs all catalyse the reversible oxidative deamination of the D-centre of *m*-diaminopimelate employing NADP(H) and ammonia as cosubtrates.

In 2017, Gao *et al*.[26] introduced the division of *m*-DAPDHs into two sub-classes: type I consists of dimeric enzymes exhibiting a narrow substrate scope for *m*-diaminopimelate (*m*-DAP); type II consists of hexameric enzymes acting also on other substrates like D-alanine, and are described as more active towards the reverse, reductive reaction. Accordingly, the sequence identity between *m*-DAPDH from *S.t.* (type I) and *C.g.* (type II) is only 28%,[26] while the sequence identity between *m*-DAPDH from *U.t.* (type I) and *C.g.* (type I) is higher (48%). In this research enzyme-variants derived from bacteria were used. The parental enzymes from *U.t.* and *C.g.* belong to class I, while the parental enzyme of *S.t.* belongs to class II. The oxidation of *m*-DAP is irreversible *in vitro* due to spontaneous cyclisation of the product. While *in vivo* class I enzymes are believed to prefer the oxidative direction, class II enzymes prefer the reductive direction, even though NADP(H) is the cosubstrate.[26]

The main mentioned, function related, differences in the primary structure between the two classes are conserved InDels that prevent oligomerization of more than two subunits in type I and very few alternated substrate- and coenzyme-binding residues.

Structure

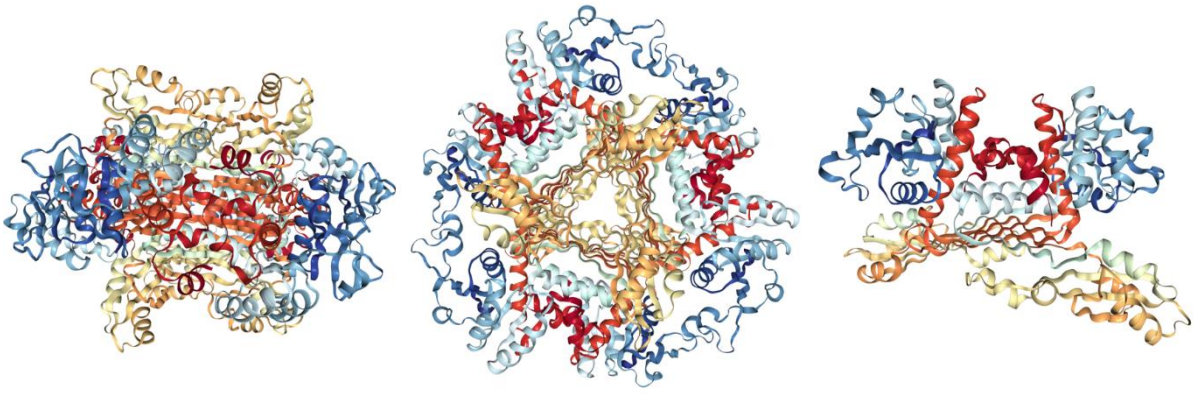

Figure 8: m-DAPDH from *Symbiobacter thermophilum* (pdbid: 3WB9, hexameric, left & middle),[31] from *Ureibacillus thermosphaericus* (pdbid: 3WYB, dimeric, right).[32]

As already mentioned, the enzyme is either dimeric or hexameric, depending on the type. The dimer shape is not easily described and should best be checked directly in the crystal structure (pdbid: 3WYB). The hexamer may be described as cyclic trimer of such dimers (pdbid: 3WYB). The shape resembles the hexameric or octameric amino acid dehydrogenases described above, except the barrel being flattened in the

direction of its symmetry axis. This leads to a more disc-like appearance with the turbine shape at the top on both sides.

Overall, the monomer-fold of the two classes exhibits a very similar tertiary structure. It is partitioned into three domains: the nicotinamide dinucleotide binding domain (amino acids 2-120, 275-304), the dimerization domain (amino acids 121-152, 247-174, 305-328), and the so-called *C*-terminal domain (amino acids 153-246).[29,32] The used amino acid numbers are derived from the crystal structure of *U.t. m*-DAPDH (pdbid: 3WYB)[32] and are similar in the other used enzymes. Enzymes of class I are indeed longer (class I: *U.t.* 328 amino acids, *C.g.* 320 amino acids; class II: *S.t.* 299 amino acids) but, since the main amino acid extension is *C*-terminal, the numbering is not affected.

The nicotinamide dinucleotide binding domain has the classical Rossmann-fold (*vide infra*), built from the helices $\alpha_{1\text{-}6,13}$ and sheets $\beta_{1\text{-}6,14}$ (as in the PDB-structure 3WYB). Since the general fold is elaborately described in other parts of this thesis, only the most important residues in coenzyme binding, as in the *C*-terminally His_6-tagged *U.t. m*-DAPDH in complex with $NADP^+$ (pdbid: 3WYC), are described. V121, P125, W123, and D124 are for nicotinamide binding; D94, S72, and S92 for nicotinamide ribose binding; N13 and L14 are for pyrophosphate binding; C69 for binding of the 3'OH of the adenine ribose; and Y11, T35, R36, and R37 are for binding of the 2'-phosphate group. The adenine moiety is bound mostly *via* hydrophobic interactions. Binding of NADP(H) in class II is largely conserved for nicotinamide, nicotinamide ribose, and pyrophosphate but differs greatly for the adenine ribose and the adenine moiety. These two moieties are much more solvent-exposed in *S.t. m*-DAPDH and even though residues at similar positions in the peptide chain are responsible for 2'-phosphate binding, their relative spatial positions differ greatly.[32,26]

The dimerization domain consists of helices $\alpha_{7,14\text{-}16}$ and sheets $\beta_{7,8,12,13}$ (as in the PDB-structure 3WYB). Class I *m*-DAPDHs have an additional *C*-terminal α_{17} which is involved in subunit assembly and stabilisation of the closed conformation. Class I oligomerization is facilitated by the formation of an antiparallel 6 β-sheet, made of 3 β-strands of each subunit, flanked on both sides by one α-helix of each subunit, which also form extensive interactions. Additionally, the *C*-terminal helix extends into a U-shaped pocket of the conjugated subunit, forming extensive interactions from V320 (L326) to H92*, D120*, and R128* (* indicates residues from the other subunit). These

interactions are in proximity to the substrate-binding region and are believed to stabilize the closed conformation. Indeed, *C*-terminally His_6-tagged class I enzymes have been shown to exhibit a lower overall activity than their untagged homologues, due to disturbance of this ion-pair network.[29] The class II subunit-assembly can be described as a trimer of this dimer forming a cylindrical unit, with a narrow solvent channel through its 3-fold symmetry axis. The trimer assembly of the dimers is achieved mainly by interaction of the turns at the side of the 6-sheets. The additional *C*-terminal helix is absent since it would hinder this trimeric assembly.

The, so-called *C*-terminal domain ($\alpha_{8\text{-}12}$, $\beta_{9\text{-}11}$) contains some of the catalytic domains and probably functions as the lid of the active site. The transition from the open to the closed conformation upon ligand binding is observed in many dehydrogenases and is assumed to be essential for catalysis. The motion is described as rigid-body movement of the *C*-terminal domain, rotating around the two linkage regions (G145-G147, H239-G241, as in *C.g. m*-DAPDH, apo PDB-structure: 5LOC, closed PDB-structure: 5LOA)[33] The finding that only one of the subunits is in the closed conformation, is assumed to indicate a “half of the sites reactivity”.[34] This “half of the sites reactivity” is also observed for other dehydrogenases and points towards a cooperative domain movement (*vide infra*).

While the substrate *m*-DAP binds with its α-carboxylate (D-centre) to M152, G153, and N253 in *S.t. m*-DAPDH, it binds to L154 and N276 in *U.t. m*-DAPDH. The α-amine group is bound to D92 in *S.t. m*-DAPDH, which in turn is bound to Y205. This tyrosine covers the active site entrance in the closed conformation, shielding it from the aqueous medium. This is believed to be essential for enabling hydride transfer (*vide infra*). Corresponding residues in *U.t. m*-DAPDH are D94 and Y224. The γ-amine group is bound to a histidine moiety *via* a hydrogen bridge mediated by an active site water molecule (H94 in *S.t.*, H96 in *U.t.*). The γ-carboxy group is bound to T171, R181, and H227 in *S.t.*, corresponding to T173, R199, and H229 in *U.t.*. Hence, the substrate binding is very well conserved between the two classes.[29]

The first attempt to widen the substrate specificity was made by Vedha-Peters *et al.*, who used *m*-DAPDH as a starting point.[27] They combined site directed saturation mutagenesis of rationally selected active site residues, binding the L-centre carboxylate, (R196, T170, H245) with two rounds of random mutagenesis over the

entire gene. The mutant Q151L-D155G-R196M-T170I-H245N has a broad substrate specificity on straight chain, branched and cyclic aliphatic and aromatic amino acids.

Even though this mutational study represents the first successful attempt to create a broad range D-AADHs, it has been argued that this enzyme would not be sufficiently stable for industrial applications. For this reason, similar mutations were applied on the thermostable *C*-terminally His_6-tagged *U.t. m*-DAPDH and indeed a broad range D-AADH was created this way.[28]

The same authors later recognized that the *C*-terminal His_6-tag disturbed the cooperativity of the enzyme subunits and indeed, removal of the tag increased the overall activity of the mutant and increased its thermostability.[29]

The additional mutation D94A was introduced into the quintuple mutant *U.t.* D-AADH (D94A-Q154L-D158G-T173I-R199M-H249N) to alleviate steric strain, observed in the structure of the enzyme in complex with phenylalanine. The enlarged binding pocket and its increased hydrophobicity has led to an increased overall activity in the oxidative direction and specifically increased the reductive activity towards phenylpyruvate.[29]

Another attempt to create a broad-spectrum D-AADH was made with the class II *S.t. m*-DAPDH. The starting point is a different one, also because natural class II *m*-DAPDHs already have a broader substrate spectrum than their class I counterparts. Five active site residues were selected in this study and subjected to site directed saturation mutagenesis. The most promising mutation H227V has a 35-fold higher activity towards phenylpyruvate than the parental enzyme.[30]

Mechanism

In the closed conformation, both the substrate and the cosubstrate lie buried in the core of the enzyme, thus no binding of either could occur after domain closure. Structural insight revealed that only the substrate is likely to influence the domain movement. Since domain closure without bound cosubstrate is unproductive, a mechanism with successive cosubstrate and substrate binding seems to be more likely than binding in a random order. The finding that there is a solvent channel, leading directly to the active site, does not lift these restrictions, since it is too small for cosubstrate and *m*-DAPDH. It may instead serve to provide ammonia for the reductive reaction. After binding of both substrates, domain closure brings the nicotinamide and the D-centre α-C into close proximity and enables catalysis. There are many aspects

of the enzymes that resemble glutamate dehydrogenases: successive binding and domain closure leads to the reaction, general domain organization and the *C*-terminal arm, governing the subunit assembly. It is also believed that these enzymes share a common mechanism and thus further aspects, like subunit cooperativity and reaction intermediates, will be discussed in the glutamate dehydrogenase chapter. An interesting difference is the differentiation of the substrate binding domain of GluDHs into the *C*-terminus and the dimerization domains. This also attributes to the flattened shape of the oligomer (*vide supra*).

Application

The quintuple mutant Q151L-D155G-R196M-T170I-H245N shows activity for the reductive amination of several amino acids in the range of 0.1 to 2.5 U mg^{-1} lyophilized solids (7.8 U mg^{-1} for D-2-aminooctanoate). Such a broad spectrum qualifies this mutant to be called a D-amino acid dehydrogenase (D-AADH).

0.22 U mg^{-1}, 0.11 U mg^{-1} and >99% e.e. were measured for D-leucine and D-phenylalanine respectively.[27]

Competitive inhibitors are for example close structural relatives to *m*-DAP like (*S*)-5-((*R*)-2-aminopropyl)-4,5-dihydroisoxazole-3-carboxylic acid.[35,36]

2.2.3 L-Hydroxy acid dehydrogenases

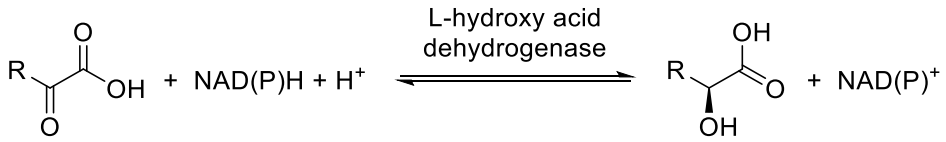

Figure 9: General reaction catalysed by L-hydroxy acid dehydrogenases.

2.2.3.1 L-Lactate dehydrogenase

The L-lactate dehydrogenase (LDH, EC: 1.1.1.27), that was used in this study, is derived from an enzyme from *Bacillus stearothermophilus* (*B.s.*). The enzyme catalyses the enantiospecific, reversible reduction of pyruvate to L-lactate and uses nicotinamide dinucleotide [NAD(H)] as cosubstrate.

Extrensive research on its structure and function is ongoing since the 1950s. The enzyme represents an important catalyst for the *anaerobic in vivo* degradation of glucose to providing energy to the cells. Close relatives of the enzyme are present in most organisms. In humans it is known to lead to muscle pain after extensive training.

While eucariotic LDHs are very specific for pyruvate,[37] bacterial LDHs are able to accept substrates with longer side chains, though forking at C(3) drastically decreases the catalytic efficiency.

Structure

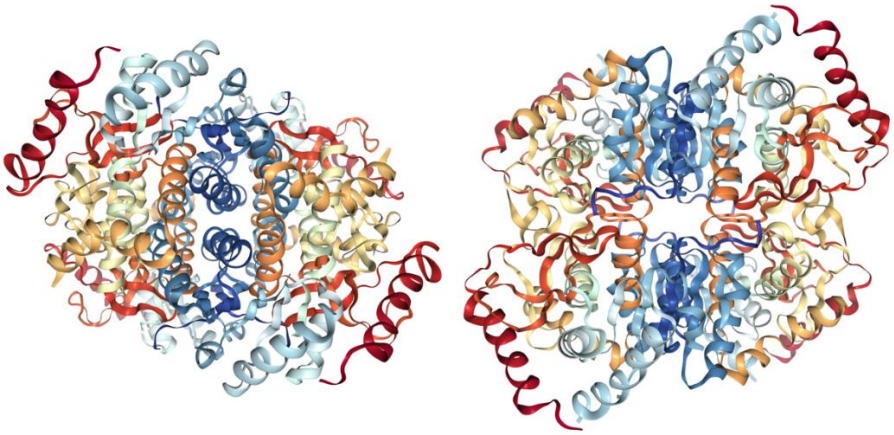

Figure 10: Lactate dehydrogenase from *Bacillus stearothermophilus* (pdbid: 1LDB).[38]

The amino acids are numbered as in the crystal structures of pig heart LDH (pdbid: 5LDH).[39] *B.s.*LDH crystal structures (pdbids: 1LDB, 1LDN),[40,38] are also available in the protein data base. In the sequence displayed at the protein data base (pdbid: 1LDN), the first fourteen residues are missing. The reason for this is that most eucariotic enzymes (pdbid: 5LDH) possess an additional, fourteen amino acid long α-helix at the *N*-terminus. For comparability reasons it was chosen to start the sequence with amino acid fifteen. This kind of counting is not employed in the mutational study by Flores *et al.*, so in the part of the discussion, referencing to this publication,[41] amino acid counting starts with 1 (for example, I37 in the mutational study equals I51 in other publications).

The enzyme is either dimeric or tetrameric depending on its concentration in solution and on the presence of an activator molecule.[42,43]

Enzyme-subunits undergo spatial rearrangements upon cosubstrate and upon substrate binding. When only the cosubstrate is bound, the enzyme is in its apo-form and when the substrate is also bound, it is in the holo-form.

The monomeric enzyme subunits can be further divided into domains, the nucleotide binding domain and the substrate binding domain. The active site sits at the interface of the substrate and cosubstrate binding domains and has a very flexible active site

loop. Additionally, two anion binding sites are located at the interface between the two dimers which form the tetramer. For differentiation between protein surfaces, representing the interfaces between subunits, Rossmann *et al.* have introduced three imaginary perpendicular axes, called the Q-, R-, and P-axis.[12] The monomer interfaces, contacting to form the dimeric enzyme, are perpendicular to the Q-axis, while the dimer-dimer interface, responsible for tetramer formation, is perpendicular to the P-axis. There is no random subunit assembly but the dimer, always with monomer-monomer contacts *via* the Q-interface, assembles with another dimer to a tetramer *via* interactions of the P-interfaces. Overall the enzyme has a highly symmetrical quarternary structure.

The nicotinamide is tightly but non-covalently bound in the cosubstrate binding domain of the enzyme. As in most nicotinamide dependent enzymes the structure of the nucleotide binding domain is defined by the so-called Rossmann fold, a pattern of alternating α-helices and β-strands. Unspecific binding of the NAD(H)'s adenine moiety takes place in a hydrophobic pocket, located at the surface of the enzyme. This moiety can move significantly during the course of catalysis, probably coupled to the closing of the active site loop. The unspecific hydrophobic pocket can also bind other aromatic systems, provided they are small enough. This circumstance can be utilised for purification of the enzyme. The adenine's ribose unit is bound *via* hydrophobic interactions and is hydrogen bound *via* its hydroxy groups. Since in NADP(H), the 2'-hydroxy group is replaced by a phosphate group, this is the locus, where discrimination between the phosphorylated and non-phosphorylated cosubstrate takes place. In the *B.s.*LDH, the 2'-hydroxy group is hydrogen bound to a negatively charged aspartate residue. In most enzymes employing NADP(H), the negatively charged phosphate group that would be subject to charge repulsion from the aspartate residue, is bound *via* ionic interactions to a positively charged arginine residue, replacing the aspartate. The pyrophosphate group, interconnecting both ribose units, is bent to a gauche-gauche conformation, negatively charged, located at the *N*-terminus of an α-helix dipole and extensively bound *via* charge interactions and hydrogen bonds. The nicotinamide's ribose unit is, as the other ribose, bound *via* hydrophobic interactions and hydrogen bonds *via* its hydroxy groups. The environment of the catalytically vital nicotinamide unit is generally hydrophobic. Additionally, the amide group is surrounded by more polar residues to increase binding strength. This hydrophobic surrounding of

the nicotinamide moiety accounts for the stronger binding of the reduced cosubstrate in contrast to the positively charged, oxidized cosubstrate.

In the substrate binding domain, close to the nicotinamide-moiety site, the substrate is bound *via* hydrogen bonds. The substrate's carboxylate group is hydrogen bound to R171[44,45] and the carbonyl or hydroxy group is bound to H195,[45] which acts as acid base catalyst and is either protonated or deprotonated, depending on the redox state of the substrate's C(2) and on the state of catalysis.

The active site is located at the interface of the nicotinamide moiety of the substrate and the C(2) of the substrate. The active site crevice is rather hydrophobic and accessible by solvent, depending on the conformation of the active site loop. As part of the active site, the active site loop (98-110), containing the catalytically important, positively charged R109 residue[46] undergoes large special rearrangement during catalysis. The positive charge of R109 is partially counterbalanced by D168, stabilizing the ternary complex.[45] Compared to eucaryotic enzymes, the loop is in a more open conformation in the apo form of the enzyme. This is attributed to tightening of the loop structure by two intra-loop H-bridges and introduction of main-chain restraints due to exchange of glutamine to proline in the bacterial enzyme. This more open conformation is attributed to a wider substrate specificity.[40]

The anion binding site is located at the dimer-dimer (perpendicular to P-axis) interface. H188 and R173, symmetrically allocated at the dimer-dimer interface repel the corresponding residues of the other subunit and thus destabilize the tetramer. Comparison with eukaryotic LDHs shows that their equivalent binding site is always occupied by small anions and that removal results in irreversible deactivation. The structural difference to bacterial LDH, known to be activated by fructose-1,6-bisphosphate (FDP) is that eucaryotic LDHs have more positively charged residues at the anion binding site, resulting in stronger anion binding and an enzyme, always in its tetrameric state. In *B.s.* LDH, FDP binds at the interface between two corresponding H188 residues, coiling around one of the imidazole units. Both phosphates of the FDP interact with both H188, while each phosphate interacts with only one R171. There are slight asymmetries, due to differentiation between the two histidine residues and the orientation of FDP (asymmetry of fructose). The planes of the two imidazole moieties are parallel and separated by only 3.5 Å, representing a distance suitable for pi-stacking.[47] H188 is connected to H195 and R173 to R171 *via* βG/H (182-196) and αF

(163-179), respectively and thus are directly communicating the binding state to the active site. As effect, the affinity of the active site for the substrate is increased. This suggests that FDP is stabilizing the tetramer, increasing the thermal stability and additionally increasing the affinity for the substrate. In nature, this makes sense, since at a high rate of glycolysis, when excess glucose is available, energy equivalents are generated as fast as possible as lactate is secreted. On the other hand, when FDP is not available, pyruvate is passed to the citric cycle for optimized total energy gain per glucose unit. Since the enzyme more closely resembles the eucaryotic enzyme in its FDP-activated form, the absence of FDP is considered a deactivation rather than FDP presence an activation.[40,15,42,43,48,49,38]

Mechanism

The catalytic mechanism is described as a sequence of successive, distinguishable steps. The reaction sequence of pyruvate reduction at one subunit of the tetrameric enzyme starts with binding of the reduced NADH at the coenzyme binding site. Then pyruvate binds to the substrate binding site, forming a ternary NADH-LDH$^+$-pyruvate complex. Upon ternary complex formation, the active site loop closes.[46] This causes extrusion of water from the active site cleavage and proper alignment of substrates and important residues. The substrate's carbonyl functionality is thus located between H195 and the nicotinamide ring of NADH. Extrusion of water renders the active site more hydrophobic and the binding of the reduced cofactor more fortunate than the oxidized. Approach of the protonated loop residue R109 to the protonated H195 imidazolium decreases its pK_A and causes proton transfer to the adjacent pyruvate's carbonyl-O atom, activating the carbonyl-C[50,51] for the subsequent hydride transfer from the adjacent NADH's nicotinamide-C(4). The developing positive charge at the nicotinamide causes charge repulsion from the hydrophobic active site wall, where it was aligned and stabilized. This charge repulsion causes the active site loop to open, facilitating lactate and subsequent cofactor release, leaving the H195 deprotonated. Reduction of pyruvate is thermodynamically favoured.[37] Its rate limiting step is release of the oxidized cosubstrate.

Lactate oxidation on the other hand is initiated by NAD$^+$ and subsequent pyruvate binding, causing the active site loop to close. This pushes the protonated nicotinamide moiety against the hydrophobic wall and charge repulsion initiates reverse electron and hydride flow. As H195 accepts the lactate hydroxy proton, charge repulsion of

R109 pushes the loop open and allows substrate and cosubstrate release. The rate limiting step of the oxidation is a conformational change prior to reduction, associated to the hydride transfer, as a primary isotopic effect with NAD^2D was observed.[46,45]

In the description of the mechanism by Grau *et al.* about LDH from pig heart,[39] it was termed “charge repulsion balance” mechanism and developed from the “oil-water-histidine” mechanism introduced by Parker and Holbrook.[51] No observations indicate that this mechanism is untrue for bacterial LDHs. The differences are that the loop is in a more open conformation in bacterial LDH,[40] giving it a broader substrate specificity and that the bacterial LDH is activated by FBP, while the eucariotic enzyme is fixed in the activated state. It should be noted that, when product concentration is high, there is the possibility of an abortive complex[39] with the product, decreasing the speed of the turnover when the reaction is coming close to completion.

The enzyme has been mutated for studying reasons,[44–46,48] to change the substrate scope[52] and to switch the cofactor specificity[23,41,53]. Since the aim of this study is to create a cascade, feasible for cloning into microalgae to use photosynthesis for NADPH regeneration, an enzyme that can utilize NADPH was required. The quintuple variant F16Q-I37K-D38S-C81S-N85R was created by Flores *et al.*,[41] in a modified consensus approach, using the results of previous studies on the mutation of the coenzyme binding domain and on the overall structure of the enzyme. They reason that the change in cofactor specificity was less due to the exchange of the negatively charge D38, which is in close vicinity to the 2’-pyrophosphate, but due to subtle changes in the overall protein structure. They were able to switch the enzyme’s cosubstrate preference from NADH to NADPH in the presence of FBP, measured as initial reaction rates of the oxidation of lactic acid.

Appliction

While the wild type enzyme exhibited an initial rate of about 13 nmol (min 7.5 pmol enzyme)$^{-1}$ with NAD^+ and only about 0.1 nmol (min 7.5 pmol enzyme)$^{-1}$ with $NADP^+$, the quintuple mutant exhibits an initial rate of 2.1 nmol (min 7.5 pmol enzyme)$^{-1}$ with NAD^+ and 4.3 nmol (min 7.5 pmol enzyme)$^{-1}$ with $NADP^+$.

Some kinetic parameters, relevant for this work, are displayed in Table 1. It is stated that the mutant's K_M's are not drastically changed.[41]

Table 1: Kinetic data of wild type and quintuple variant (F16Q-I37K-D38S-C81S-N85R) lactate dehydrogenase from *Bacillus stearothermophilus*.[41]

Substrate	K_M [mM]
$NADP^+$ (quintuple variant)	4.7 ± 0.7
Pyruvate (wild type)	0.04
Phenylalanine (wild type)	0.67

2.2.3.2 L-2-Hydroxyisocaproic acid dehydrogenase

L-2-hydroxyisocaproate dehydrogenase (LHicDH, EC: 1.1.1.-, last number not defined) from *Lactobacillus confuses* (*L.c.*) has a very high structural similarity to L-LDH (29% identity to L-LDH from *Lactobacillus confuses*, 31% to *B.s.*LDH, 23% to L-LDH from dogfish)[54,55] and thus the mechanism will not be discussed in detail again.

The enzyme was found by Schütte *et al.* 1984, during the purification of L-LDH from the same organism. The researchers noticed a loss in activity for phenylpyruvate during a distinct partition step and deduced the presence of a second enzyme.[56]

As LDH, it catalyses the reversible, L-specific, NADH dependent reduction of α-keto acids. The main differences between L-LDH and LHicDH are the different substrate scope and the absence of FBP activation.

Due to the high catalytic activity, good stability and broad substrate scope, the enzyme presents an outstanding candidate for industrial dynamic resolution of racemates and the production of synthons. Research for the establishment of advantageous biocatalytic cascades is in progress, incorporating also the present thesis.[57,58]

Structure

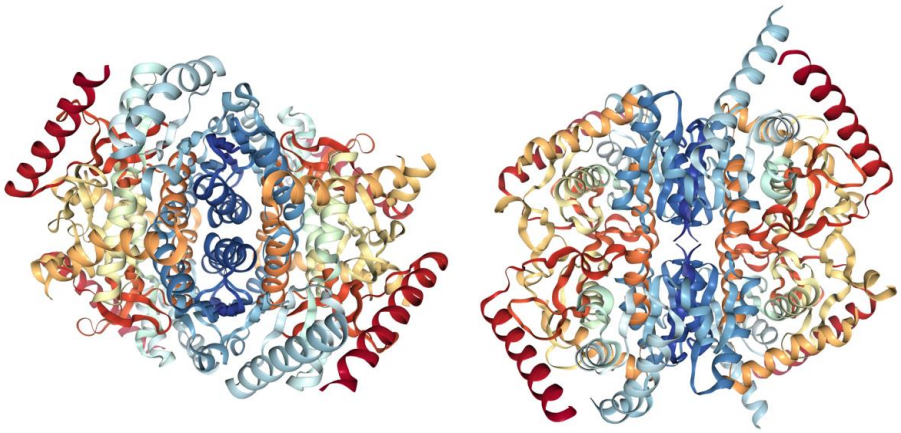

Figure 11: L-2-Hydroxyisocapric acid dehydrogenase from *Lactobacillus confuses* (pdbid: 1HYH).[59]

The crystal structure of L-HicDH with NAD^+ and sulphate-ions as ligands has been solved and compared to two distinct crystal structures of dogfish M4 L-LDH, a crystal structure of *Bacillus stearothermophilus* L-LDH and a crystal structure of L-LDH from wild boar (pdbids: 1HYH, 1LDM, 6LDH, 1LDN, 9LDT respectively).[59–61]

Since the resemblance of the enzyme to microbial LDHs is extraordinary, only the main differences are described.

Different to other microbial L-LDHs, the quarternary structure is stabilized by the additional *N*-terminal α-helix and not by FBP, as in L-LDHs from higher organisms. Consequently, a concentration dependent dissociation of the protein tetramer has not been found in the literature. Fittingly, there is a serine residue at the position, equivalent to H186 (as in the PDB-structure 1LDN), the anion binding site of *B.s.*LDH.

The known activity related residues are all well conserved, except for one isoleucine residue is alternated to valine in the substrate side chain environment, maybe to make room for larger substrates.

The active site loop is elongated compared to bacterial L-LDHs, noticeable by the insertion of two amino acids at each active site loop hinge regions (I100-K101, N106-P107, as in the PDB-structure 1HYH). It has been suggested that an elongated active site loop may facilitate closure over larger substrates. However, deletion of all four residues in LHicDH did not lead to favouring of pyruvate but rendered phenylpyruvate the only substrate. Maybe the phenyl substituent renders complete loop closure completely unnecessary. Anyways, deletions in the region of I100-K101 decreased the

overall catalytic efficiency, while deletions in the N106-P107 region drastically altered the substrate specificity towards larger substrates, contrary to the prediction. This shows that the dynamic structural changes in the loop region, essential for the catalysis, is not easily deduced from static crystal structures and cannot be ascribed to just sterics.

An inner active site cofactor loop is described which, to our knowledge, has not yet been described for LDHs. In fact, a very similar sequence has been found in the same region of *B.s.*LDH, in which I141 is exchanged by alanine, S142 by threonine, representing residues with different steric demand but similar chemical functionality. So, an additional mutational study of these residues may prove worthwhile.

Worth mentioning is also that, to our knowledge, in contrast to all LDH crystal structures, the four monomer subunits of the tetrameric enzyme are not in the same conformation. Instead, two of the subunits are in the open while the other two are in the closed conformation. Niefind *et al.* assumed that this asymmetry would probably be induced by NAD^+-binding.[59]

The fact that the enzyme is also active with NADPH, contrary to the reported exclusive NADH facilitation declared by Schütte *et al.*,[56] renders this enzyme interesting for this research.

The different substrate scope is mainly attributed to the following differences: the Q103 residue is fixed to the back, providing space, while it points towards the substrate side chain in *B.s.*LDH., I100 substitutes a glutamine present in *B.s.*LDH, increasing the hydrophobicity of the active site pocket, L242 substitutes isoleucine in *B.s.*LDH, providing more structural flexibility in the area of the substrate side-chain and to further differences in the contact zone between the active site loop and αG1/G2 in the closed conformation.

Application

All these changes combined supposedly lead to the emphasised differences in the substrate scope. While native microbial LDHs mainly accept pyruvate, have low activity towards other small straight-chain α-hydroxy acids and have only marginal activity with branched substrates, L-HicDH exhibits its highest catalytic efficiency with 2-oxocaproate while it is five orders of magnitude less effective towards pyruvate, mainly due to a reduced k_{cat} (Table 2).

Table 2: Kinetic parameters of L-HicDH.[62]

Substrate	K_M [mM]	k_{cat} [s^{-1}]
2-oxoisocaproate	0.067	2400
2-oxocaproate	0.11	3.6×10^5
2-phenylpyruvate	0.026	7300
pyruvate	3.5	90

The maximum activity of the purified enzyme from the natural source was measured as 479 U mg^{-1}.

The enzyme is inhibited presumably by the same substrate mimetics as LDH with a preference towards larger mimetics. Reports in the literature were not found. Feil *et al.* reported cosubstrate inhibition.[62] Inhibition due to absent FBP is not present.

The optimum pH for the reduction of keto acids is 7.0, different than 8 – 8.5, representing the optimum pH for the oxidative direction, as also described for LDHs and reasoned to be attributed to the protonation or deprotonation of the active site acid base catalyst histidine residue (see mechanism of LDH). As in LDHs, the reductive direction is favoured.[56]

The enzyme is reportedly stable between pH 5.5 and 9.0.[56]

Maximum activity is reached at 50 °C (3 × more active than at 30 °C).[56]

Stability is maintained up to 40 °C.[56]

2.2.4 D-Hydroxy acid dehydrogenases

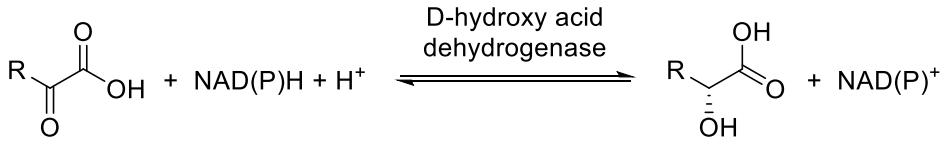

Figure 12: General reaction catalysed by D-2-hydroxy acid dehydrogenases.

2.2.4.1 D-Lactate dehydrogenases

All used enzymes with this reactivity belong to the large family of D-2-hydroxy acid dehydrogenases. Part of this family are for example D-lactate dehydrogenases (D-LDH, EC: 1.1.1.28), D-3-phosphoglycerate dehydrogenases (EC: 1.1.1.95), D-2-hydroxyisocaproate dehydrogenases (D-HicDH, EC: 1.1.1.-, not defined),

glyoxylate/hydroxypyruvate reductase (EC: 1.1.1.81), and, quite surprisingly, formate dehydrogenase (EC: 1.2.1.2), even though formate is not chiral.[63,64,65,66]

The single sub-groups of the enzyme family mainly differ in their substrate specificity.

The enzymes used in this work are: D-2-hydroxyisocaproic acid dehydrogenase from *Lactobacillus paracasei* (D-HicDH from *L.p.*),[67,68] the *C*-terminally His_6-tagged D-2-hydroxyisocaproic acid dehydrogenase from *Haloferax mediterranei* (D-HicDH from *H.m.*)[69,70,71] the hydroxypyruvate reductase from *Escherichia coli* K12 (YiaE),[72,73,74,75] and the *C*-terminally His_6-tagged triple variant D-lactate dehydrogenase from *Lactobacillus delbrueckii* ssp. *bulgaricus* (D-LDH from *L.b.*, D176S-I177R-F178T).[76,77,78,79] All four enzymes catalyse the reversible reduction of α-keto acids to α-hydroxy acids. Like with all dehydrogenases, nicotinamide dinucleotide (NAD(P)(H)) is used as cofactor. While the first three mentioned enzymes prefer NADH over NADPH, the latter was engineered to use NADPH. Special attention has to be paid to *L.b.* D-LDH because the species harbours at least five different D-HADHs and another, tetrameric version of the D-LDH is discussed in the literature.[80,69]

The enzymes' *in vivo* function is to take part in the metabolism of fatty acids, for example in the glyoxylate bypass. The production of hydroxy acids as a sink for NADPH from photosynthesis in plants has been proposed as natural function.[73]

Structure

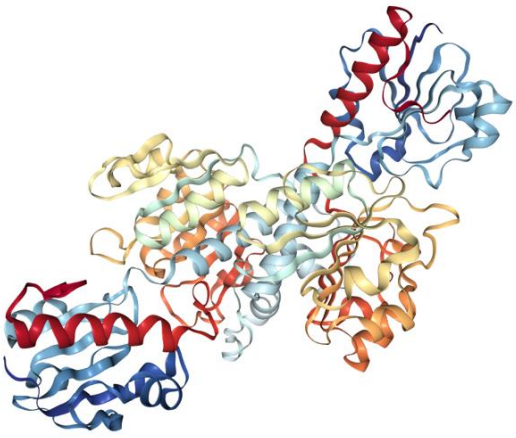

Figure 13: D-2-Hydroxy acid dehydrogenase from *Haloferax mediterranei* (pdbid: 5MHA).

The enzyme class can be further divided into one consisting of tetrameric enzymes and one consisting of dimeric enzymes. All four enzymes discussed herein are reported to be dimers of about 80 kDa mass in solution.[66,77,75] The crystal structure of D-HADH from *Haloferax mediterranei* is solved (pdbid: 5MHA) but has yet to be published in a journal.

The monomer subunit can be further divided into two domains: the nicotinamide dinucleotide binding domain and the substrate binding domain, in some publications also called the catalytic domain. This designation is misleading, since it implies that this domain would include the active site, which is not the case. In fact, the catalytic signature triade residues (*vide infra*) are all located in the cosubstrate binding domain. The active site lies at the bottom of a deep cleft, framed by both domains and is constructed from residues of both domains and made whole only upon rolling[81] inter-domain movement.[77] The overall monomer structure is described as dumb-bell-like.[66]

The two monomers bind *via* the *N*-terminus of the substrate binding domain. The contact zone is predominantly hydrophobic.[66] The possible structural role, induction of anti-cooperative domain movement, will be discussed below.[77]

Based on the concept of modularity, the Rossmann folded NAD(H) binding domain will not be described in detail. It is found in the middle of the protein chain. Functionalities like the hydrophobic patch, activating the nicotinamide for hydride transfer, are conserved. The wild type enzymes D-HicDH, *L.b.* D-LDH, and *H.m.* D-HADH are specific for NADH and retain about 1/10 of their activity when NADH is replaced by NADPH.[74] In YiaE and *H.m.* D-HADH the cofactor specificity is switched to NADPH.[73] A special feature, namely a loop (175-179, numbered like in the PDB-structure 1J49), controls the selectivity towards NAD or NADP.

Based on a sequence alignment with the NADP dependent glyoxylate reductase from *Pyrococcus horikoshii* OT3 (pdbid: 2DBQ), this selectivity control loop was altered in the NAD(H) dependent *C*-terminally His_6-tagged D-LDH from *Lactobacillus bulgaricus* to accept NADP(H). For this reason, three unconserved central residues, contrary to the two hinge residues at the ends of the loop, were exchanged.[76] The triple mutant D176S-I177R-F178T has a 184-fold increased catalytic efficiency with NADPH compared to the wild type and has not lost its activity towards NADH. Additionally, the overall activity increased. While the residues prior to mutation made two H-bonds to

the adenine ribose hydroxy groups (*via* D176) and one hydrophobic interaction with the adenine moiety, the variant residues form three H-bonds with the phosphate's hydroxy groups (*via* R177 and T178) and one H-bond to the ribose hydroxy group (*via* S176). Additionally, the negative charge at the aspartate, excluding the negatively charged residue from the binding site, is replaced by two positively charged residues, dragging the negative charge into the binding site. These findings are extraordinary since they suggest that the first successful attempt to alter the cofactor specificity upon exclusively rational design has been made and because the authors provide the reasons for their success and the reasons for the failure of other attempts. Consequently, the results have been published in nature.[76] With respect to the ultimate goal of this work, to clone the whole cascade into cyanobacteria, it is important to point out that the variant mutant not only has been designed to fit to the NADP(H) dependent photosystem of cyanobacteria but has also already been tested in cyanobacteria.[82] For more information on the general organization of the NAD-binding domain, see the descriptions of the other dehydrogenases or the literature.[66,65]

The substrate binding domain is Rossmann-fold derived, since it also consists of alternating α-helices and β-sheets and the β-strands form a parallel sheet, lined by the helices. Compared to the coenzyme binding domain it consists of fewer sheets and helices and is overall smaller. It is composed of the two ends of the protein chain. The overall temperature factor of the substrate binding domain has been found to be larger, associated with the inter-domain movement, since the coupled cosubstrate domain movement is masked by association with other monomers.[80]

There are two flexible hinges, connecting both ends of the cofactor binding domain protein chain to the two parts of the substrate binding domain, allowing flexible inter domain movement in a rolling motion. This rolling motion describes the interdomain movement in a way, rotating around a central hinge. It opposes a sliding interdomain movement.[81]

The active site lies, as already mentioned, at the bottom of the deep cleft between the two domains. The signature triade histidine, glutamate, and arginine is highly conserved among members of the family. The residues are located at the *C*-terminus of the cosubstrate binding domain. The function and position of the functional atoms are highly conserved even between members of D- and L-2-hydroxy acid dehydrogenases even though the residues are found at different positions of the

protein chain in the members of D-HADHs and L-HADHs. This fact strongly supports the concept of convergent evolution. Histidine is the acid base catalyst, protonating and activating the carbonyl functionality of the substrate or accepting the proton from the hydroxy acid. Glutamate, taking the role of aspartate in L-LDHs, stabilizes the protonated histidine residue and arginine binds the carboxyl group of the substrate and further activates the carbonyl functionality, in agreement with kinetic data.[83,84] Special attention should be paid to the gatekeeper residues Y52 and F299 (as in the PDB structure 1J49 of D-LDH from *L.b.*) at the opposite site of the active site wall, playing the role of a size exclusion filter, defining the available space and the electrostatic potential of the substrate side chain environment, especially at C(3). In D-3-phosphoglycerate dehydrogenase for example, the phenyl residue is replaced by glycine to make room for the sterically demanding phosphate group.[77] Further residues restricting the active site space are Y101, M308, and W135* from the other subunit. All residues except Y101 and M308 are subject to extensive variations between D-HADHs of different origin, depending on the substrate specificity. These residues are also subject to extensive variations between the sub-groups of the enzyme family, also in alignment with the hypothesis that these residues play an important role in recognition of the individual substrates. For example lysine is exchanged by an arginine residue in the D-3-phosphoglycerate dehydrogenase from *E. coli* to compensate the phosphate's negative charge.[80,85]

Mechanism

The catalytic mechanism is initiated by either coenzyme binding or independent binding of coenzyme and substrate. Interdomain rolling[81] constructs the active site and initiates the redox reaction. Whether the coenzyme binding prior to substrate binding is necessary or whether both molecules can bind independently and what exactly causes the inter-domain movement is still being investigated.[65,] The general accessibility of the active site for pyruvate has been confirmed for *L.b.* D-LDH.[77] While Holton *et al.* found crystals of a binary NAD^+-enzyme complex of another *L.b.* D-LDH in the open conformation and stated that a 10 ° movement around the two hinges between the domains would be necessary to construct the actual active site,[80] Lamzin *et al.* found crystals of a binary complex of FDH from *Pseudomonas sphaericus* with NAD^+ to be in a closed conformation, rolled 7.5 ° compared to the apo-enzyme.[65] They reasoned that the substrate may pass through a distinct channel of the closed holo-

enzyme into the active site.[65,77] It is also possible that interdomain movement is masked in the crystal structures because of free energy compensation from extensive intra-crystal contacts between tetramers. Razeto *et al.* proposed an anti-cooperative mode of domain movement between the two dimer subunits, because they identified the subunits to be in different conformations in a crystal structure of *L.b.* D-LDH. However structural elements enabling the subunits to communicate *via* the monomer interface were not found.[77] Identification of the rate determining step has not been found in the literature. In the L-specific enzymes, either protein rearrangement prior to hydride transfer or cofactor release are the two possible rate determining steps. Since loop closure seems to be more advanced in evolution, compared to movement of bigger domains, hence more effective, the free energy of protein rearrangement supposedly has a lower free energy difference. This would render the free energy difference of cosubstrate release smaller compared to protein rearrangement, and thus more likely to be the rate determining step.

Application

The optimum pH for the reduction, is 7.0-7.5, the optimum pH for the oxidation is 8.0. This is due to the protonation state of the acid base catalyst histidine residue. Replacing this residue by lysine in *L.b.* D-LDH, lowers the optimum pH to 6 even though lysine is more basic. This is attributed to the different spatial arrangement of the lysine residue, for example the missing H-bond to the polarizing glutamate residue.[77,74,73,] D-HicDH is special because it tolerates acidic solvents up to pH 3.3 and it is even reported to increase its activity, if crude extracts are treated with acidic solutions, probably due to refolding of inclusion bodies.[67,68,66]

The enzymes are reported to be stable up to 45 °C and deactivate rapidly until 60 °C.[74]

The used enzymes have different substrate specificity. More information about the experimental data on the selected enzymes are given in Table 3.

Table 3: Kinetic and thermodynamic data on the selected enzymes (for *L.b.* D-LDH, activity of the mutant but K_M of the wild type are given).

Enzyme	Activity [U mg^{-1}]	K_M [mM]
D-HicDH[67]	240 (NADH, 2-ketoisocaproate)	0,06 (2-ketoisocaproate) 5 (C(3) branched)
YiaE[74,73]	345 (NADH, glyoxylate) 123 (NADH, hydroxypyruvate)	42 (pyruvate) 0.7 (hydroxypyruvate)
H.m. D-HADH[69]	2.1 (NADH, 2-ketobutyrate, highest)	Lowest: 2-ketoisoleucine
L.b. D-LDH variant[79]	3100 (NADPH, pyruvate)	1.6 (pyruvate) >100 (phenylpyruvate)

The ee of the products of all four enzymes is declared to be >99%.[74,67,69,79,77]

Competitive inhibitors like oxamate have already been discussed for L-amino acid dehydrogenases. Azide is reported to be a potent competitive inhibitor for FDH.[65]

Dependence on anorganic ions has only been reported for the halophilic D-HADH from *Haloferax mediterranei*. This enzyme has a very high content of acidic residues, compared to other members of the family (D + E = 18%). This high content of acidic residues must be counteracted by cations in solution, to maintain stability and activity of the enzyme. This is a challenge when expressing the enzyme in *E. coli* because the lower salt concentrations necessary to create viable conditions for expression causes misfolding and inclusion body formation. Partly refolding can be achieved by rapid dilution with 4 M brine. Potassium chloride has been shown to be less effective.[69]

2.2.5 D-Amino acid oxidases

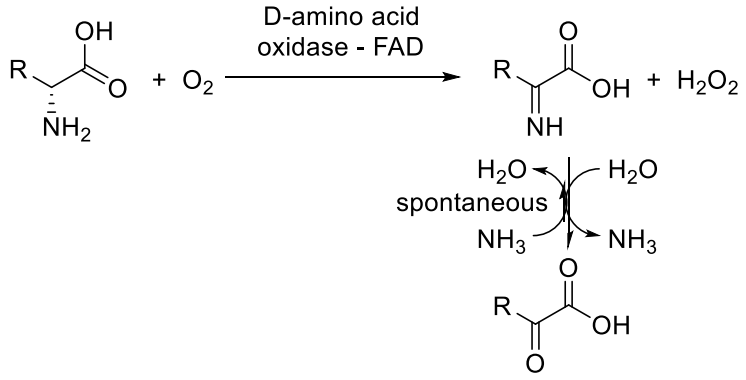

Figure 14: General reaction catalysed by D-amino acid oxidases.

D-Amino acid oxidases (EC 1.4.3.3, D-AAO) are flavoproteins, facilitating the oxidative dehydrogenation of D-amino acids in the presence of molecular oxygen, yielding the corresponding α-keto acids and hydrogen peroxide.

The presence of a distinct enzymatic system catalysing the oxidative deamination of D-amino acids was first published 1935 by Krebs, who found already in 1933 that slices of kidney and liver were able to oxidize both enantiomers of α-amino acids.[86,87] Other authors were working on similar topics. For example, Bergheim, Bergheim and Dorothy Webster found that microorganisms were also able to facilitate the oxidation of D-amino acids and they published in 1935 the oxidation of D-alanine and D-valine using a resting cell preparation of *Bacillus proteus*. In 1938, Warburg and Christian published that flavin adenine dinucleotide (FAD) is the enzyme's cofactor.[88]

Research of D-amino acid oxidases picked up pace in the early 70s, when Mazzeo and Romeo found that purified D-amino acid oxidase from porcine kidney (p.k. D-AAO) facilitates oxidative deamination of Cephalosporin C.[89] Following decarboxylation in the presence of the side-product hydrogen peroxide, enables enzymatic glutamine cleavage. The two-step process liberates the β-lactam core 7-amino-cephalosporanic acid (7-ACA) which readily undergoes chemical modification to yield members of the important cephalosporin family broad-spectrum antibiotics.[90] The first enzymatic large-scale process for the synthesis of 7-ACA was reported in 1995.[91]

Today the use of D-amino acid oxidases is mainly in the production of 7-ACA but there are also other examples like biosensors for continuous measurement of D-amino acid concentration or the production of chemical synthons.[92,93]

Herein, D-amino acid oxidases from different sources, namely from porcine kidney, and the two different yeasts, *Trigonopsis variabilis* (*T.v.*) and *Rhodotorula gracilis* (*R.g.*), were used. Additionally, the *N*-terminally His_6-tagged M213G mutant of the D-amino acid oxidase from *Rhodotorula gracilis* was used.

In vivo mammalian D-AAOs mainly facilitate detoxification after natural racemisation of L-amino acids and D-amino acid uptake through food. Since hydrogen peroxide is toxic for cells, mammalian D-AAOs are located inside peroxisomes, where developing peroxide is quenched by catalase. Additionally, it has been proposed that D-AAOs play a crucial role in the regulation of the brain's D-serine concentration, an amino acid, which interacts with the NMDA receptor.[94]

In microorganisms D-AAO's facilitate the use of D-amino acids as growth substrates.[95]

There are several challenges that still need to be overcome regarding the expression of D-AAO's in *E. coli* cells. pET28a utilizes the T7-lac operator to achieve high levels of protein expression. At this level endogenous catalase is not capable of quenching all developing peroxide which leads to cell damage and apoptosis.[96] Eukaryotic cell walls contain D-amino acid derived compounds and consumption of endogenous D-amino acids leads to serious disturbance of natural cell growth, disabling the cells to divide in a natural fashion.[96] Therefore the formation of vast amounts of the enzyme is a major threat to the viability of the host. Additionally, high levels of aeration, desired in the cultivation of *E. coli*, increases the activity of the oxygen dependent enzyme, leading to even more prominent negative effects arising from D-AAO activity inside the host.[49] Endogenous FAD is not sufficient to saturate all the newly formed protein so that most of the enzyme is produced in the form of an inactive apoenzyme.[96] The formation of insoluble inclusion bodies is reported which also poses a big challenge in the development of a highly efficient biocatalyst.[49]

Most attempts to overcome some of these challenges are valid for the three expressed yeast D-AAO's and include: coexpression of haemoglobin to reduce intracellular free oxygen levels,[97] decrease of aeration and supplementation of the growth medium with sacrificial amounts of D-alanine and D-methionine,[49] addition of FAD to the biocatalyst to render a part of inactive apoenzyme active,[96] tight regulation of expression by selection of suitable expression vectors to avoid premature expression,[98] growth at

lower temperatures and addition of sorbitol and glycyl betaine to stabilize the enzyme and therefore to reduce inclusion body formation.[99]

Structure

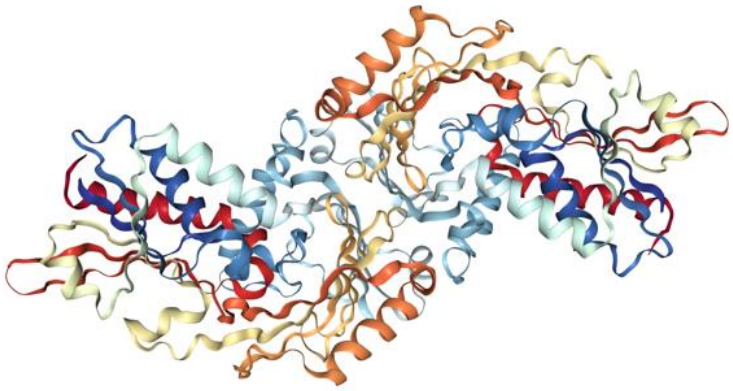

Figure 15: D-Amino acid oxidase from porcine kidney (pdbid: 1VE9, dimeric structure).[100]

D-amino acid oxidases can remove disturbing D-amino acids and enable D-amino acids as a source of nutrition and are therefore very useful enzymes for all organisms. This led to development in an early stage of evolution, maybe independently for different organisms, and to a high diversity between D-amino acid oxidases from different sources which have a homology score below 30-40%.[101]

Nevertheless, there are some homologies: Each enzyme-monomer contains one non-covalently bound FAD, when in its reduced state, being oxidized spontaneously with molecular oxygen. The large active site cavity is restricted by a β-sheet, representing the substrate binding area and on the other site by the isoalloxazine group of FAD, the prosthetic group. The *N*-terminal sequence GXGXXG is typical for nucleotide binding domains. The three key catalytic residues asparagine, arginine and tyrosine are highly conserved. While the arginine residue has a highly restricted mobility, tyrosine, which is responsible for substrate access, is very mobile. The S-(K/H/R)-L *C*-terminus is important for the transport to peroxysomes.[101]

Some of the most prominent differences are: While the active form of D-AAO from porcine kidney is monomeric and oligomer formation upon high concentrations leads to inhibition, *T.v.* and *R.g.* D-AAO's holoenzyme is a head-to-tail homodimer. This leads not only to a higher stability of yeast D-AAO's but to a completely different deactivation mechanism. Direct, concentration independent deactivation, probably through globule unfolding, in D-AAO from porcine kidney contradicts a two-step

mechanism in yeast D-AAO, starting with concentration dependent, reversible dissociation into monomers and subsequent irreversible deactivation of the monomers.

Yeast D-AAO's bind FAD much stronger than mammalian ones, which can be seen in the differences in their dissociation constants for FAD (D-AAO from *Rhodotorula gracilis*: K_d (FAD) = 2×10^{-8} M, D-AAO from porcine kidney: K_d (FAD) = 2×10^{-7} M).

There are significant differences in the substrate binding domain reflecting the wide variety in substrate affinities. While the substrate binding domain of *T.v.* D-AAO is more closely related to *R.g.* D-AAO, reflecting the more prominent ability to convert cephalosporins, compared to p.k. D-AAO, the FAD binding domain of *T.v.* D-AAO is more closely related to p.k. D-AAO since *R.g.* D-AAO there has an additional loop, which is not reflected in FAD binding constants. Mutational studies have showed that this loop contains key residues, critical for dimer formation and FAD binding.[102][103]

Mechanism

There are two possible kinetic pathways for the reaction. Both pathways start with formation of the Michaelis complex between the substrate and the enzyme which has the oxidized flavin tightly bound. In this complex, the substrate is bound to the *Re*-side of the flavin isoalloxazine ring with the α-hydrogen atom in close proximity (3.4 Å C(α)-N(5) D-alanine, p.k. D-AAO) to the flavin N(5).[104] In this state, the α-amino group is already in its deprotonated neutral form. Practically irreversible redox reaction between the flavin and the substrate then leads to imine formation. Regeneration of the flavin can now either happen after, representing a classical ping-pong mechanism, or prior (ternary complex with oxygen) to product dissociation. In fact, steady-state, stopped-flow and kinetic isotope effect measurements showed that the classical ping-pong mechanism only holds true for the oxidation of basic amino acids with the oxidase from porcine kidney. In general, O_2 reactivity of flavoenzymes is very diverse and defined by the electrostatic environment (compensation of the developing negative charge at the flavin isoalloxazine) and dioxygen accessibility.[105] For the yeast D-AAO's reactions and for the oxidation of non-basic amino acids with porcine kidney D-AAO reoxidation of the flavin happens prior to product release and thus *via* a ternary [product-enzyme-O_2] complex. MD simulations of *R.g.* D-AAO helped to identify distinct channels with high O_2 affinity leading to the *Si*-side of the isoalloxazine system, the more relevant one leading to the N(5)-C(4a). The authors also identified a H^+

transport chain consisting of four water atoms, possibly channelling the imino proton from the isoalloxazine *Re*-side to the *Si*-sided HO_2^- species, only present in complex with the ligand and not in the free reduced enzyme. This may explain the preference for ternary complex over the classical ping pong mechanism.[106] The kinetic measurements also revealed the rate determining step, being the product release in mammalian D-AAO's and the substrate reduction in yeast D-AAO's.[94]

The microscopic mechanism is nicely summed up by Molla et al.: "L-AAO [,analogous to D-AAO,] catalyzes the dehydrogenation of the L-amino acid through a hydride transfer mechanism by steering the trajectory of the αC-H orbital of the substrate to the LUMO of the FAD cofactor N(5), without direct involvement of active site residues."[107,108,109]

The reduction of the prosthetic group can be nicely followed spectroscopically *via* the disappearance of its longest wavelength absorption maxima (272, 360, 455 nm as in *T.v.* D-AAO) in the course of reduction.[110,111] During turnover most of the enzyme is present in the oxidized form indicating that the oxidation reaction is always faster than the reduction.

There has been a debate concerning the mode of electron transfer from the substrate to the flavin. Whilst some authors favoured a direct hydride shift, others thought it would proceed *via* deprotonation of the substrate by a base and then addition of the amino acid α C – atom to the N(5) of the flavin isoalloxazine ring, followed by imine release and protonation of the N(5). Mutational studies proved the absence of basic residues in the active site that would be able to take the role of the base thereby deciding in favour of direct hydride shift.

Only three amino acid residues have been found, by sequence alignment, comparison with other flavoenzymes, crystal structure studies, kinetic isotope effect studies and mutagenesis studies,[110,112,113,114,115,116] to play a major role in the active site: Y224(223), Y228(238) and R283 [labelled as in p.k. D-AAO (*R.g.* D-AAO)]. These studies also show that the three amino acids do not play a role as base catalysts but instead guide and orient the substrate into the electrostatic environment so that the amino acid is more readily deprotonated and readied for the hydrogen shift. All three residues fix the amino acid carboxylate: the tyrosines through H-bonding and the arginine through salt bridging. Hydrophobic amino acids line the active site, explaining

the enzyme's preference for amino acids with hydrophobic side chains and why charged amino acid side chains are rendering these amino acids no or bad substrates.[104]

P.k. D-AAO has an additional lid-loop (AA217 – AA228), containing both tyrosines, that limits active site space to approx. 160 $Å^3$, rendering it too small for amino acids with residues of a chain length of >5 C-atoms. The effects can be seen in significantly increased K_M – values and in drastically increased catalytic efficiency of yeast D-AAO's towards Cephalosporins. The loop exists in either an open or closed conformation depending on substrate presence, tightly controls substrate orientation and renders the substrate surroundings more hydrophobic in the closed conformation. This lid also explains why the product release is rate determining for p.k. D-AAO.[117]The M213G mutant of *R.g.* D-AAO was specially designed for the conversion of unnatural naphthyl-substituted D-amino acids. *In silico* analysis of the wild type enzyme provided insight that steric hindrance occurs when D-naphthylglycine substrates are fitted into the active site and that mainly M213's residue is responsible for it. In fact, the M213G variant showed increased yields when D-2-Naphtylglycine was used as substrate.[118]

The used D-AAO's are all described as highly specific for D-amino acids.[94] The additional lid in p.k. D-AAO decreases activity towards larger substrates.[117] P.k. D-AAO does not accept acidic amino acids and basic amino acids are less suitable substrates.[94] The two acidic amino acids aspartic acid and glutamic acid are oxidized *in vivo* by a separate enzyme, D-aspartate oxidase (DASPO, EC 1.4.3.1).[94]

Application

Competitive inhibition occurs with substances that somehow mimic the natural substrates like benzoates, crotonates or sulfites.[119] L-amino acids are not inhibitors. For more selective inhibitors with potential medical applications see the literature.[120]

2.2.6 L-Amino acid deaminases

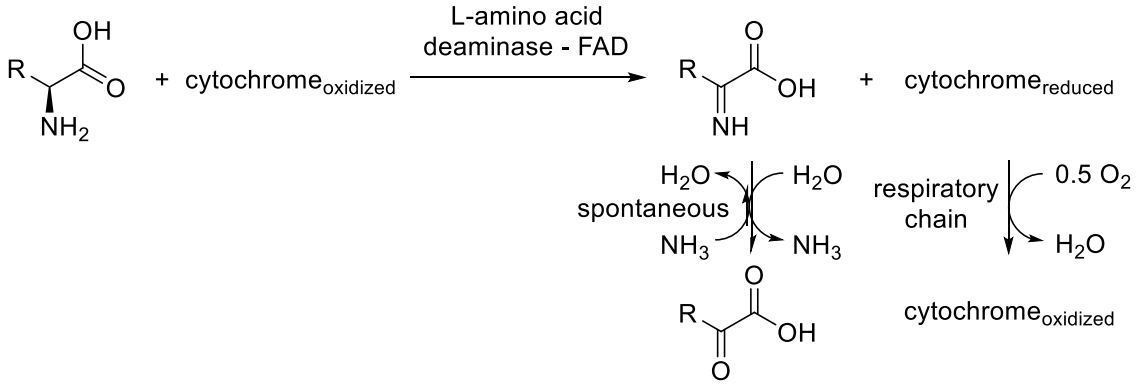

Figure 16: General reaction scheme for L-amino acid deaminases.

L-Amino acid deaminases (L-AAD, EC 1.4.99.B3, preliminary) are flavoproteins, facilitating the oxidative deamination of L-amino acids in the presence of water and a cytochrome *b*-like protein, yielding the corresponding α-keto acids, ammonia and the reduced cytochrome. They are differentiated from L-amino acid oxidases mainly through the absence of hydrogen peroxide production.

The first report about an enzymatic system capable of oxidizing L-amino acids comes from Zeller and Maritz in 1944.[121] They identified the oxidizing effect of different snake venoms on L-amino acids.

The type I L-amino acid deaminase from *Proteus myxofaciens* (*P.m.*), which is well known for its wide substrate scope and high activity, was used herein.

These deaminases are monomeric enzymes that are anchored into the bacterial cell wall.[122] There are two different types of deaminases present in members of the genus *Proteus* and *Providencia*, for example *Proteus vulgaris*, *Proteus mirabilis*, *Proteus myxofaciens*, and *Providencia alcalifaciens*.[123,124,125,126] The two types of deaminases differ in their substrate specificity, which is reflected by a very high degree of structural conservation among deaminases of one type (91% structural identity for type II deaminases from *P. mirabilis* and *P. vulgaris*) and significantly less conservation between deaminases of different types (56% structural identity for type I and type II deaminases from *P. mirabilis*).[127] While type I deaminases catalyse the deamination of most L-amino acids (no activity for L-threonine measured by Baek *et al.*) except basic ones, type II deaminases are specialized in the oxidation of basic L-amino acids, especially L-histidine and L-arginine.[127] Interestingly, though the used L-AAD from *Proteus myxofaciens* clearly belongs to the type I L-AAD's (highest activity with L-

phenylalanine), it also displays activity with L-histidine (10% activity compared to L-phenylalanine) and L-arginine, but not with L-glutamine or L-asparagine.[128]

Structure

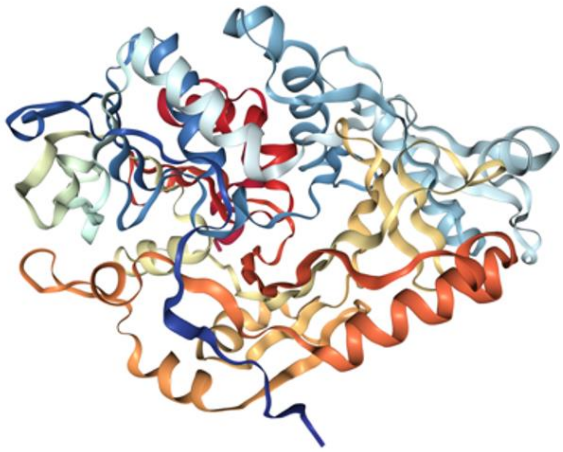

Figure 17: L-amino acid deaminase from *Proteus myxofaciens* (pdbid: 5FJN).[122]

The enzyme's structural identity to other known microbial L-AAOs and D-AAOs is quite low (around 15%). Especially one subdomain containing the transmembrane α-helix (anchoring the enzyme at cell membranes) at its *N*-terminus and a very flexible region (α-helix A9 and the following loop) at its *C*-terminus is not found in D-AAOs and L-AAOs.

This flexible region especially establishes the positions of the catalytically active residues R316 (amino acid α-carboxyl binding) and F318 (non-polar amino acid residue binding) upon substrate binding.

Of twelve known L-AADs in *Proteus* and *Providencia*, four have been expressed in recombinant form and characterized.[107] Mechanistic research is difficult, because the enzyme's oxidation reaction seems to be rate limiting.[107] Therefore, the natural electron acceptor needs to be isolated to perform kinetic measurements. Two findings indicate that the enzyme's oxidation is rate limiting: the enzyme's cofactor is rapidly reduced in the presence of *E. coli*-membranes, when mixed with a large excess of L-phenylalanine[122] and the addition of artificial electron acceptors increases the reaction rate also in the presence of *E. coli*-membranes.[107] The most efficient known artificial acceptor, 2,6-dichlorophenol indophenol which increases the reaction rate 8-fold, when applied to the purified enzyme in solution (compared to ~100 fold with *E. coli*-membranes).[122] In summary, the first step in finding the mechanism is identification of

the cytochrome. Additionally, maximizing the activity of the enzymatic system may require optimization of the cytochrome expression and research about the influence of oxygen pressure.

Mechanism

Under anaerobic conditions, the enzyme does not recover from its reduced state and therefore is not catalytically active. This proves oxygen to be an essential cosubstrate. Despite this fact, most authors believe that, instead of direct oxidation of the reduced flavin, it transfers the electrons to a cytochrome *b* like small membrane protein and therefore to the respiratory chain. This hypothesis is not only supported by the absence of hydrogen peroxide production and the absence of flavin reoxidation when there are no suitable membranes present but also by the appearance of the typical, narrow absorption bands of a reduced cytochrome b at 429 nm (large), 532 nm, (very small) and 560 nm (small), when the reaction is performed anaerobically or when the substrate concentration exceeds the oxygen concentration in the medium. These three absorption bands resemble the spectrum of a cytochrome *b* present in complex II of *Proteus mirabilis* not only in wavelength but also in peak shape and size.[129,130] The fact that, the involved cytochrome is present in the reduced form at higher substrate concentrations renders oxygen solvation rate limiting, at least if there are no additional measures for increased oxygen dissolution. Direct oxidation of the reduced flavin happens only at a very low rate or not at all. In nature, the electrons are transferred to dioxygen at the end of the respiratory chain, yielding water.[129,122]

Preferred substrates are aromatic and neutral L-amino acids. Limited activity is shown on small, charged or polar amino acids. Interestingly the enzyme also exhibits activity on L-phenylalanine ethyl ester and L-DOPA.[122]

In contrast to D-AAOs, carboxylates like benzoates are not competitively inhibiting the enzyme. Instead an amino group seems to be crucial for ligand binding. Therefore, anthranilate and kojic acid are excellent inhibitors, with dissociation constants of K_d = 18.4 ± 4.4 mM and K_d = 3.0 ± 0.3 mM, respectively. Also, in contrast to D-AAOs, sulphite is not an inhibitor because of the absence of stabilization of reduced FAD and steric clash with the A2-β4 loop.[112,113,94,114]

Cofactor of the enzyme is FAD which is tightly bound inside the protein (43 residues are directly involved in FAD-binding). It’s redox potential is amongst others defined by

the α_{14}-helix dipole, of which the *N*-terminus points towards the O(2) of the isoalloxazine and therefore compensates the negative charge of its reduced form. Further stabilization (i.e. positively charged amino acid residues in proximity to N(1)-C(2)=O) of negative charge, developing during transition, is absent which may be a possible explanation for the absence of direct dioxygen reactivity. The isoalloxazine's N(5), extensively hydrogen- and van der Waal's-bound, is located at the interface between the substrate binding domain and the flavin binding domain, its *Re*-side pointing towards the substrate binding domain.

Application

Maximum activity of the recombinant type I L-AAD from *Proteus myxofaciens* was detected at pH between 7.0 and 7.5 and a temperature of around 50 °C as also reported for the L-AAD from *Proteus mirabilis*. The enzyme is stable between pH 5.5 and 8.8 and no significant activity has been measured above 75 °C.[107,127] Type I L-AAD from *Proteus mirabilis* was found to possess a K_M(L-phenylalanine) = 31.55 mM and a V_{max}(L-phenylalanine) = 119.7 µmol/(min mg protein).[127] Motta *et al.* reported K_M(L-phenylalanine) = 3.27 ± 0.96 mM and a V_{max}(L-phenylalanine) = 1.35 ± 0.08 u/(mg protein) for the recombinant pmaL-AAD.

2.2.7 Transaminases

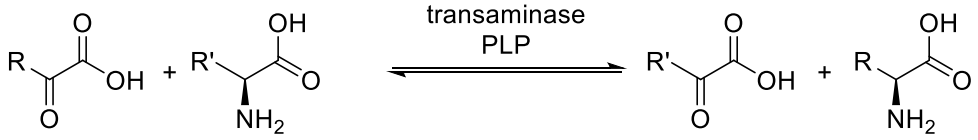

Figure 18: General reaction scheme for transaminases, PLP: pyridoxal-5'-phosphate.

Aminotransferases, also called transaminases constitute another important enzyme family, catalysing formal reductive aminations of ketones. Similar to dehydrogenases these enzymes play an important role in amine anabolism, for example in the synthesis of amino acids or neurotransmitters.

In contrast to dehydrogenases, they use an amine donor as cosubstrate, instead of NAD(P)H and ammonia. The amine group is transferred from the donor substrate to an acceptor substrate, bearing a keto-group. The amine functionality is shuttled *via* the prosthetic group pyridoxal-5'-phosphate (PLP).

In this research, two very specific wild type transaminases were used, namely the aromatic transaminase from *Paracoccus denitrificans* (*P.d.*) and the transaminase from *Vibrio fluvialis* (*V.f.*, EC 2.6.1.57). The enzymes have a very high amino acid identity of 94%[131] and belong to the sub-class of ω-transaminases. However, this is misleading and outdated since these transaminases are not limited to ω-amino acids. For this reason, in this work, they will be referred to as transaminases (TA).

Structure

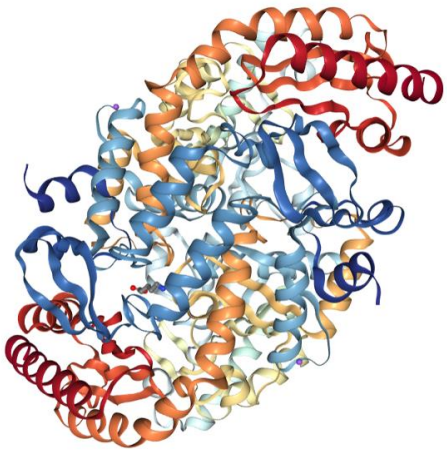

Figure 19: Transaminase from *Vibrio fluvialis* in complex with PLP (pdbid: 4E3Q; an equivalent crystal structure from the enzyme from *Paracoccus denitrificans* is also available in the pdb under the id 4GRX).[132]

Both used transaminases are homodimeric enzymes with protein chains of 353 amino acids length. The subunits consist of two domains (small domain: amino acids 1-65 and 344-353, large domain: amino acids 66-343), characterized by different temperature factors and relative movements upon substrate binding. The active site is positioned at the interface of both subunits and is constructed of the small domain of one subunit and the large domain of the other subunit. Consequently, the homodimeric enzyme bears two active sites in total.

Mechanism

When no substrate is bound, the prosthetic group PLP forms a Schiff-base with the side chain of K285. Upon cosubstrate binding, transaldimination towards the substrate occurs, thus K285 is released. After a 1,3-prototropic shift from the substrate's α-C atom towards PLP, hydrolysis of the aldimidine releases the oxidized cosubstrate. The prosthetic group, present as pyridoxamine-5'-phosphate, is now ready to transfer the amine group to an acceptor substrate, closing the catalytic cycle.[133]

The rate determining step is still unclear and may depend on specific substrates. However, the reactivity of the respective substrate is determined by the susceptibility of its carbonyl C-atom towards the nucleophilic attack from the amine.[133]

Since focus herein is on different substrates for these two transaminases, the structural prerequisites for the determination of enantioselectivity are of special interest. The enzyme distinguishes the two residues of the prochiral ketone substrate by limiting the available space and definition of the electrostatic environment. This way two distinct pockets, a small and a large one, are constructed.[134,135] Different acetophenones were tested herein and as it is known that the enzymes accept only little variation in the small residue,[133] only the large pocket, harbouring the aromatic large residue is of interest here. This pocket bears the following amino acid's residues at its surface: phenylalanine, tyrosine, threonine, alanine, leucine, glycine, arginine, and lysine (F19, 85*, 86*, 321*, Y150, 165, T322*, A228, L417, G320*, R415, K163). There are aromatic and aliphatic hydrophobic amino acid residues, basic amino acids, and hydrogen donating hydroxy groups but no acidic amino acid residues available for interaction with the aromatic substrate side-chain. When small substrates are bound, (e.g. alanine) R415 is in a suitable position for polar interactions with the carboxy group, while it is pinned back when larger substrates are bound. Instead, larger substrate's carboxy-groups are bound by K216.[131,132] Generally spoken, the large pocket exhibits structural flexibility to fit a variety of aromatic substrates. *Para*- and hydroxy- substituted aromates possess a reportedly lower reaction rate.[133,135]

Application

Examples for inhibitors are benzaldehyde[136] and compounds bearing an aromatic residue on one side and a carboxylic acid residue at the opposite side of a linear ethene- or propene-chain.[135]

The activity of *V.f.*-TA on pyruvate with 1-phenylethan-1-amine as amine donor is given as 20.0 ± 0.4 U/mg and the K_M of pyruvate is 3.98 ± 0.05 mM.[132]

3 Results and discussion

3.1 Transaminases

The here described reductive amination of acetophenone derivates is based on a work from Michael Fuchs *et al.* from 2010, who established the stereoselective enzymatic amination of *1-(3-(methoxymethoxy)phenyl)ethan-1-one*. The produced amine can be further converted to (*S*)-rivastigmine, a potent drug for the treatment of early stage Alzheimer's disease, in three more reaction steps.[137] It was reported that the transaminase from *Vibrio fluvialis* (*V.f.* TA) is the most suitable transaminase for this reductive amination. However, in 2012 an improved version of the protocol was reported, using a transaminase from *Paracoccus denitrificans* (*P.d.* TA) converting 3-acetylphenyl ethyl(methyl)carbamate (**6a**) to the corresponding amine, which after methylation of the newly formed amine group represents the target compound (*S*)-rivastigmine.[138] Alanine was used as the amine donor, which was converted to pyruvate during the course of the reaction and then withdrawn from the equilibrium using a commercial "pyruvate reductase mix" (PRM). PRM contains glucose dehydrogenase, lactate dehydrogenase and glucose and converts pyruvate to lactic acid (Figure 20).

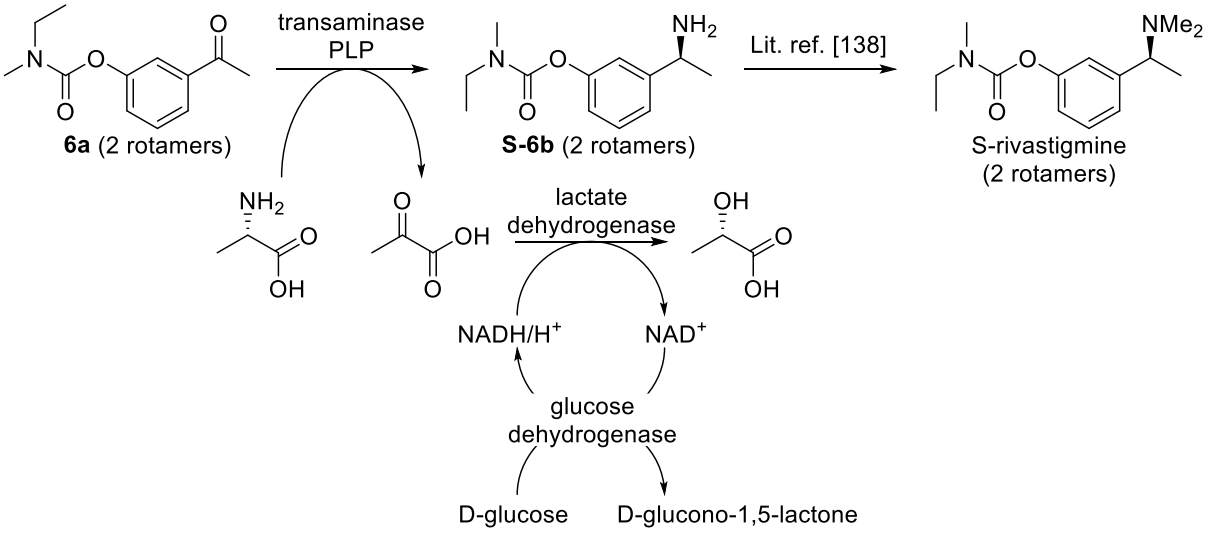

Figure 20: Enzymatic reductive amination of 3-acetylphenyl ethyl(methyl)carbamate (**6a**) by Fuchs *et al.*,[138] PLP: pyridoxal-5'-phosphate.

Before the coupling of a transaminase to *Synechocystis'* photosystem, the reported amination was reproduced,[138] starting with the synthesis of the ketone precursor 3-

acetylphenyl ethyl(methyl)carbamate (**6a**) from *m*-hydroxyacetophenone (**7a**, yield, 373 mg, >90%).

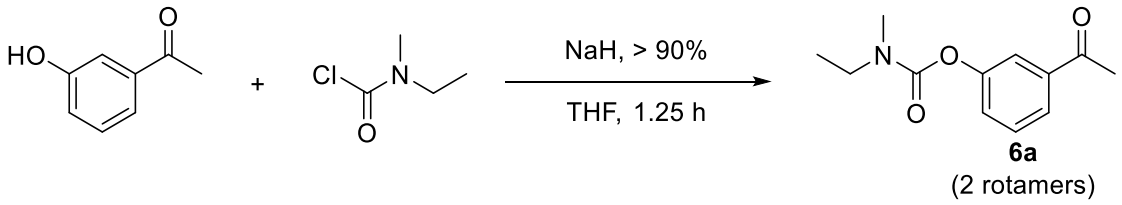

Figure 21: Synthesis of 3-acetylphenyl ethyl(methyl)carbamate (**6a**).[138]

The ester synthesis is convenient, except the amount of sodium hydride needs to be kept slightly below one equivalent to prevent double esterification. As the PRM was several years old (2012), diminished activity was expected. To investigate the residual activity and reproduce the reaction conditions[138] four model reactions varying the originally published conditions were run with 3-acetylphenyl ethyl(methyl)carbamate (**6a**) as substrate. Additionally, a blank reaction without transaminase was included, which showed no conversion as expected.

The results of this screening are summarized in Figure 22.

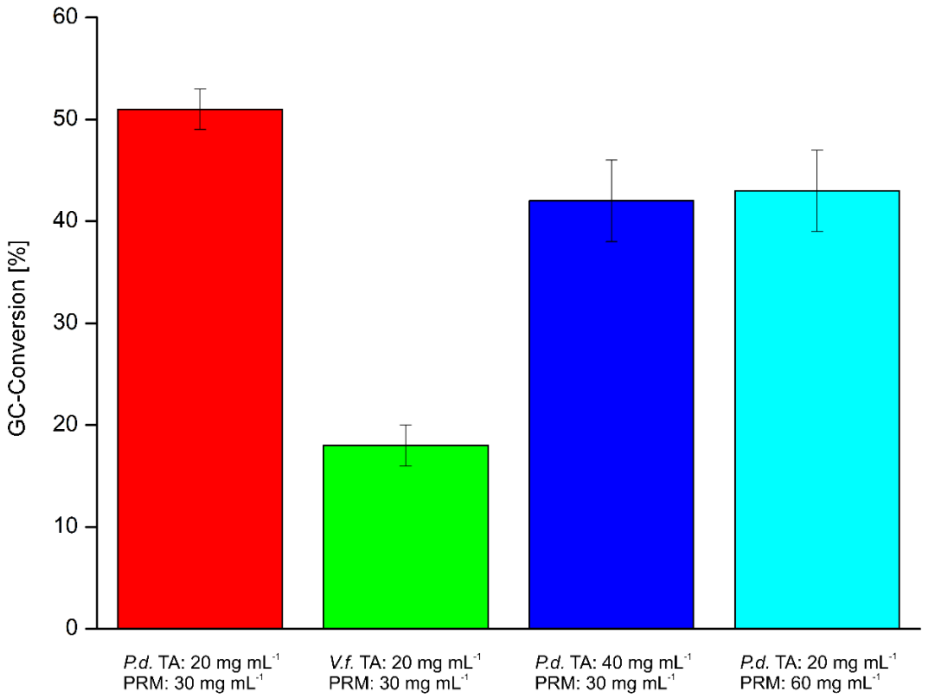

Figure 22: Optimization of the amination of **6a**; red: reaction conditions from [138] with the transaminase from *Paracoccus denitrificans*; green: reaction conditions from [138] with the transaminase from *Vibrio fluvialis*; dark blue: twice the amount (compared to [138]) of *P.d.* TA; light blue: twice the amount (compared to [138]) of PRM; standard conditions from [138]: 1 mL total volume, 20 mg whole lyophilized cells with overexpressed transaminase, 30 mg PRM, 0.25 M L-alanine, 50 mM 3-acetylphenyl ethyl(methyl)carbamate (**6a**), 1 mM pyridoxal-5'-phosphate, 24 h, 30 °C, sodium phosphate buffer (100 mM, pH 7.0), 120 rpm; the conversion is based on integrated GC-MS peaks.

The essayed variations of the published standard conditions gave decreased yields [double amount of *P.d.* TA: 42%, double amount of PRM: 43%], leading to the conclusion that the published conditions are optimal. However, the yield of the amination decreased compared to the original results (optimized *V.f.* TA: 29%, optimized *P.d.* TA: 83%),[138] indicating a loss of activity of the enzyme preparations. The optimized amination with *P.d.* TA displayed a conversion of 51% which is more than twice the conversion with *V.f.* TA 18%. Concluding, the transaminase from *Paracoccus denitrificans* is superior in the amination of acetophenone under the given conditions.

Furthermore, the substrate scope of the two different transaminases was investigated using the optimized conditions. All tested substrates and the respective products are displayed in Figure 23.

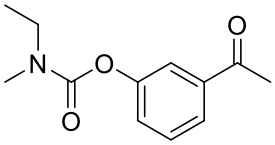

6a
3-acetylphenyl ethyl(methyl)carbamate
(2 rotamers)

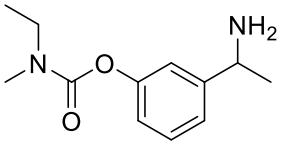

6b
3-(1-aminoethyl)phenyl ethyl(methyl)carbamate
(2 rotamers)

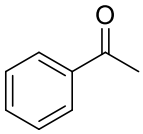

7a
acetophenone

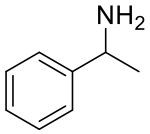

7b
1-amino-1-phenylethane

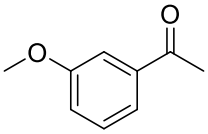

8a
m-methoxyacetophenone

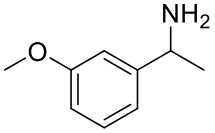

8b
1-(3-methoxyphenyl)ethan-1-amine

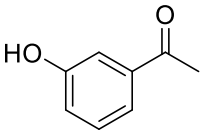

9a
m-hydroxyacetophenone

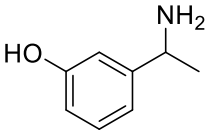

9b
3-(1-aminoethyl)phenol

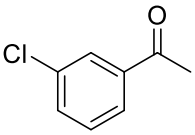

10a
m-chloroacetophenone

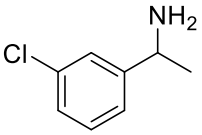

10b
1-(3-chlorophenyl)ethan-1-amine

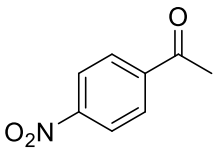

11a
p-nitroacetophenone

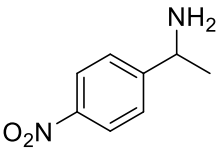

11b
1-(4-nitrophenyl)ethan-1-amine

Figure 23: Substrates and products of the enzymatic amination reaction.

The results of this screening for the transamination of **7a** – **11a** are summarized in Figure 24.

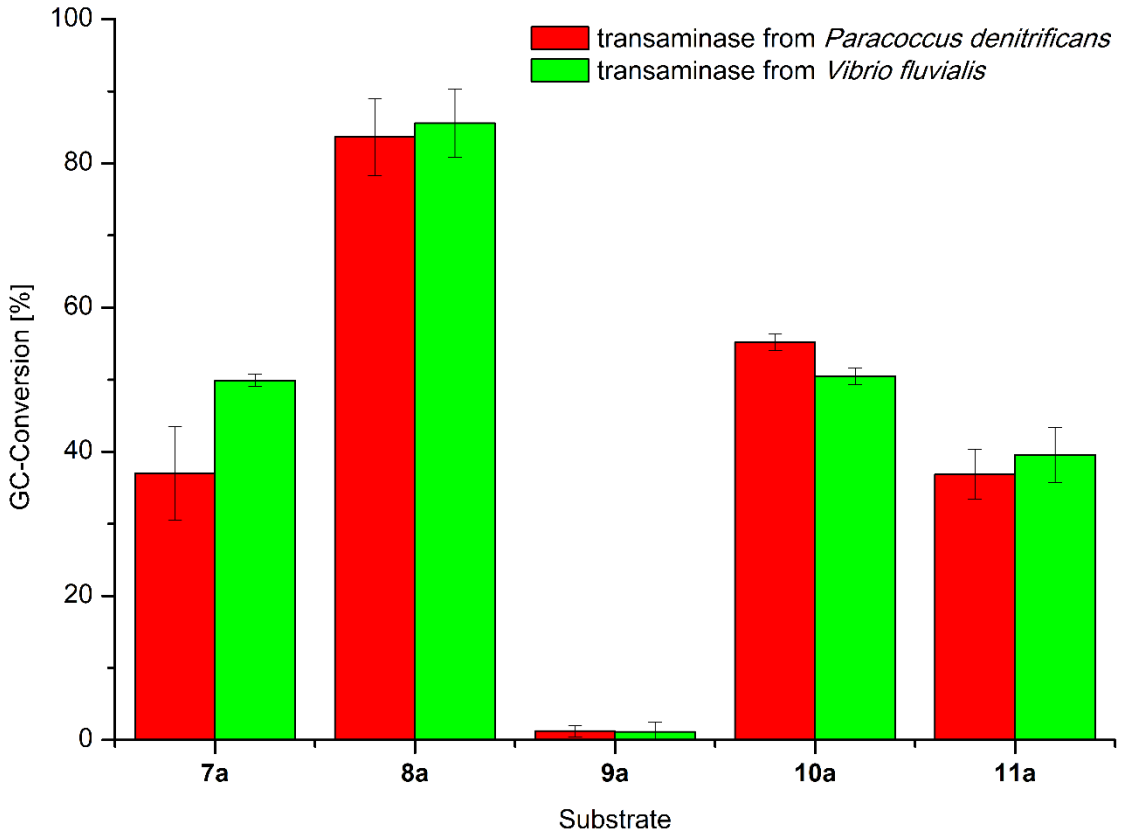

Figure 24: Enzymatic amination of **7a**-**11a** with the transaminases from *Vibrio fluvialis* and *Paracoccus denitrificans*; reaction conditions: 1 mL total volume, 20 mg whole lyophilized cells, 30 mg PRM, 0.25 M L-alanine, 50 mM substrate, 1 mM pyridoxal-5'-phosphate, 24 h, 30 °C, sodium phosphate buffer (100 mM, pH 7.0), 120 rpm.

The highest conversion (*P.d.* TA: 84%, *V.f.* TA: 86%) was achieved with *m*-methoxyacetophenone (**8a**), whereas *m*-hydroxyacetophenone (**9a**) showed only very little conversion (both enzymes 1%). This difference may be attributed to an altered substrate binding as the hydroxy group has hydrogen-donor properties. *p*-Nitroacetophenone (**11a**) showed less than 50% conversion, which was surprising, as the decreased electron density in α-position to the carbonyl function was expected to facilitate the nucleophilic attack. This may be attributed to a decreased efficiency in substrate binding or inefficient protonation in the transamination cycle due to the lowered pK_A value of the benzylic position. However, this is well in accordance with literature, where decreased yields were already reported for *para*-substituted acetophenones.[137]

A Hammett-plot was prepared to correlate the substrates electronic properties with the velocity of the reaction in accordance with the following equation (Formula 1).

$$log\frac{k}{k_0} = \rho \cdot \sigma$$

Formula 1: Hammett equation: k: rate constant with specific substrate, k_0: rate constant with reference substrate, ρ: reaction constant, σ: substituent-parameter.

The substituent-parameter σ quantifies the influence of the phenyl's substituent on the reaction centre. This empiric value depends on the nature of the substituent and on its relative position at the phenyl-ring.[139] The rate constant k describes the reaction velocity and the rate constant k_0 describes the reaction velocity with a substrate, carrying a hydrogen atom instead of the respective substituent. The reaction constant ρ provides information about the sensitivity of the reaction velocity towards the substituent and also about the electronic nature of the rate determining step. The higher the absolute value of the reaction constant, the more sensitive is the reaction towards the electronic induction of the substituent. In the rate determining step of reactions with positive reaction constants, the reaction centre builds negative charge. The value is negative, if positive charge is built. As the substituent-parameters are determined for benzoic acid, reaction constants larger than one indicate that the respective substrate is more sensitive towards the substituent's electronic induction in the respective reaction.

Figure 25 displays the Hammett-plot for both enzymes. It needs to be pointed out that using conversions instead of initial velocities is a strong simplification especially for high conversions. Furthermore, only substrate-inherent electronic effects can be rationalized. Enzyme electronics as well as sterics are ignored. *m*-Methoxyacetophenone (**8a**), for example, does not fit into the plot at all which may be due to its high conversion or due to an altered binding within the enzyme. Consequently, the results of the Hammett correlation must be examined with caution. Nonetheless, the Hammett plot might give an additional clue towards the nature of the rate determining step. In a classical chemical understanding of reductive aminations, for example the Leuckart-Wallach reaction, the substrate reversibly forms the imine in an upstream equilibrium before being reduced. In such a reaction scheme, the reduction represents the rate determining step,[140] leading to a negative Hammett-reaction constant.[141] On the other hand, it has been reasoned that the attack of the amine would represent the rate determining step on the basis that substrates more

susceptible towards amine attack have higher reaction rates.[133] Since such an amine-attack would be electronically influenced in a similar way as the attack by a hydride it is not surprising that the Hammett constant, found for the model reaction in this work, also is negative (- 0.93 ± 0.10 for *V.f.* TA; - 1.1 ± 0.3 for *P.d.* TA).

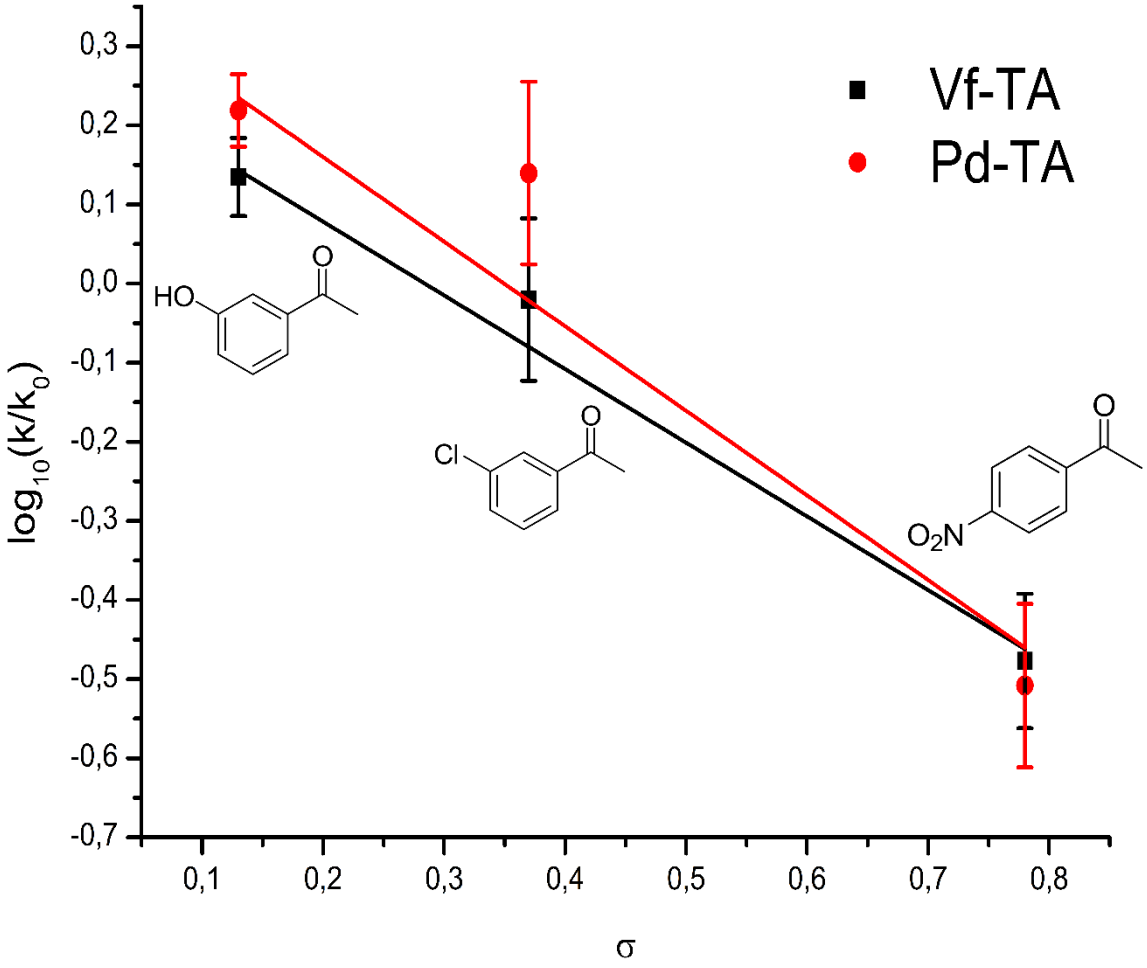

Figure 25: Hammett-plot for the aminations of **9a**, **10a** and **11a**. k Is simplified (peak area of product)/(peak area of product & substrate), Hammett constant for *V.f.* TA: - 0.93 ± 0.10 (R^2 = 0.98), Hammett constant for *P.d.* TA: - 1.1 ± 0.3 (R^2 = 0.89).

Both enzymes were absolutely (*S*)-selective for all substrates (ee >99%).

The results show that both, *P.d.* TA and *V.f.* TA are potent transaminating enzymes with broad substrate scope.

Thus, cloning of either transaminase into *Synechocystis* sp. PCC 6803 seems to be promising. Regeneration of the cosubstrate alanine will be achieved by the heterologous expression of an additional NADPH-dependent alanine dehydrogenase

in the cyanobacterium. Overall, the modified cyanobacterium will be capable to perform the amination of the carbonyl-carrying substrates, utilizing L-alanine as cosubstrate of the transaminase. L-Alanine, present in catalytic amounts, in turn is oxidized to pyruvate and regenerated by the NADPH-dependent alanine dehydrogenase, consuming one equivalent of NADPH and ammonia. NADPH regeneration will be facilitated by the *Synechocystis*' photosystem (Figure 26).

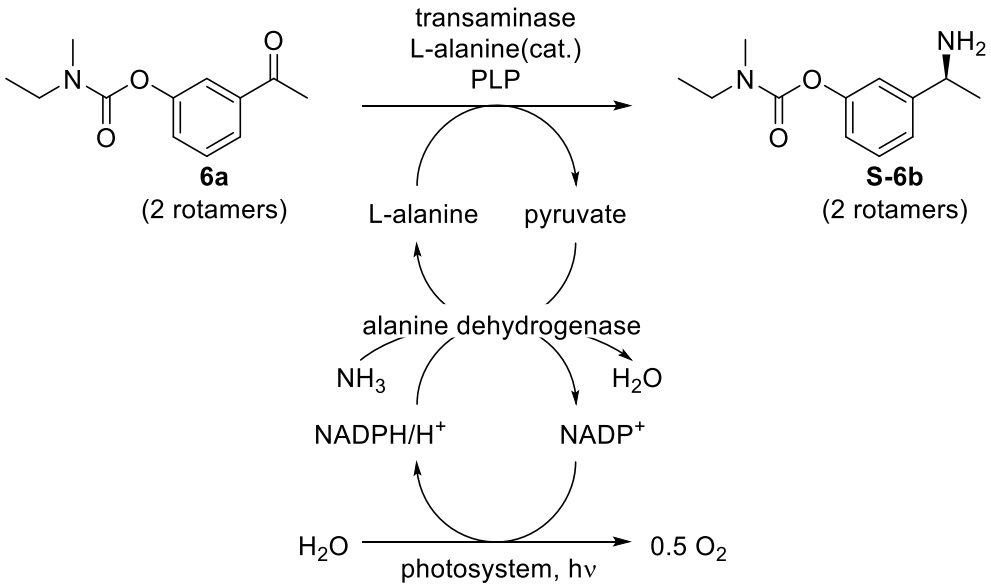

Figure 26: Targeted coupling of the transaminase and the alanine dehydrogenase to the photosystem of *Synechocystis sp* PCC 6803 to demonstrate a light dependent reductive amination. PLP: pyridoxal-5'-phosphate.

3.3 Cascades

Herein, artificial biocatalytic hydrogen-borrowing cascades were developed and tested *in vitro*.

α-Amino acids were used as substrates which, were transformed to the corresponding α-keto acid by amino acid oxidases or deaminases in the first step of the linear cascade. This oxidation results in the loss of stereoinformation at the α-carbon. Subsequent stereospecific reduction of the α-keto acid represents the second reaction step of the cascade. Depending on the enzyme employed in the second step, the cascade either yields the enantioenriched or stereoinverted α-amino acid, or the corresponding α-hydroxy-acid. While D- or L-amino acid dehydrogenases are used to produce the corresponding amino acids, D- or L-2-hydroxyisocaproic acid dehydrogenases yield the corresponding α-hydroxy acid. Figure 27 provides an overview pf all four cascades and demonstrates the modularity of the general concept.

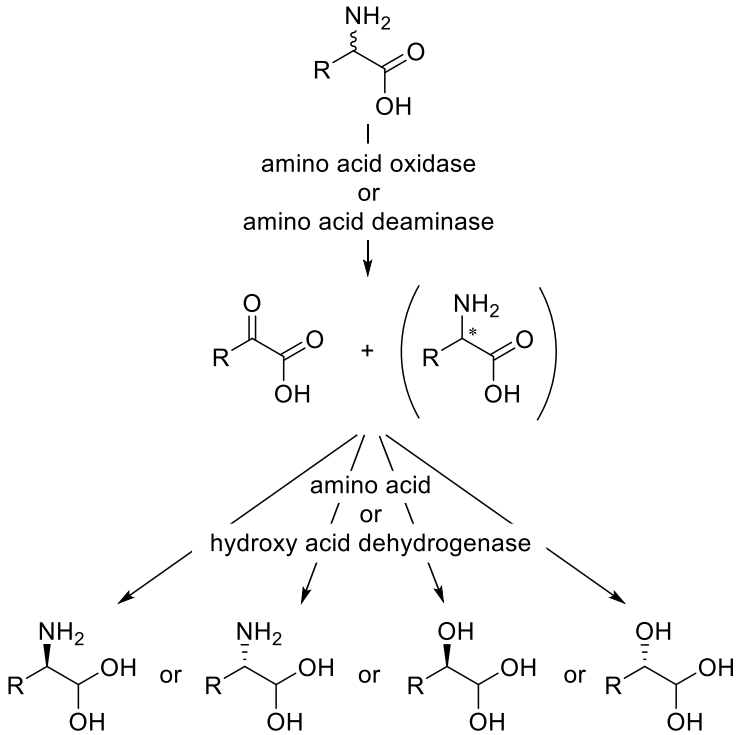

Figure 27: General reaction scheme of envisioned cascades for production of enantiopure amino or hydroxy acids.

Individual biocatalysts were selected from a pool of fifteen pre-selected enzymes (Table 4 to Table 6) which were previously evaluated individually.

3.3.1 Cultivation

A library of amino acid dehydrogenases, keto acid dehydrogenases, amino acid oxidases, and amino acid deaminases, previously cloned into *E. coli* BL21 were cultivated. The following yields of lyophilized whole cells were collected from 2 L of medium.

Table 4 displays yields of cultivated enzymes that were used for reductions of keto acids.

Table 4: Yields of cultivated, lyophilized whole cells of *E. coli* BL21, herterologously expressing the target enzymes (enzymes used for reductions).

pEG[1]	No.[2]	Expressed enzyme	His_6-tag	Mass[3] [kDa]	Yield[4] [g]
86	1	L-Leucine dehydrogenase (variant D203A-I204R-D210R) from *Thermoactinomyces intermedius*[24]	No tag	40.6	2.40
491	3	L-Glutamate dehydrogenase (variant F18: K92A-A166G-V377A) from *E. coli*[10]	*N*-term	50.4	1.87
489	5	*meso*-D-Aminopimelate dehydrogenase (variant B: D94A-Q154L-D158G-T173I-R199MH249N) from *Ureibacillus thermosphaericus*[28,29]	No tag	35.9	2.11
488	6	*meso*-D-Aminopimelate dehydrogenase (variant H227V) from *Symbiobacter thermophilum*[30]	*N*-term	34.4	1.70
220	L-HicDH	L-2-Hydroxyisocaproic acid dehydrogenase from *Lactobacillus confuses* DSM 20196[56]	No tag	33.8	n.d.
479	7	L-Lactate dehydrogenase from *Bacillus stearothermophilus*[37,53,41]	*C*-term	36.5	1.37
221	D-HicDH	D-2-Hydroxyisocaproic acid dehydrogenase from *Lactobacillus paracasei* DSM 20008[68]	No tag	37.9	n.d.
480	8	D-2-Hydroxy acid dehydrogenase from *Haloferax mediterranei*[69]	No tag	33.4	3.84
493	9	YiaE from *E. coli* K12[74]	*C*-term	37.0	2.28

[1] pEG: plasmid number, [2] No.: internal reference number, [3] including tag, [4] lyophilized whole cells; n.d.: not detected.

Table 5 displays yields of cultivated enzymes that were used for oxidations of amino acids.

Table 5: Yields of cultivated, lyophilized whole cells of *E. coli* BL21, herterologously expressing the target enzymes (enzymes used for oxidations).

pEG[1]	No.[2]	Expressed enzyme	His_6-tag	Mass[3] [kDa]	Yield[4] [g]
219	-	L-Amino acid deaminase from *Proteus myxofaciens*[122]			
485	11	Soluble, dye-linked D-amino acid deaminase “dauA” (wild type) from *Pseudomonas aeruginosa* PAO1[142]	*N*-term	42.5	5.09
484	12	Membrane bound, dye-linked D-amino acid deaminase “dadA” (wild type) from *Pseudomonas aeruginosa*[143]	*N*-term	49.1	1.87
481	13	D-Amino acid oxidase (wild type) from *Rhodotorula gracilis*[144]	*N*-term	42.0	1.71
483	14	D-Amino acid oxidase (variant: M213G) from *Rhodotorula gracilis*[118]	*N*-term	42.0	3.21
482	15	D-Amino acid oxidase (wild type) from *Trigonopsis variabilis*[145]	*N*-term	41.3	4.26

[1] pEG: plasmid number, [2] No.: internal reference number, [3] including tag, [4] lyophilized whole cells

.

Table 6 provides information about enzymes that are available in house.

Table 6: Enzyme preparations that are available in house as lyophilized whole cells. Commercial oxidase from porcine kidney available as purified enzyme.

pEG[1]	No.[2]	Expressed enzyme	His_6-tag	Mass[3] [kDa]
487	10	D-Lactate dehydrogenase (variant: D176S-I177R-F178T) from *Lactobacillus bulgaricus*[80]	*C*-term	38.6
490	2	L-Glutamate dehydrogenase (variant F11: K92C-A166G-V377A-S380A) from *E. coli*[10]	*N*-term	50.4
492	4	L-Glutamate dehydrogenase (variant F18-T195A: K92A-A166G-T195A-V377A) from *E. coli*[10]	*N*-term	50.4
206	-	*meso*-D-Aminopimelate dehydrogenase (variant Q151L-D155G- R196M-T170I-H245N) from *Corynebacterium glutamonicum*[146]	No tag	35.4
207	-	*meso*-D-Aminopimelate dehydrogenase (variant A: Q154L-D158G-T173I-R199M-H249N) from *Ureibacillus thermosphaericus*[32]	No tag	37.1
Commercial (Sigma)		D-Amino acid oxidase from porcine kidney	No tag	40.3

[1] pEG: plasmid number, [2] No.: internal reference number, [3] including tag, [4] lyophilized whole cells

To examine overexpression and solubility of the enzymes, SDS-pages of supernatants and cell pellet suspensions of digested (sonication) and undigested cells were performed. The following figures (Figure 29 to Figure 35) show the SDS-pages and the amount of suspended lyophilized cells, equivalent to 3 µg protein (Bradford assay)

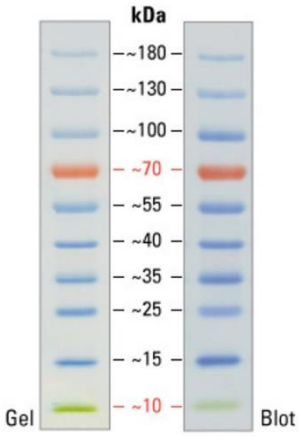

Figure 28: Pageruler (thermofisherscientific)[147]

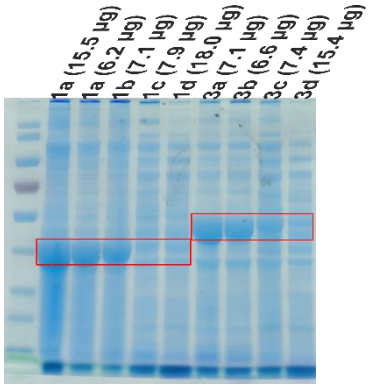

Figure 29: SDS-page of enzymes 1 (L-leucine dehydrogenase (variant: D203A-I204R-D210R) from *Thermoactinomyces intermedius*) and 3 (L-glutamate dehydrogenase (variant F18: K92A-A166G-V377A) from *E. coli*), the mass refers to the amount of lyophilized whole cells containing 3 µg of total protein (except the leftmost lane of 1a). Leftmost lane: pageruler standard (*Figure 28*). a: insoluble fraction of ultrasonicated cells, b: insoluble fraction of untreated lyophilized whole cells, c: soluble fraction of ultrasonicated cells, d: soluble fraction of untreated lyophilized whole cells

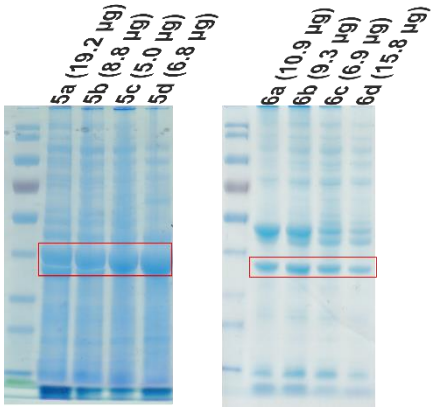

Figure 30: SDS-pages of enzymes 5 (D-amino acid dehydrogenase (variant: D94A-Q154L-D158G-T173I-R199M-H249N) from *Ureibacillus thermosphaericus*) and 6 (D-amino acid dehydrogenase (variant: H227V) from *Symbiobacterium thermophilum*), the mass refers to the amount of lyophilized whole cells containing 3 µg of total protein (except the leftmost lane of 1a). Leftmost lane: pageruler standard (*Figure 28*). a: insoluble fraction of ultrasonicated cells, b: insoluble fraction of untreated lyophilized whole cells, c: soluble fraction of ultrasonicated cells, d: soluble fraction of untreated lyophilized whole cells

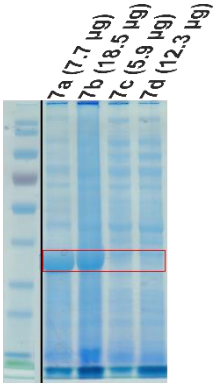

Figure 31: SDS-page of enzyme 7 (L-lactate dehydrogenase (variant: I37K-D38S-F16Q-C81S-N85R) from *Bacillus stearothermophilus*), the mass refers to the amount of lyophilized whole cells containing 3 µg of total protein (except the leftmost lane of 1a). Leftmost lane: pageruler standard (*Figure 28*). a: insoluble fraction of ultrasonicated cells, b: insoluble fraction of untreated lyophilized whole cells, c: soluble fraction of ultrasonicated cells, d: soluble fraction of untreated lyophilized whole cells

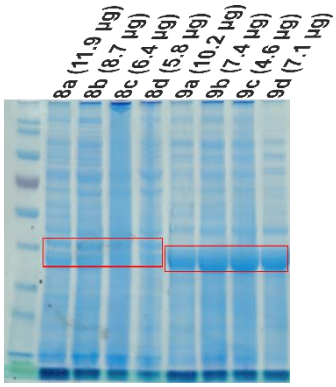

Figure 32: SDS-page of enzymes 8 (D-2-hydroxy acid dehydrogenase (wild type) from *Haloferax mediterranei*) and 9 (YiaE (wild type) from *E. coli* K12), the mass refers to the amount of lyophilized whole cells containing 3 µg of total protein (except the leftmost lane of 1a). Leftmost lane: pageruler standard (*Figure 28*). a: insoluble fraction of ultrasonicated cells, b: insoluble fraction of untreated lyophilized whole cells, c: soluble fraction of ultrasonicated cells, d: soluble fraction of untreated lyophilized whole cells

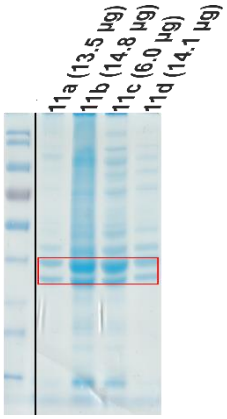

Figure 33: SDS-page of enzyme 11 (Soluble, dye-linked D-amino acid deaminase “dauA” (wild type) from *Pseudomonas aeruginosa* PAO1), the mass refers to the amount of lyophilized whole cells containing 3 µg of total protein (except the leftmost lane of 1a). Leftmost lane: pageruler standard (*Figure 28*). a: insoluble fraction of ultrasonicated cells, b: insoluble fraction of untreated lyophilized whole cells, c: soluble fraction of ultrasonicated cells, d: soluble fraction of untreated lyophilized whole cells

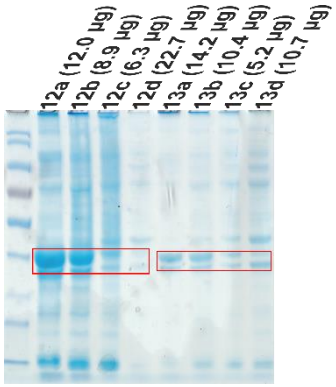

Figure 34: SDS-page of enzymes 12 (Membrane bound, dye-linked D-amino acid dehydrogenase “dadA” (wild type) from *Pseudomonas aeruginosa*) and 13 (D-amino acid oxidase (wild type) from *Rhodotorula gracilis*), the mass refers to the amount of lyophilized whole cells containing 3 µg of total protein (except the leftmost lane of 1a). Leftmost lane: pageruler standard (*Figure 28*). a: insoluble fraction of ultrasonicated cells, b: insoluble fraction of untreated lyophilized whole cells, c: soluble fraction of ultrasonicated cells, d: soluble fraction of untreated lyophilized whole cells

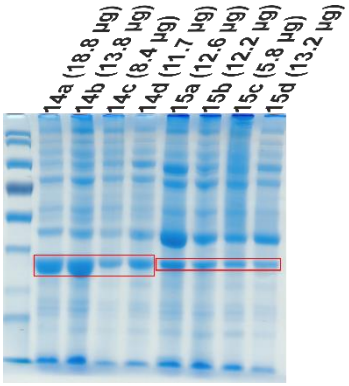

Figure 35: SDS-page of enzymes 14 (D-amino acid oxidase (variant: M213G) from *Rhodotorula gracilis*) and 15 (D-amino acid oxidase (wild type) from *Trigonopsis variabilis*), the mass refers to the amount of lyophilized whole cells containing 3 µg of total protein (except the leftmost lane of 1a). Leftmost lane: pageruler standard (*Figure 28*). a: insoluble fraction of ultrasonicated cells, b: insoluble fraction of untreated lyophilized whole cells, c: soluble fraction of ultrasonicated cells, d: soluble fraction of untreated lyophilized whole cells

All enzymes except the D-2-hydroxy acid dehydrogenase from *Haloferax mediterranei* are well overexpressed. However, enzymes 1, 3, 6, 7, 12, and 13 are poorly soluble. It seems like digestion increases the amount of soluble enzyme only for enzymes 3 and 12.

3.3.2 Analytics

To be able to evaluate the single enzyme's performance individually, as well as in the cascade, the product concentrations need to be determined.

3.3.2.1 Photometric assays

Since productivity of the dehydrogenases is coupled to consumption of the cosubstrate nicotinamide dinucleotide, it is feasible to determine the enzyme's performance by determining the cosubstrate concentration under certain circumstances. Oxidized and reduced nicotinamide dinucleotide cosubstrates have different UV-absorption spectra, allowing a convenient coupled photometric assay to be used. The photometric plate-reader then allows a high degree of parallelization and thus fast and resource-saving determination of initial reaction velocities of dehydrogenases.

The downside of such a coupled assay is that it only reaches high accuracies if certain requirements are met: e.g. there must not be any other components in the solution which alter the UV-absorption at the measured wavelength. Furthermore, the enzyme to evaluate must be the sole system in the preparation that is reactive towards the measured cosubstrate. This may be an issue especially when whole-cell preparations are used. The SDS pages (Figure 29 to Figure 35) show that there are several different proteins present in significant concentrations. Some of these might interfere with the coupled assay. Additionally, some blanks of the photometric plate reader experiments, containing only cosubstrate but not the substrate, already showed a decreasing cosubstrate concentration. Even though simple subtraction of the blank's activity is feasible to improve the quality of the measured enzyme's initial velocity, overall result comparability is diminished. A third observation pointing towards decreased result accuracy is that some of those cascade reaction-mixtures, meant to produce enantiopure amino acids, show small concentrations of hydroxy acids after cultivation. This may indicate the presence of an additional hydroxy acid dehydrogenase in either an amino acid dehydrogenase preparation or in a preparation of an oxidizing enzyme. However, such uncertainties were accepted, since measuring the single enzymes' initial velocities was planned to provide a rough overview of their performance and as the enzymes finally will be used in whole cyanobacterial cells.

3.3.2.2 Chromatographic essay

The discussed photometric assay is limited for the dehydrogenases. For both, the assembled cascades or the oxidases an alternative chromatographic assay was

developed to enable the parallel determination of the concentrations of the substrate, the reaction intermediate and the reaction product namely the respective α-amino acid, α-oxo acid, and α-hydroxy acid. Additionally, a whole array of different amino acids and their derivates was planned to be tested (Figure 36). The array was chosen to represent a wide range of different amino acids, namely small-polar, aliphatic, aromatic, aromatic-polar, natural, and non-natural ones.

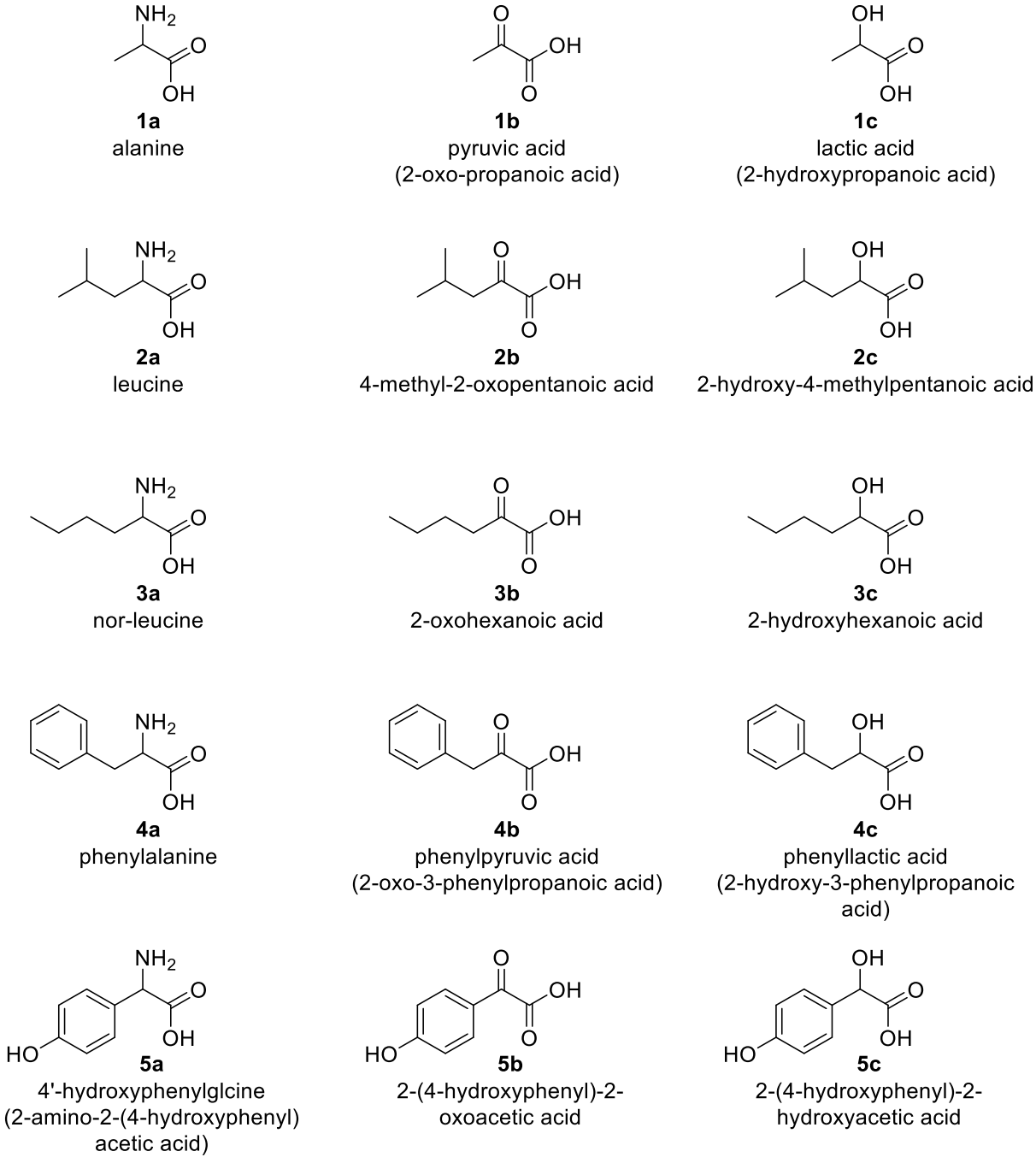

Figure 36: Amino acids and their oxo-, and hydroxy- derivates, to be analysed *via* HPLC-MS.

Previous unpublished experiments suggested separation by HPLC with aqueous solvent and detection with quadrupole MS, due to the setup's convenient sample preparation, low limits of detection, wide range of linearity, and little restrictions on physical properties of molecules.

Even though initial results seemed promising, several challenges needed to be overcome.

Firstly, separation of the three species proved to be difficult because of high molecular similarities and consequently low differences in polarity. Especially small amino acids and amino acids with polar groups are highly hydrophilic. This high polarity and hydrogen-bonding capacity leads to little interactions with the column material and outweighs any differences between the three species on C-18 reverse phase columns. However, separation of alanine, pyruvate, and lactic acid as well as separation of 4'-hydroxyphenylglycine and its derivates could not be achieved on such columns. Separation of these analytes is possible if normal phase HPLC is used. In fact, separation of alanine and its derivates was achieved using a Zorbax SCX 300 normal phase column with a gradient of H_2O, acetonitrile and formic acid (0.1%) as the eluent.

Secondly phenylpyruvate showed keto-enol tautomerism on the column during separation (Figure 37).

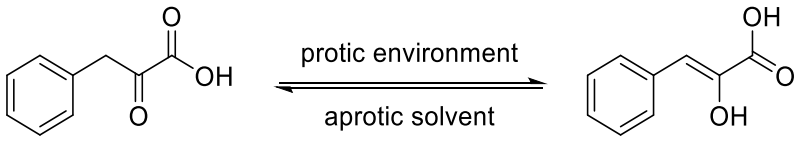

Figure 37: Keto-enol tautomerism of phenylpyruvic acid (**4b**).

The relatively high acidity of the benzylic proton leads to a high tendency of phenylpyruvate to form an equilibrium between the α-oxo acid and its enol-form. This tautomerism is easily observable with the naked eye looking at solid phenylpyruvate. When phenylpyruvate is recrystallized from dichloromethane, it appears as shiny flakes, while these flakes are slowly converted to an amorphous material when stored under atmosphere (Figure 38).

Figure 38: shiny flakes of phenylpyruvic acid (**4b**, left) and amorphous enol-form (right).

In aprotic solvents, the equilibrium lies on the side of the ketone. When the solid comes in contact with moist air, the equilibrium shifts towards the enol due to solvation.[148,149] By employing either of the two forms as substrates for dehydrogenations and comparison of the HPLC-MS data of these experiments, it was investigated whether there is an effect on the velocity of the enzymatic reaction. However, such an effect was not found, supposedly due to the fast equilibration in the acidic aqueous reaction medium. This fast equilibration was also observed on the column of the HPLC instrument as an alleviated baseline between the peaks of ketone and enol (Figure 39).

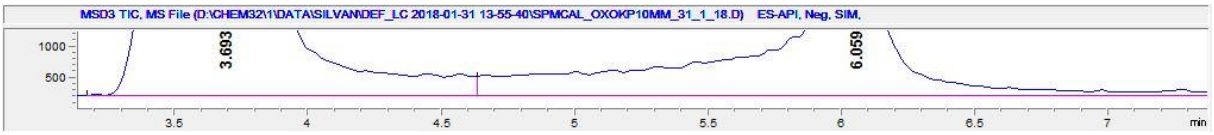

Figure 39: HPLC-MS spectrum of equilibrating phenylpyruvic acid (**4b**) (at 6.06 min) and its enol (at 3.69 min).

There is a significant difference between spectra obtained from recrystallized enol and amorphous ketone if the respective material was dissolved in the HPLC solvent and analysed right away or stored previously to injection. However, the position of this equilibrium is not only dependent on solvent and length of exposure to it, but also on other conditions such as temperature. Calibration on the peak-area of either the ketone or the enol or of both peaks revealed that the detector response for each of the two species was significantly different. This finding may be explained by the mild atmospheric pressure ionization used and tendencies to absorb or emit protons are different between the two species. These findings together with the difficulty to control the equilibrium position in this assay rendered direct analysis on aqueous HPLC-MS impossible.

The first upcoming strategy to overcome this issue was derivatization (Figure 40). Two derivatization strategies were tested: reaction with hydroxylamine to yield the oxime and reaction with *o*-phenylenediamine to yield cyclic 3-phenylquinoxalin-2-ol (products not isolated). Synthesis of the oxime revealed formation of two products, namely the (*E*)-oxime and the (*Z*)-oxime. Even though this strategy may be valid because both products may exhibit similar detector response, rendering calibration over both product peaks a viable strategy, it was not further investigated. The other derivatization strategy also yielded promising initial results but was also dropped after it was found that HPLC with organic solvent resulted in a single peak and therefore represents the more efficient analytics. However, the method may only be applied for UV-active analytes.

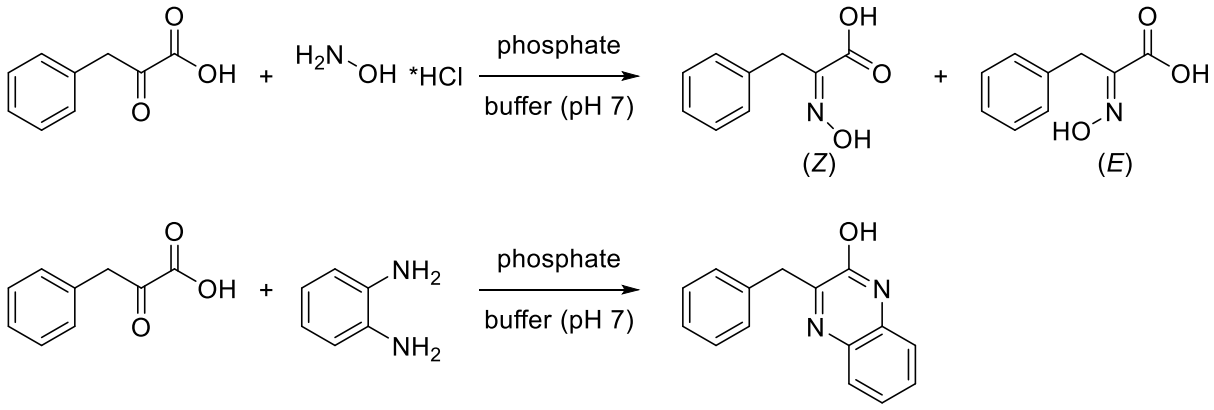

Figure 40: Derivatization strategy for phenylpyruvic acid (**4b**); top: derivatization with excess hydroxylamine in phosphate buffer (pH 7), bottom: derivatization with excess phenylene diamine in phosphate buffer (pH 7).

A third obstacle to overcome was that the three respective derivates of each amino acid exhibit large differences in detector response corresponding to their tendency to be ionized. For example, leucine induces a detector response, which is about 200-fold more intense than that of its hydroxy acid derivate. Keeping in mind that the ideal cascade should yield a high concentration of the product analyte (in our case 10 mM) and very low concentration of the substrate and intermediate analytes (ideally below 0.1 mM), linear calibrations over several orders of magnitude are required. Even though the used instrument has a large linear range it certainly cannot meet such requirements. The strategy to individually analyse the derivates in customized dilutions interfered with already large numbers of samples. That is why it was chosen to accept calibration equations of second order polynomials.

Finally, the MS-detector's response not only depended on the tendency of molecules to be ionized, it also exhibited an intrinsic drift of up to about 20% over time. This became evident when measuring the same sample at different times producing a large

fault when measurements of multiple samples exceeded 5 hours. By measuring each sample multiple times and by randomizing the order in which samples are measured, the systematic errors caused by the detector drift can be compensated using statistical analysis of the data. This way the large uncertainty about whether the detector response is the same when measuring calibrations and samples could be reduced and recovery rates could be drastically improved. However, this requires higher sample numbers, and that is why it was chosen to carry out only double measurements of the experimental triplicates.

3.3.3 Initial reaction rates

Enzyme performances were tested as initial reaction rates and in four-hour measurements of model reactions (Figure 41).

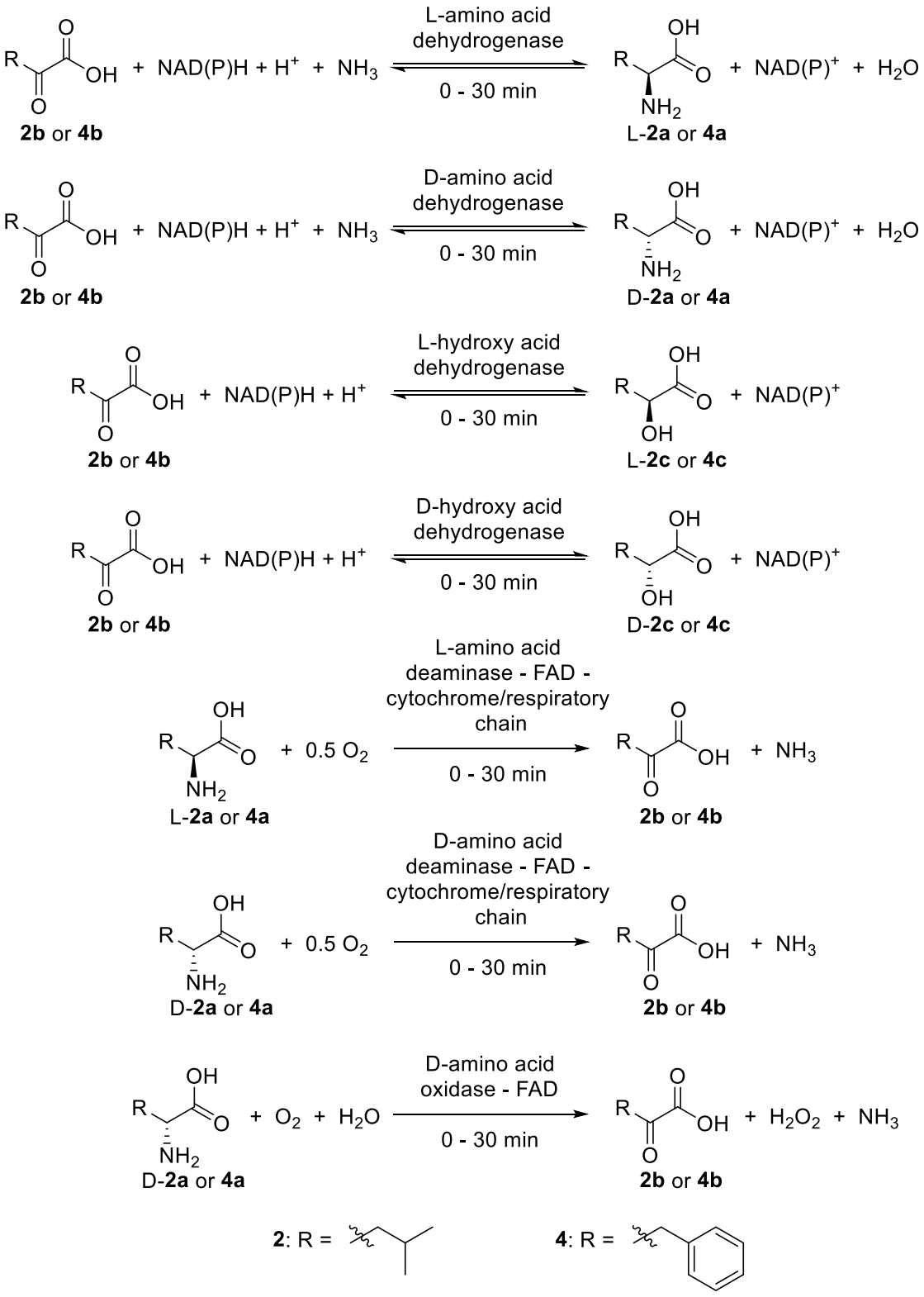

Figure 41: Model reactions for the measurement of initial reaction velocities.

While initial reaction rates of dehydrogenases can be determined in a coupled photometric assay, allowing the use of a plate reader and thus a high degree of parallelization, the oxidases' and deaminases' initial reaction rates were determined by quenching the model-reactions at specific time points and quantification on HPLC-MS or HPLC-UV. More information regarding the analytics can be found in chapter 3.3.2. Table 7 to Table 13 summarize the collected data.

Table 7 displays the initial reaction rates of the L-amino acid dehydrogenases.

Table 7: Initial reaction rates of L-amino acid dehydrogenases with the 2-oxocarboxylic acids **2b** and **4b** to produce the amino acids **2a** or **4a**, based on the photometric measurement of NADH or NADPH consumption. Reaction conditions: substrate 2 mM, NADH or NADPH 2 mM, ammonium chloride buffer pH 8.5, 300 mM, 30 °C); enzymes in the form of suspended whole lyophilized cells or, where indicated as lysates; n.d.: no significant activity detected.

L-Amino acid dehydrogenases	Substrates	Initial reaction rates [U/mg]
L-Leucine dehydrogenase (variant D203A-I204R-D210R) from *Thermoactinomyces intermedius* (pEG 486)	**2b** and NADH	0.17 ± 0.04
	4b and NADH	n.d.
	2b and NADPH	72 ± 16 (lysate); 1.7 ± 0.5
	4b and NADPH	n.d.
L-Glutamate dehydrogenase (variant F11: K92C-A166G-V377A-S380A) from *E. coli* (pEG 490)	**2b** and NADH	n.d.
	4b and NADH	n.d.
	2b and NADPH	0.034 ± 0.001
	4b and NADPH	0.17 ± 0.01
L-Glutamate dehydrogenase (variant F18: K92A-A166G-V377A) from *E. coli* (pEG 491)	**2b** and NADH	n.d.
	4b and NADH	0.0068 ± 0.0001
	2b and NADPH	11 ± 1 (lysate); 0.29 ± 0.03
	4b and NADPH	1.6 ± 0.1

Reaction conditions: substrate 2 mM, NADH or NADPH 2 mM, ammonium chloride buffer (pH 8.5, 300 mM, 30 °C); enzymes used in the form of suspended whole lyophilized cells (*T.i.* L-LeuDH: 0.34 mg mL^{-1}, *E.coli* GluDH F11: 0.31 mg mL^{-1}, *E.coli* GluDH F18: 0.37 mg mL^{-1}), or where indicated as lysates (from equivalent amounts of cells); n.d.: no significant activity detected, initial rates are given as U/mg of the enzyme preparation.

L-Leucine dehydrogenase (variant D203A-I204R-D210R) from *Thermoactinomyces intermedius* was selected as preferred enzyme for the reductive amination of aliphatic 2-oxo acids and L-glutamate dehydrogenase (variant F18: K92A-A166G-V377A) from *E. coli* was selected for reductive aminations of aromatic 2-oxo acids. They were chosen, because they were the most active enzymes under the given conditions. For the L-Leucine dehydrogenase (variant D203A-I204R-D210R) from *Thermoactinomyces intermedius,* no activity towards **4b** was detected. While for this

enzyme a considerable activity with NADH was detected, the other two enzymes exhibited no or very little activity with NADH.

Table 8 displays the initial reaction rates of the D-amino acid dehydrogenases.

Table 8: Initial reaction rates of D-amino acid dehydrogenases with the 2-oxocarboxylic acids **2b** and **4b** to produce the amino acids **2a** or **4a**, based on the photometric measurement of NADH or NADPH consumption.

D-amino acid dehydrogenase	Substrates	Initial velocity [U/mg]
meso-D-Aminopimelate dehydrogenase (variant Q151L-D155G-R196M-T170I-H245N) from *Corynebacterium glutamonicum* (pEG 206)	**2b** and NADH	n.d.
	4b and NADH	n.d.
	2b and NADPH	0.0072 ± 0.0006 (lysate)
	4b and NADPH	0.0029 ± 0.0002 (lysate)
meso-D-Aminopimelate dehydrogenase (variant A: Q154L-D158G-T173I-R199M-H249N) from *Ureibacillus thermosphaericus* (pEG 207)	**2b** and NADH	0.0067 ± 0.0035
	4b and NADH	0.0079 ± 0.0002
	2b and NADPH	0.028 ± 0.004
	4b and NADPH	0.040 ± 0.001
meso-D-aminopimelate dehydrogenase (variant B: D94A-Q154L-D158G-T173I-R199M-H249N) from *Ureibacillus thermosphaericus* (pEG 489)	**2b** and NADH	0.022 ± 0.003
	4b and NADH	0.037 ± 0.003
	2b and NADPH	0.024 ± 0.002
	4b and NADPH	0.040 ± 0.001
meso-D-Aminopimelate dehydrogenase (variant H227V) from *Symbiobacter thermophilum* (pEG 488)	**2b** and NADH	0.014 ± 0.001
	4b and NADH	0.020 ± 0.005
	2b and NADPH	0.016 ± 0.002
	4b and NADPH	0.024 ± 0.001

Reaction conditions: substrate 2 mM, NADH or NADPH 2 mM, ammonium chloride buffer (pH 8.5, 300 mM, 30 °C); enzymes used in the form of suspended whole lyophilized cells (*C.g. m*-DAPDH: 2.6mg mL^{-1}, *U.t. m*-DAPDH var. A: 1.4 mg mL^{-1}, *U.t. m*-DAPDH var. B: 1.5 mg mL^{-1}, *S.t. m*-DAPDH: 1.4 mg mL^{-1}), or where indicated as lysates (from equivalent amounts of cells); n.d.: no significant activity detected, initial rates are given as U/mg of the enzyme preparation.

meso-D-Aminopimelate dehydrogenase (variant A: Q154L-D158G-T173I-R199M-H249N) from *Ureibacillus thermosphaericus* was selected as preferred enzyme for the reductive amination of aliphatic 2-oxo acids and variant B was selected for reductive aminations of aromatic 2-oxo acids. They were chosen, because they were the most active enzymes under the given conditions. Variant A showed only little activity with NADH but variant B exhibits activity with NADH in the same range as with NADPH. The *meso*-D-aminopimelate dehydrogenase (variant Q151L-D155G-R196M-T170I-H245N) from *Corynebacterium glutamonicum* did on one hand not have significant activity with NADH, but on the other hand, also had very low activity with NADPH, which was only detectable in the lysate.

Table 9 displays the initial reaction rates of the L-2-hydroxy acid dehydrogenases.

Table 9: Initial reaction rates of L-hydroxy acid dehydrogenases with the 2-oxocarboxylic acids **2b** and **4b** to produce the 2-hydroxy acids **2c** or **4c**, based on the photometric measurement of NADH or NADPH consumption.

L-α-Hydroxy acid dehydrogenase	Substrates	Initial velocity [U/mg]
L-2-Hydroxyisocaproic acid dehydrogenase from *Lactobacillus confuses* (pEG 220)	**2b** and NADH	15 ± 5
	4b and NADH	22 ± 1
	2b and NADPH	7.4 ± 0.2 (lysate) 2.6 ± 0.1
	4b and NADPH	4.7 ± 0.1
L-Lactate dehydrogenase from *Bacillus stearothermophilus* (pEG 479)	**2b** and NADH	n.d.
	4b and NADH	n.d.
	2b and NADPH	n.d.
	4b and NADPH	n.d.

Reaction conditions: substrate 2 mM, NADH or NADPH 2 mM, potassium phosphate buffer (pH 7.0, 100 mM, 30 °C); enzymes used in the form of suspended whole lyophilized cells (L-HicDH: 0.1 mg mL^{-1},*S.t.* L-LacDH: 0.3 mg mL^{-1}); or where indicated as lysates (from equivalent amounts of cells); n.d.: no significant activity detected, initial rates are given as U/mg of the enzyme preparation.

L-HicDH is active towards both substrates and both coenzymes and thus was selected for the cascade reactions. NADH is the more effective cosubstrate. The L-lactate dehydrogenase from *Bacillus stearothermophilus* was not found to be active. Activation of this enzyme may be achieved by addition of the allosteric activator fructose-5-phosphate to enable dimerization of enzyme monomers (*vide infra*).

Table 10 displays the initial reaction rates of the D-2-hydroxy acid dehydrogenases.

Table 10: Initial reaction rates of D-hydroxy acid dehydrogenases with the 2-oxocarboxylic acids **2b** and **4b** to produce the 2-hydroxy acids **2c** or **4c**, based on the photometric measurement of NADH or NADPH consumption.

D-α-Hydroxy acid dehydrogenase	Substrates	Initial velocity [U/mg]
D-2-Hydroxyisocaproic acid dehydrogenase from *Lactobacillus paracasei* (pEG 221)	**2b** and NADH	10 ± 1
	4b and NADH	13 ± 8
	2b and NADPH	3.9 ± 0.1 (lysate) 1.8 ± 0.1
	4b and NADPH	13 ± 1
D-2-Hydroxy acid dehydrogenase from *Haloferax mediterranei* (pEG 480)	**2b** and NADH	n.d.
	4b and NADH	n.d.
	2b and NADPH	n.d.
	4b and NADPH	0.0028 ± 0.0001
YiaE from *E. coli* K12 (pEG 493)	**2b** and NADH	0.063 ± 0.018)
	4b and NADH	0.075 ± 0.018
	2b and NADPH	0.20 ± 0.02
	4b and NADPH	0.45 ± 0.01

Reaction conditions: substrate 2 mM, NADH or NADPH 2 mM, potassium phosphate buffer (pH 7.0, 100 mM, 30 °C); enzymes used in the form of suspended whole lyophilized cells (D-HicDH: 0.13 mg mL^{-1}, *H.m.* D-HADH: 0.35 mg mL^{-1}, YiaE: 0.1 mg mL^{-1}), or where indicated as lysates (from equivalent amounts of cells); n.d.: no significant activity detected, initial rates are given as U/mg of the enzyme preparation.

D-HicDH is active towards both substrates and both coenzymes. NADH is the more effective cosubstrate. D-2-Hydroxy acid dehydrogenase from *Haloferax mediterranei* only displays activity with NADPH towards phenylpyruvate. YiaE from *E. coli* K12 is active with both cosubstrates and both substrates and exhibits higher activities with NADPH than with NADH. However, the activity of the YiaE preparation is lower than that of the D-HicDH preparation. For this reason, D-HicDH was selected for the cascade reactions.

Table 11 displays the initial reaction rates of the L-amino acid deaminases.

Table 11: Initial reaction rates of L-amino acid deaminase with the amino acids D/L-**2a** and D/L-**4a** to produce the 2-oxocarboxylic acids **2b** or **4b**, based on the photometric measurement of NADH or NADPH consumption.

L-Amino acid deaminases	Initial velocity with 2a [U/mg]	Initial velocity with 4a [U/mg]
L-Amino acid deaminase from *Proteus myxofaciens* (pEG 219)	0.31 ± 0.01	0.041 ± 0.003

Reaction conditions: substrate 10 mM, FAD 0.2 mM, O_2 1 atm, potassium phosphate buffer (pH 7.0, 100 mM, 30 °C); enzymes used in the form of suspended whole lyophilized cells (0.1 mg mL^{-1}), initial rates are given as U/mg of the enzyme preparation.

The L-amino acid deaminase from *Proteus myxofaciens* is well known as effective enzyme for oxidations of L-amino acids. For this reason and because it is the only L-amino acid oxidizing enzyme at hand, it was used in all cascades. However, it proves to be more effective towards the oxidation of aliphatic amino acids.

Table 12 displays the initial reaction rates of the D-amino acid deaminases.

Table 12: Initial reaction rates of D-amino acid deaminases with the amino acids **2a** and **4a** to produce the 2-oxocarboxylic acids **2b** or **4b**, based on the photometric measurement of NADH or NADPH consumption.

D-Amino acid deaminases	Initial velocity with 2a [U/mg]	Initial velocity with 4a [U/mg]
Soluble, dye-linked D-amino acid deaminase "dauA" (wild type) from *Pseudomonas aeruginosa* PAO1 (pEG 485)	0.0065 ± 0.0001	0.0087 ± 0.0013
Membrane bound, dye-linked D-amino acid deaminase "dadA" (wild type) from *Pseudomonas aeruginosa* (pEG 484)	0.049 ± 0.001	0.077 ± 0.003

Reaction conditions: substrate 10 mM, FAD 0.2 mM, O_2 1 atm potassium phosphate buffer (pH 7.0, 100 mM, 30 °C); enzymes used in the form of suspended whole lyophilized cells (dauA: 0.1 mg mL^{-1}, dadA: 0.1 mg mL^{-1}), initial rates are given as U/mg of the enzyme preparation.

Both enzymes are active towards the oxidation of both substrates. However, since in direct concurrence with the D-amino acid oxidases, they were not selected for the cascade reaction because their preparations exhibited lower reaction rates.

Table 13 displays the initial reaction rates of the D-amino acid oxidases.

Table 13: Initial reaction rates of D-amino acid oxidases with the amino acids **2a** and **4a** to produce the 2-oxocarboxylic acids **2b** or **4b**, based on the photometric measurement of NADH or NADPH consumption.

D-Amino acid oxidase	Initial velocity with 2a [U/mg]	Initial velocity with 4a [U/mg]
D-Amino acid oxidase (wild type) from *Rhodotorula gracilis* (pEG 481)	0.39 ± 0.23	0.52 ± 0.18
D-Amino acid oxidase (variant: M213G) from *Rhodotorula gracilis* (pEG 483)	0.38 ± 0.25	0.48 ± 0.06
D-Amino acid oxidase (wild type) from *Trigonopsis variabilis* (pEG 482)	0.18 ± 0.01	0.37 ± 0.06
Commercial D-amino acid oxidase from porcine kidney	5.9 ± 4.3	Not measured

Reaction conditions: substrate 10 mM, FAD 0.2 mM, potassium phosphate buffer pH (7.0, 100 mM, 30 °C, catalase >650 U); enzymes used in the form of suspended whole lyophilized cells (*R.g.* DAAO w.t.: 0.1 mg mL^{-1}, *R.g.* DAAO M213G: 0.1 mg mL^{-1}, *T.v.* DAAO: 0.1 mg mL^{-1}, p.k. DAAO: 0.025 mg mL^{-1}), initial rates are given as U/mg of the enzyme preparation.

All amino acid oxidases, grown in house, were active towards both substrates. The highly active amino acid oxidase from porcine kidney was not used, because non-commercial enzymes were preferred. For the cascade reactions, the preparation with the highest activity towards the oxidation of both D-amino acids was selected [D-amino acid oxidase (wild type) from *Rhodotorula gracilis*].

3.3.4 Conversion after four hours

After initial reaction rates were determined, the single enzyme's performance was measured in four-hour measurements.

The results of these four-hour measurements are displayed in Table 14 to Table 20.

Table 14 displays conversions of **2b** or **4b** to **2a** or **4a** with L-amino acid deaminases.

Table 14: Conversion of the 2-oxocarboxylic acid **2b** or **4b** to **2a** or **4a** with L-amino acid dehydrogenases after four hours reaction time.

L-Amino acid dehydrogenases	c of **2b** [%]	ee of L-**2a** [%]	c of **4b** [%]	ee of L-**4a** [%]
L-Leucine dehydrogenase (variant D203A-I204R-D210R) from *Thermoactinomyces intermedius* (pEG 486)	89 ± 4	n.d.	2.7 ± 0.3	n.d.
L-Glutamate dehydrogenase (variant F18: K92A-A166G-V377A) from *E. coli* (pEG 491)	91 ± 7	n.d.	97 ± 4	n.d.

Reaction conditions: substrate 10 mM; NADPH 12 mM; ammonium chloride buffer (300 mM, pH 8.5, 30 °C); enzymes in the form of suspended whole lyophilized cells; amino acid dehydrogenases: pEG 486 3.0 mg mL^{-1}, pEG 491 17.3 mg mL^{-1}; 120 rpm; c = conversion; n.d. = not determined.

Both tested L-amino acid dehydrogenases show high conversions with **2b**, but the leucine dehydrogenase does convert only little of **4b**. For this reason, L-glutamate dehydrogenase (variant F18: K92A-A166G-V377A) from *E. coli* was chosen to be used in the cascades for the conversion of **4b** to L-**4a**. L-Leucine dehydrogenase (variant D203A-I204R-D210R) from *Thermoactinomyces intermedius* was chosen to convert **2b** to L-**2a** because the two enzymes' conversion after four hours is not significantly different, but the leucine dehydrogenase has a higher initial reaction rate.

Table 15 displays conversions of **2b** or **4b** to **2a** or **4a** with D-amino acid dehydrogenases.

Table 15: Conversion of the 2-oxocarboxylic acid **2b** or **4b** to **2a** or **4a** with D-amino acid dehydrogenases after four hours reaction time.

D-Amino acid dehydrogenases	c of **2b** [%]	ee of D-**2a** [%]	c of **4b** [%]	ee of D-**4a** [%]
meso-D-Aminopimelate dehydrogenase (variant A: Q154L-D158G-T173I-R199M-H249N) from *Ureibacillus thermosphaericus* (pEG 207)	44.1 ± 0.9	n.d.	48 ± 4	n.d.
meso-D-Aminopimelate dehydrogenase (variant B: D94A-Q154L-D158G-T173I-R199M-H249N) from *Ureibacillus thermosphaericus* (pEG 489)	39 ± 2	n.d.	39 ± 2	n.d.

Reaction conditions: substrate 10 mM; NADPH 12 mM; ammonium chloride buffer (300 mM, pH 8.5, 30 °C); enzymes in the form of suspended whole lyophilized cells; amino acid dehydrogenases: pEG 207 19.9 mg mL^{-1}, pEG 489 19.9 mg mL^{-1}; 120 rpm; c = conversion; n.d. = not determined.

Both tested D-amino acid dehydrogenases show good conversions with **2b** and **4b**. For this reason, the selection was based on their initial reaction rates. To be used in the cascade, *meso*-D-Aminopimelate dehydrogenase (variant A: Q154L-D158G-T173I-R199M-H249N) from *Ureibacillus thermosphaericus* was selected for the conversion of **2b** to D-**2a** and *meso*-D-aminopimelate dehydrogenase (variant B: D94A-Q154L-D158G-T173I-R199M-H249N) from *Ureibacillus thermosphaericus* for the conversion of **4b** to D-**4a**.

Table 16 displays conversions of **2b** or **4b** to **2c** or **4c** with L-2-hydroxy acid dehydrogenases.

Table 16: Conversion of the 2-oxocarboxylic acid **2b** or **4b** to **2c** or **4c** with L-2-hydroxy acid dehydrogenases after four hours reaction time.

L-α-Hydroxy acid dehydrogenase	c of **2b** [%]	ee of L-**2c** [%]	c of **4b** [%]	ee of L-**4c** [%]
L-2-Hydroxyisocaproic acid dehydrogenase from *Lactobacillus confuses* (pEG 220)	90 ± 6	99.9	86 ± 6	n.d.

Reaction conditions: substrate 10 mM; NADPH 12 mM; potassium phosphate buffer (100 mM, pH 7.0, 30 °C); enzymes in the form of suspended whole lyophilized cells; hydroxy acid dehydrogenase pEG 220 2 mg mL^{-1}; 120 rpm; c = conversion; n.d. = not determined.

L-HicDH from *Lactobacillus confuses* proves to be highly efficient in the conversion of 2-oxo acids to L-2-hydroxy acids. It is used in the cascades.

Table 17 displays conversions of **2b** or **4b** to **2c** or **4c** with D-2-hydroxy acid dehydrogenase.

Table 17: Conversion of the 2-oxocarboxylic acid **2b** or **4b** to **2c** or **4c** with D-2-hydroxy acid dehydrogenases after four hours reaction time.

D-α-Hydroxy acid dehydrogenases	c of **2b** [%]	ee of D-**2c** [%]	c of **4b** [%]	ee of D-**4c** [%]
D-2-Hydroxyisocaproic acid dehydrogenase from *Lactobacillus paracasei* (pEG 221)	89 ± 22	99.9	84 ± 5	n.d.
YiaE from *E. coli* K12 (pEG 493)	87 ± 26	99.9	58 ± 43	n.d.

Reaction conditions: substrate 10 mM; NADPH 12 mM; potassium phosphate buffer (100 mM, pH 7.0, 30 °C); enzymes in the form of suspended whole lyophilized cells; hydroxy acid dehydrogenase pEG 221 3.1 mg mL^{-1}, pEG 493 20.1 mg mL^{-1}; 120 rpm; c = conversion; n.d. = not determined.

Both enzymes are effective enzymes for the conversion of **2b** or **4b** to **2c** or **4c**. D-HicDH was chosen for application in the cascades due to higher initial reaction rates.

Table 18 displays conversions of **2a** or **4a** to **2b** or **4b** with L-amino acid deaminases.

Table 18: Conversion of the amino acid *rac*-**2a** or *rac*-**4a** to **2b** or **4b** with L-amino acid deaminases after four hours reaction time.

L-Amino acid deaminase	c of *rac*-**2a** [%]	ee of D-**2a** [%]	c of *rac*-**4a** [%]	ee of D-**4a** [%]
L-Amino acid deaminase from *Proteus myxofaciens* (pEG 219)	52 ± 2	n.d.	48 ± 5	3.2 ± 0.4

Reaction conditions: substrate 10 mM; O_2 0.2 atm; FAD 0.02 eq; potassium phosphate buffer (100 mM, pH 7.0, 30 °C); enzymes in the form of suspended whole lyophilized cells; amino acid deaminase: pEG 219 16.1 mg/mL; 120 rpm; c = conversion, n.d. = not determined.

L-Amino acid deaminase from *Proteus myxofaciens*, is the only enzyme at hand for the conversion of L-**2a** or L-**4a** to **2b** or **4b**. It displays good conversions in the four-hour measurements.

Table 19 displays conversions of *rac*-**2a** or *rac*-**4a** to **2b** or **4b** with D-amino acid deaminases.

Table 19: Conversion of the amino acid *rac*-**2a** or *rac*-**4a** to **2b** or **4b** with D-amino acid oxidases after four hours reaction time.

D-Amino acid deaminases	c of **2a** [%]	E-value/ee [%] for D-**2a**	c of **4a** [%]	E-value/ee [%] for D-**4a**
Soluble, dye-linked D-amino acid deaminase "dauA" (wild type) from *Pseudomonas aeruginosa* PAO1 (pEG 485)	2.9 ± 0.4	>200/ 7 ± 2	1.4 ± 0.8	>200/ 12 ± 2
Membrane bound, dye-linked D-amino acid deaminase "dadA" (wild type) from *Pseudomonas aeruginosa* (pEG 484)	13 ± 3	3.5 ± 0.4/ 17 ± 2	33 ± 4	2.0 ± 0.4/ 45 ± 15

Reaction conditions: substrate 10 mM; O_2 0.2 atm; FAD 0.02 eq; potassium phosphate buffer (100 mM, pH 7.0, 30 °C); enzymes in the form of suspended whole lyophilized cells; amino acid oxidases: pEG 485 20.4 mg mL^{-1}, pEG 484 19.6 mg mL^{-1}; 120 rpm; c = conversion, n.d. = not determined.

Both enzymes display conversions that are lower than those of the D-amino acid oxidases. For this reason, they were not used in the cascades.

Table 20 displays conversions of *rac*-**2a** or *rac*-**4a** to **2b** or **4b** with D-amino acid oxidases.

Table 20: Conversion of the amino acid *rac*-**2a** or *rac*-**4a** to **2b** or **4b** with D-amino acid oxidases after four hours reaction time.

D-Amino acid oxidases	c of **2a** [%]	ee of D-**2a** [%]	c of **4a** [%]	ee of D-**4a** [%]
D-Amino acid oxidase (wild type) from *Rhodotorula gracilis* (pEG 481)	39 ± 3	n.d.	26 ± 7	n.d.
D-Amino acid oxidase (wild type) from *Trigonopsis variabilis* (pEG 482)	34.4 ± 0.9	n.d.	20 ± 6	n.d.
Commercial D-amino acid oxidase from porcine kidney	51 ± 5	n.d.	40 ± 4	n.d.

Reaction conditions: substrate 10 mM; O_2 0.2 atm; FAD 0.02 eq; potassium phosphate buffer (100 mM, pH 7.0, 30 °C); enzymes in the form of suspended whole lyophilized cells; catalase as commercial solution (sigma); amino acid oxidases: pEG 481 13.0 mg mL^{-1}, pEG 482 19.7 mg mL^{-1}, porcine 0.9 mg mL^{-1}; catalase >650 U; 120 rpm; c = conversion, n.d. = not determined.

The D-amino acid oxidase (wild type) from *Rhodotorula gracilis* converted roughly a third of both substrates which is a little more than the D-amino acid oxidase (wild type) from *Trigonopsis variabilis*. The commercial enzyme is highly effective but was only to be used if no non-commercial enzyme would have displayed good conversions. For this reason, the D-amino acid oxidase (wild type) from *Rhodotorula gracilis* was selected for the conversion of D-**2a** and D-**4b** to **2b** and **4b**.

Concluding, there are effective enzymes at hand for all envisioned enzyme functionalities to be applied in the cascade reactions.

3.3.5 Cascades

Four different cascades were chosen as representative examples for the target-reactions, following the general scheme, depicted in Figure 27. The following schemes show reactions with phenylalanines (**4a**) as substrates, (a[phe] – d[phe]), however, each reaction system was also applied for leucine (**2a**, a[leu] – d[leu]) The starting material in the cascades was either the respective L- or the racemic amino acid. D-amino acids were not chosen as starting materials, because they are more expensive than L- or racemic amino acids. Sigma Aldrich for example sells 50 g of L-leucine for 22,40 € while the same supplier sells 25 g D-leucine for 116 € and 25 g of racemic leucine for 78.30 €. In the first step of the linear cascades, depending on the target compound and the starting material, either the L-amino acid deaminase from *Proteus*

myxofaciens or the D-amino acid oxidase (wild type) from *Rhototorula gracilis* or both were used. If a racemic starting material and only one oxidizing enzyme was used, one enantiomer is converted to the respective oxo acid. This was done in the production of L-amino acids, increasing the overall efficiency of the cascade, since only half of the total starting material needs to be converted by the oxidizing and reducing enzyme. If the L-enantiomer was used as starting material, the amino acid deaminase from *Rhodotorula gracilis* was employed. For the production of hydroxy acids from racemic amino acids, both oxidizing enzymes were employed. The oxidizing step of the linear cascade requires O_2 as cosubstrate. To allow diffusion of air into the reaction mixture, the cascades were carried out in open Eppendorf tubes. To avoid side reactivities and enzyme deactivation by H_2O_2, catalase was added to the reaction mixture, if the amino acid oxidase from *Rhodotorula gracilis* was used. In the second step of the liner cascade, the enzyme, that most efficiently converts the oxo acid to the targeted compound was applied. For example, if the targeted compound was the L-2-hydroxy acid, L-HicDH from *Lactobacillus confuses* was employed. The dehydrogenation reaction was run with NADPH as the cosubstrate in catalytic amounts. Cofactor recycling was done with the glucose dehydrogenase recycling system and an excess of glucose (Figure 42).

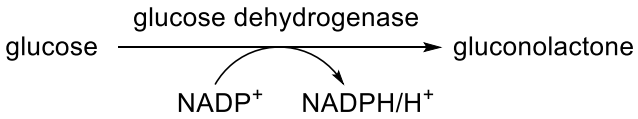

Figure 42: Reaction scheme of the glucose dehydrogenase reregeneration system.

One equivalent of ammonia, required by the amino acid dehydrogenase, was provided in the form of the ammonium chloride buffer (300 mM, pH 8.5). This buffer is more basic and more concentrated than the potassium phosphate buffer (100 mM, pH 7.0), used when 2-hydroxy acid dehydrogenases were applied, to drive the reaction equilibrium to the product side.

The selection of enzymes is based on the data, obtained from the measurements of initial reaction rates and the four-hour conversions. The enzymes displaying the highest efficiencies were selected.

Similar cascades were previously established for example by Busto *et al.*, Seo *et al.* and Gourinchas *et al.*.[57,136,150]

For more general information about cascades *vide supra*.

3.3.5.1 Cascade a – production of L-amino acids

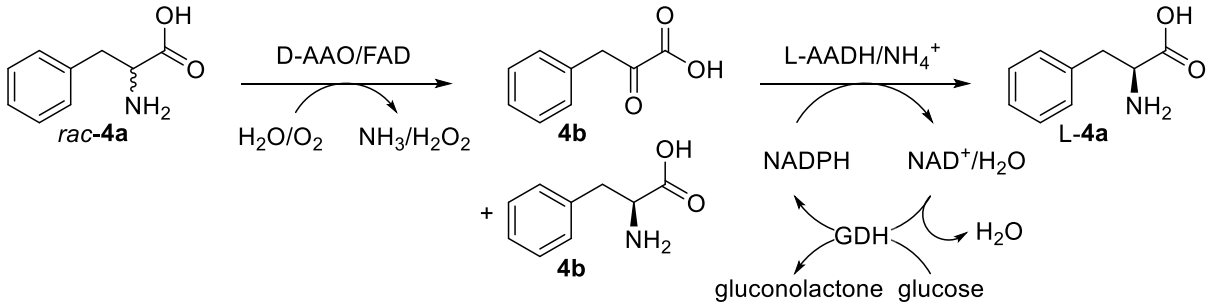

Figure 43: Reaction scheme of cascade a[phe]: conversion of racemic phenylalanine (*rac*-**4a**) to L-phenylalanine (L-**4a**), employing a D-AAO in combination with a L-AADH. The same reaction system was also used for leucine (**2a**, a[leu]).

Cascade a was designed to produce L-amino acids from the respective racemic amino acids.

The enzymes, that were selected for the respective substrate are listed in Table 21.

Table 21: Selection of enzymes for cascade a[leu] and a[phe].

Cascade	Dehydrogenase	Oxidase
a[leu]	L-Leucine dehydrogenase (variant D203A-I204R-D210R) from *Thermoactinomyces intermedius* (pEG 486)	D-amino acid oxidase (wild type) from *Rhodotorula gracilis* (pEG 481)
a[phe]	L-Glutamate dehydrogenase (variant F18: K92A-A166G-V377A) from *E. coli* (pEG 491)	D-amino acid oxidase (wild type) from *Rhodotorula gracilis* (pEG 481)

Table 22 displays the results of cascades a[leu] and a[phe].

Table 22: Results of cascade a[leu] and a[phe]: conversion of *rac*-amino acid (*rac*-**2a,** *rac*-**4a**) to L-amino acid (L-**2a**, L-**4a**).

Cascade	Substrate	Amino acid **a**		Oxo acid **b** [%]	Hydroxy acid **c** [%]
		[%]	ee [%]		
a[leu]	*rac*-**2a**	99.8 ± 0.5	>99 (L)	<0.3	<0.1
a[phe]	*rac*-**4a**	99.8 ± 0.5	29.0 ± 0.7 (L)	n.d.	<0.3

Reaction conditions: substrate 10 mM, $NADP^+$ 0.5 mM, FAD 0.2 mM, 0.2 atm O_2, 2 U reductive enzyme, 1 U oxidative enzyme; enzymes applied as suspended whole lyophilized cells; 30 °C, 120 rpm, 48 h reaction time, glucose dehydrogenase 15 U, glucose >5 eq, catalase >5000 U, ammonium chloride buffer (100 mM, pH 8.5).

Cascade a[leu] produced the targeted species in excellent conversion and excellent ee.

In cascade a[phe], the targeted compound was produced but the enantiomeric enrichment was only 29% ± 0.7%, thus the conversion was not complete.

3.3.5.2 Cascade b – production of D-amino acids

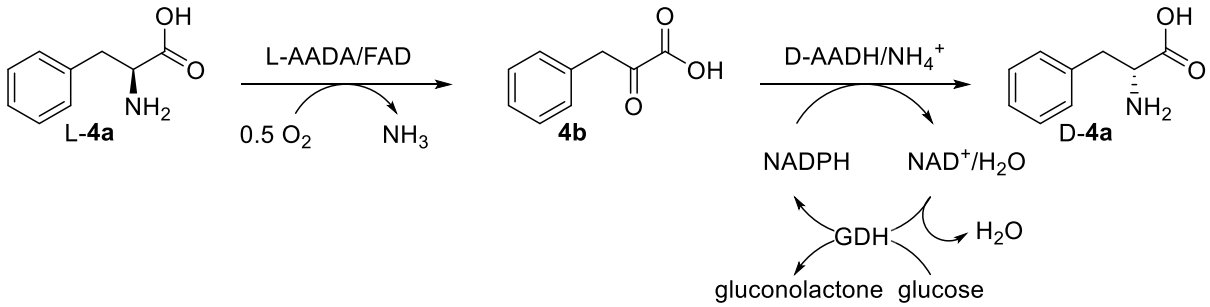

Figure 44: Reaction scheme of cascade b[phe]: conversion of L-phenylalanine (L-**4a**) to D-phenylalanine (D-**4a**), employing a L-AADA in combination with a D-AADH. The same reaction system was also used for leucine (**2a**, b[leu]).

Cascade b was designed to produce D-amino acids from the respective L-amino acids.

The enzymes, that were selected for the respective substrate are listed in Table 23.

Table 23: Selection of enzymes for cascade b[leu] and b[phe].

Cascade	Dehydrogenase	Deaminase
b[leu]	*meso*-D-Aminopimelate dehydrogenase (variant B: D94A-Q154L-D158G-T173I-R199M-H249N) from *Ureibacillus thermosphaericus* (pEG 489)	L-Amino acid deaminase from *Proteus myxofaciens* (pEG 219)
b[phe]	*meso*-D-Aminopimelate dehydrogenase (variant B: D94A-Q154L-D158G-T173I-R199M-H249N) from *Ureibacillus thermosphaericus* (pEG 489)	L-Amino acid deaminase from *Proteus myxofaciens* (pEG 219)

Table 24 displays the results of cascades b[leu] and b[phe].

Table 24: Results of cascades b[leu] and b[phe]: conversion of L-amino acid (L-**2a,** L-**4a**) to D-amino acid (D-**2a**, D-**4a**).

Cascade	Substrate	Amino acid **a**		Oxo acid **b** [%]	Hydroxy acid **c** [%]
		[%]	ee [%]		
b[leu]	L-**2a**	97.9 ± 0.9	1 ± 6 (D)	<1	<2
b[phe]	L-**4a**	81 ± 4	n.d.	n.d.	19 ± 4

Reaction conditions cascade b[leu]: substrate 10 mM, $NADP^+$ 0.5 mM, FAD 0.2 mM, 0.2 atm O_2, 2 U reductive enzyme, 1 U oxidative enzyme; enzymes applied as suspended whole lyophilized cells; 30 °C, 120 rpm, 48 h reaction time, glucose dehydrogenase 15 U, glucose >5 eq, ammonium chloride buffer (100 mM, pH 8.5). Reaction conditions cascade b[phe] similar to b[leu], but 0.5 U oxidative enzyme.

In cascade b[leu], the product ee is close to zero, which means that only about half of the substrate was transformed. The reductive step seems to have worked nicely, since there is only little of the oxo acid visible. A little bit of 2-hydroxy-4-methylpentanoic acid was also produced which may be due to reductive enzymes, present in the host cells.

Since the ee of this cascade was not measured for cascade b[phe], no evaluation of the result is possible. However, assuming the ee of the desired product is >99%, there was still significant side reactivity to the production of the respective 2-hydroxy acid observable.

3.3.5.3 Cascade c – production of L-2 hydroxy acids

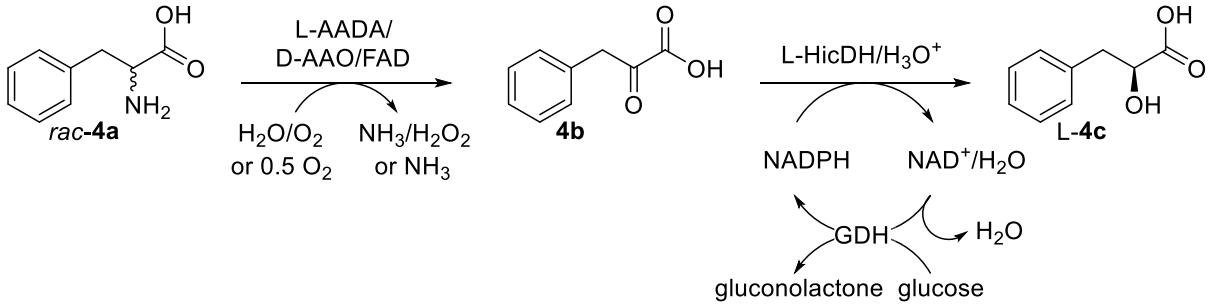

Figure 45: Reaction scheme of cascade c[Phe]: conversion of racemic phenylalanine (*rac*-**4a**) to L-2-hydroxy-3-phenypropionic acid (L-**4c**), employing a D-AAO and a L-AADA in combination with L-HicDH. The same reaction system was also used for leucine (**2a**, c[leu]).

Cascade c was designed to produce L-2-hydroxy acids from the respective racemic amino acids.

The enzymes, that were selected for the respective substrate are listed in Table 25.

Table 25: Selection of enzymes for cascade c[leu] and c[phe].

Cascade	Dehydrogenase	Oxidase/deaminase
c[leu]	L-2-Hydroxyisocaproic acid dehydrogenase from *Lactobacillus confuses* (pEG 220)	D-amino acid oxidase (wild type) from *Rhodotorula gracilis* (pEG 481) and L-Amino acid deaminase from *Proteus myxofaciens* (pEG 219)
c[phe]	L-2-Hydroxyisocaproic acid dehydrogenase from *Lactobacillus confuses* (pEG 220)	D-amino acid oxidase (wild type) from *Rhodotorula gracilis* (pEG 481) and L-Amino acid deaminase from *Proteus myxofaciens* (pEG 219)

Table 26 displays the results of cascades c[leu] and c[phe].

Table 26: Results of cascades c[leu] and c[phe]: conversion of *rac*-amino acid (*rac*-**2a,** *rac*-**4a**) to L-2-hydroxy acid (L-**2c**, L-**4c**).

Cascade	Substrate	Amino acid **a** [%]	Oxo acid **b** [%]	Hydroxy acid **c**	
				[%]	ee [%]
c[leu]	*rac*-**2a**	<2	n.d.	98.7 ± 0.5	>99 (L)
c[phe]	*rac*-**4a**	21 ± 7	n.d.	79 ± 7	>99 (L)

Reaction conditions: substrate 10 mM, $NADP^+$ 0.5 mM, FAD 0.2 mM, 0.2 atm O_2, 2 U reductive enzyme, 1 U oxidative enzyme; enzymes applied as suspended whole lyophilized cells; 30 °C, 120 rpm, 48 h reaction time, glucose dehydrogenase 15 U, glucose >5 eq, catalase >5000 U, potassium phosphate buffer (100 mM, pH 7.0).

In cascade c[leu], the targeted compound was produced with excellent conversion and excellent ee.

Cascade c[phe] produced the targeted species in excellent ee and 80% conversion.

3.3.5.4 Cascade d – production of D-2-hydroxy acids

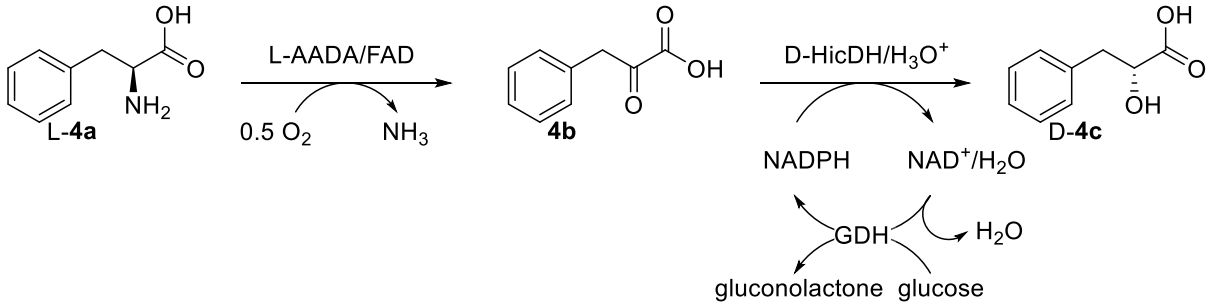

Figure 46: Reaction scheme of cascade d[Phe]: conversion of L-phenylalanine (L-**4a**) to D-2-hydroxy-3-phenylpropionic acid (D-**4c**), employing a L-AADA in combination with D-HicDH. The same reaction system was also used for leucine (**2a**, d[leu]).

Cascade d was designed to produce D-2-hydroxy acids from the respective L-amino acids.

The enzymes, that were selected for the respective substrate are listed in Table 27.

Table 27: Selection of enzymes for cascade d[leu] and d[phe].

Cascade	Dehydrogenase	Deaminase
d[leu]	D-2-Hydroxyisocaproic acid dehydrogenase from *Lactobacillus paracasei* (pEG 221)	L-Amino acid deaminase from *Proteus myxofaciens* (pEG 219)
d[phe]	D-2-Hydroxyisocaproic acid dehydrogenase from *Lactobacillus paracasei* (pEG 221)	L-Amino acid deaminase from *Proteus myxofaciens* (pEG 219)

Table 28Table 28 displays the results of cascades d[leu] and d[phe].

Table 28: Results of cascades d[leu] and d[phe]: conversion of L-amino acid (L-**2a,** L-**4a**) to D-2-hydroxy acid (D-**2c**, D-**4c**).

Cascade	Substrate	Amino acid **a** [%]	Oxo acid **b** [%]	Hydroxy acid **c**	
				[%]	ee [%]
d[leu]	L-**2a**	2.7 ± 0.5	n.d.	97.3 ± 0.5	>99 (D)
d[phe]	L-**4a**	2.7 ± 0.5	<0.2	96.4 ± 0.5	>99 (D)

Reaction conditions: substrate 10 mM, $NADP^+$ 0.5 mM, FAD 0.2 mM, 0.2 atm O_2, 2 U reductive enzyme, 1 U oxidative enzyme; enzymes applied as suspended whole lyophilized cells; 30 °C, 120 rpm, 48 h reaction time, glucose dehydrogenase 15 U, glucose >5 eq, potassium phosphate buffer (100 mM, pH 7.0).

In both cascades d[leu] and d[phe], the targeted compound was produced with excellent conversion and excellent ee.

3.3.5.5 Evaluation of the cascade reactions

Based the results of the concentration measurements, the cascade reactions appear promising: most of them deliver the desired amino- or hydroxy acid as major product and oxo acids were measured to be in very low concentrations, if found at all. Cascade b[leu] did not run to completion and needs further investigation. Cascade b[phe] cannot be evaluated, since the ee was not measured and significant side reactivity to the 2-hydroxy acid was observed. Both experiments need to be repeated. The side reactivity may be avoided, when purified enzymes are used.

Concluding, a proof of concept was achieved, demonstrating the systems' modularity. By combining different enzymes, product- and stereoselectivity can be easily switched. To drive the reaction to completion, the last step of the cascade should be downhill, which is achieved by cofactor regeneration and in the case of amino acid dehydrogenases through excess of ammonium ions and also the increased pH, favouring the reductive direction of the dehydrogenase. The dehydrogenase defines the buffer-system, since amino acid dehydrogenases need ammonium ions.

The cascades were purposefully designed in a way that would allow coupling to the photosystem of *Synechocystis* bacterium, which would allow a theoretically nearly absolute atom efficiency (Figure 47).

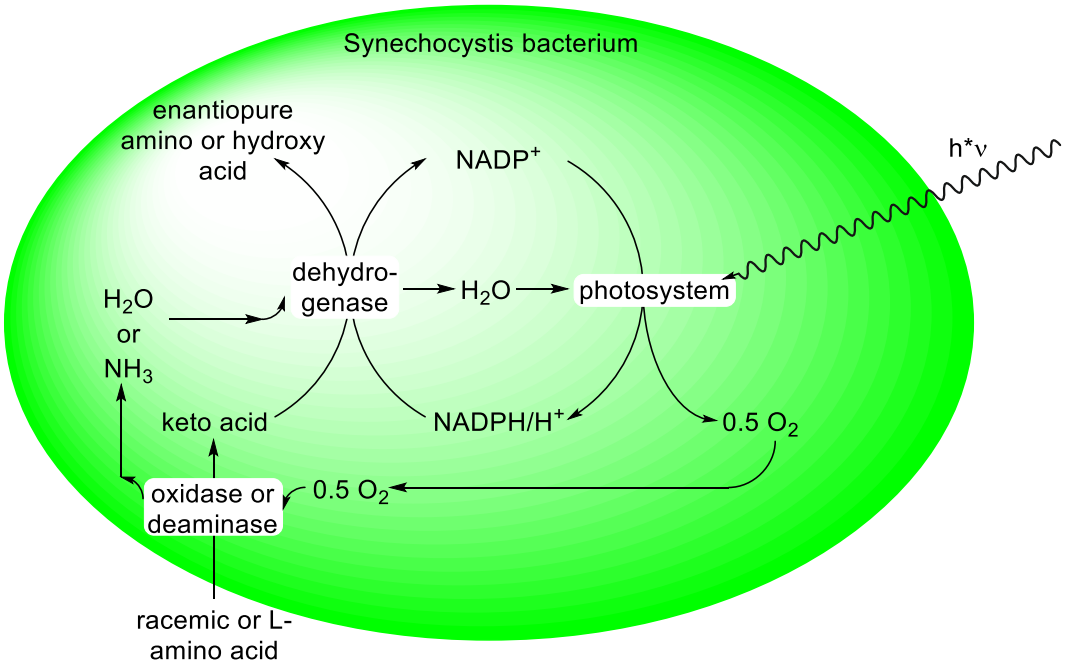

Figure 47: Theoretically total atom efficiency in the coupled cascade reaction.

3.5 Development of LED marbles

To enable photosynthesis in cyanobacteria, light is required. From a green chemist's point of view, the sun represents the ideal photon-source. Not only is it providing light, free of charge but it is also with high intensity and a broad spectrum. Thus, the sun's light provides all wavelengths from UV to IR. From a researcher's and also from industry's point of view, there are important drawbacks in the use of sunlight. Firstly, it is not constant over time. For research purposes, this represents a major disadvantage because tight control of the amount of light in the experimental setup is a prerequisite for its optimization. For example, one major goal in optimizing such a system is to maximize the product-output per light-input. In addition, living photosynthetic organisms optimize their antenna systems towards a certain spectrum during their life-span.[151] This implies that any changes in the light source would decrease the efficiency of the photosystem below its genetically defined maximum. Secondly, sunlight is not provided in a way, securing any short-term security of supply.

These facts explain why artificial illumination of *cyanobacteria* is preferred. Since the used cyanobacteria are employed as an aqueous suspension, an electric, constant and dense light source with a spectrum, optimized for cyanobacteria, is desired. This light source should evenly distribute its energy throughout the cell suspension with as little loss as possible. Also, the amount of energy, absorbed by the solution has to be known and, for research purposes, a high degree of parallelization should be possible.

There are not many photoreactors available on the market, meeting these requirements and compatible with living organisms. For this reason, a photoreactor, using an illuminated rack for small glass vials, placeable into a tempered shaker was developed in our group. This reactor provides a high degree of control and parallelization but no possibility for scaleup. Thus, the decision to develop a more universal approach to bring light into any reaction vessel was made.

Battery powered LED marbles were built. These devices not only enable easy scaleup with basically no limit and control over the amount of energy that is introduced into the solution, they also represent an internal illumination device. Internal illumination makes it possible to avoid the loss of energy by scattering or absorption when the light passes the wall of the reaction vessel. Furthermore, for statistical reasons, an even distribution of energy into the solution should be possible with an increasing number of marbles. Last but not least, the LED marbles are designed in a way that opens their field of

application, for example as light source for other chemical reactions or in other types of reactors (e.g. tubular ones). The LED marbles use is not restricted by the shape of the reactor and they can be used in any existing reaction system. Further reduction of the marble's diameter is planned as well as a change of material to polyethylene. This will lead to even more possibilities for application. A smaller diameter will not only make the application more convenient but also will allow the use of a higher number of light sources per reaction vessel. Avoiding metal as material for the marble's body will decrease weight and increase chemical resistance. Concluding, further improvement will lead to a convenient, broad field of application, for use in research as well as in industry.

The LED-marble prototypes were constructed in SolidWorks with the aid of Armesca ProCon GmbH. The two parts of the casing's main body were shaped with a CNC-mill from solid aluminium (diameter: 2.5 cm) at the university's workshop and the transparent lenses were ordered from i.materialise.com, where they were sintered from transparent, epoxy-like material (stereolithography). Seals were crafted from thin Teflon plates. Two lithium button cell batteries (3 V, 125 mAh, 16.0 mm × 3.2 mm) were used to power two LEDs (NHSW046A, 2.9 V, 5 mA, 270 mcd, for qnd spectrum see Figure 48) per LED-marble. The required voltage was adjusted, using an appropriate electrical resistance. Assembly of electronic parts into the aluminium body was done at the workshop of Pascal Poschenrieder.

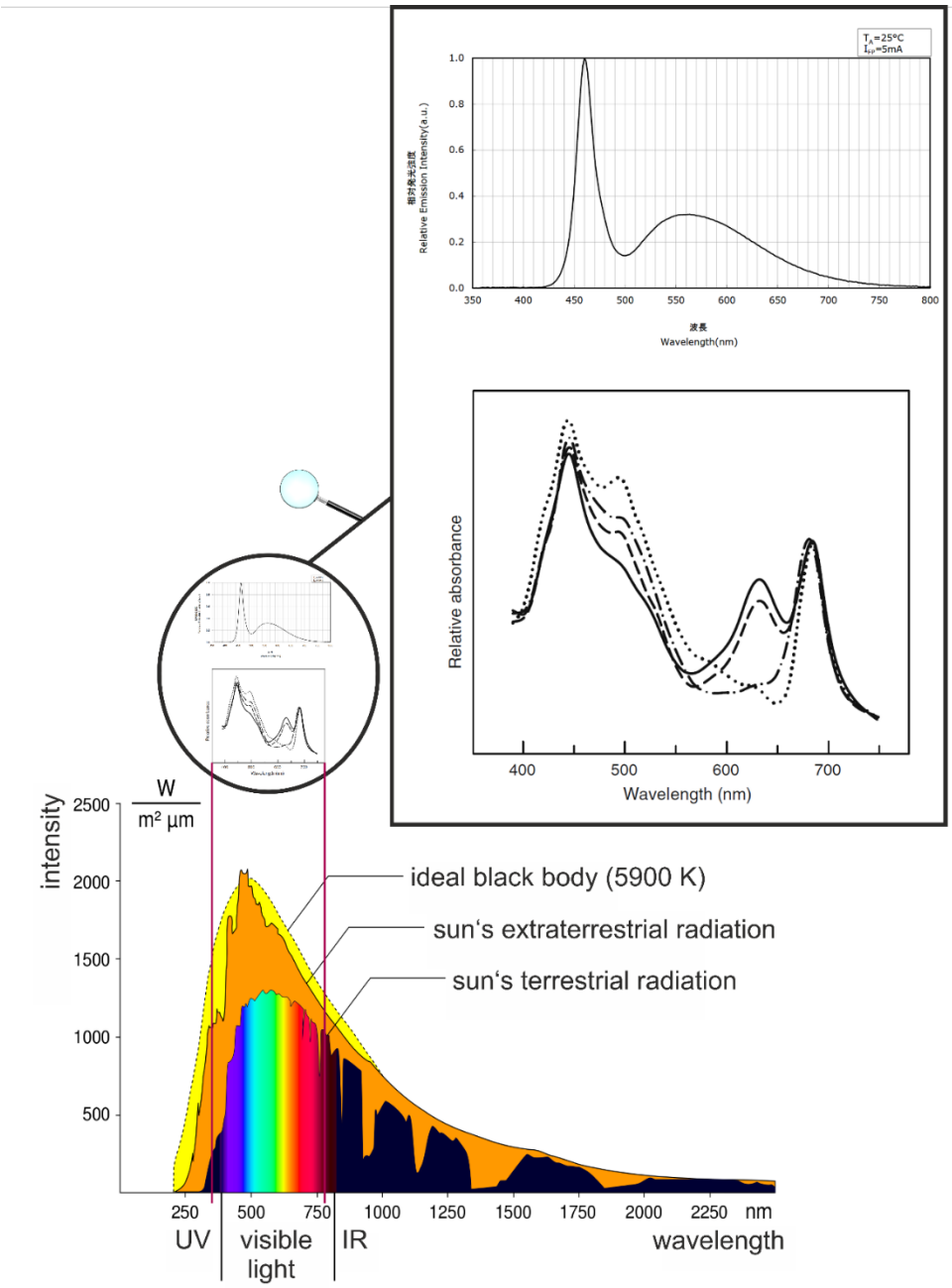

Figure 48: top: LED emission spectrum[152]; middle: *Synechocystis sp.* PCC 6803 absorption spectrum, solid line: wild type[151]; bottom: emission spectrum of the sun.[153]

The LED-marbles were tested with living *Synechocystis* cyanobacteria and after two days of incubation, (80 rpm, 25 °C) neither visible weakening of the marble's light was apparent, nor significant cell bleaching was detected at the biophotometer.

Figure 49: LED-marble in action.

For further proof of concept, an assay for continuous measurement of the oxygen production or determination of metabolite concentration is going to be developed and applied.

4 Experimental

4.1 Enzyme sources

The DAAO from porcine kidney is commercially available and were obtained from Sigma Aldrich. GDH001 and PRM are available in-house. Catalase from *Micrococcus lysodeikticus* is commercially available and was obtained from Fluka Analytics. All other used enzymes are available in the in-house plasmid database.

4.2 Chemical sources

All chemicals are available at the in-house chemical library and are from commercial sources (Sigma Aldrich, Merck, Fluka, Lancaster and Roth).

4.3 General procedures, instruments

4.3.1 Spectrophotometric activity measurements

Spectrophotometric measurements were done on a Spectra Max and M2 plate reader from Molecular Devices and analysed in Soft Max. 4220.0 mM^{-1} cm^{-1} was used as absorption coefficient of NAD(P)H.[154] For determination of the pathlength a single measurement utilizing the water constant was performed after the kinetic measurement. All measurements were performed in triplicates.

4.3.2 Spectrophotometric determination of cell densities of cultivations, Bradford assay

Cell densities of cell cultivations and enzyme concentrations of enzyme preparations were determined on an Eppendorf Biophotometer Plus.

4.3.3 Thin layer chromatography

TLC was carried out on pre-coated aluminium sheets (TLC Silica gel 60 F254, Merck) with detection at UV (254 nm) and/or by staining with ninhydrin solution [ninhydrin (1.5 g) and acetic acid (glacial, 3 mL) in 100 mL n-butanol] or ceric ammonium molybdate solution [phosphomolybdic acid (25 g), $Ce(SO_4)_2 \times H_2O$ (10 g), conc. H_2SO_4 (60 mL), H_2O (940 mL)].

4.3.4 Nucleus magnetic resonance spectrometry

^{1}H- and ^{13}C-NMR spectra were recorded at 20 °C on a Bruker Advance 300 NMR unit (300 MHz). Chemical shifts are given in ppm relative to the resonance of the solvent (^{1}H: $CDCl_3$ = 7.26 ppm; ^{13}C: $CDCl_3$ = 77.0 ppm). Multiplets were termed as follows: s (singlet), bs (broad singlet), d (doublet), dd (double doublet), qd (quadruple doublet), t(triplet), q (quadruplet), p (quintuplet), m (multiplet).

4.3.5 Aqueous high-performance liquid chromatography mass spectrometry

Aqueous HPLC-MS analysis was carried out on an Agilent 1260 Infinity system equipped with Agilent Q6120 quadrupole mass spectrometer using electrospray ionization (HPLC-MS).

4.3.6 Organic high-performance liquid chromatography with UV detection

Organic HPLC-UV was carried out on a Shimadzu system (DGU-20A5 degasser, LC-20AD liquid chromatograph, SIL-20AC autosampler, CBM-20A communication module, SPD-M20A diode array detector, and CTO-20AC column oven).

4.3.7 Gas chromatography with mass spectrometry

GC-MS spectra were recorded with an Agilent 7890A GC-system, equipped with an Agilent 5975C quadrupole mass-selective detector and a HP-5 MS column (30 m × 0.25 mm × 0.25 µm) using helium as carrier gas (flow = 0.5 mL min^{-1}).

4.3.8 Gas chromatography with flame ionization detector

GC-FID spectra were recorded with an Agilent 7890A GC-FID System equipped with a 7693 Autosampler and a Chirasil DexCB column (25 m × 0.32 mm × 0.25 µm).

4.3.9 Cell digestion

Cell disruption is carried out with a BRANSON Digital Sonifier.

4.3.10 General procedure for SDS-page

A small amount of the gathered cell pellets (approx. 50 mg) was suspended in wash buffer (1 mL) and ultrasonicated (amplitude 30%, 0.1 sec on, 0.5 sec off, 15 sec). After digestion all cell preparations were stored on ice. The lysate and pellet were separated

by centrifugation (5 min, 14800 rpm) and the pellet was re-dissolved in aqueous urea (500 µL, 5 M). The protein concentration was determined by a Bradford Assay on the biophotometer and the volume containing 15 µg protein was mixed with Laemmli[155] (1:1) and heated to 95 °C for 5 min before loading to the gel (100 V, MOPS buffer). SDS page was performed with Gene Script ExpressPlusTM page gels (10×8 cm, 12 wells, each 60 µL volume), using Gene Script Tris-MOPS-SDS running buffer powder for buffer preparation.

4.4 Cell cultivation

4.4.1 Cultivation of amino acid dehydrogenases, hydroxy acid dehydrogenases, amino acid oxidases and amino acid deaminases

Either Lysogeny Broth medium (LB: 5 g/L yeast extract, 5 g/L NaCl, 10 g/L tryptone)-medium or Terrific Broth medium [TB: 9/10 TB-base (24 g/L yeast extract, 5 g/L glycerol, 12 g/L tryptone) + 1/10 TB-buffer (23.1 g/L KH_2PO_4, 125.4 g/L)] was prepared and sterilized by autoclaving. An overnight culture was grown from the appropriate glycerol stock (5 µL) in LB-medium [10 mL, 30 µg kanamycin mL^{-1} (or 100 µg ampicillin mL^{-1} in case of L- and D-HicDH)] and used for the inoculation of sterile LB- or TB-medium in 1 or 2 L flasks, 400 mL or 700 mL medium containing 30 µg kanamycin mL^{-1} (or 100 µg ampicillin mL^{-1} for L- and D-HicDH), 2 L in total of each culture. The flasks were incubated at 37 °C and 120 rpm until an optical density of 0.6 to 1.2 was reached, then protein expression was induced by adding IPTG (1 mM). The culture was further incubated overnight at 20 °C, 25 °C, or 30 °C and 120 rpm.

Which conditions were used on which enzyme is displayed in Table 29.

Table 29: Cultivation conditions of the individual enzymes.

Enzyme	Medium	Temperature [°C]
L-leucine dehydrogenase (variant: D203A-I204R-D210R) from *Thermoactinomyces intermedius*	LB	30
L-glutamate dehydrogenase (variant F18: K92A-A166G-V377A) from *E. coli*	LB	30
D-amino acid dehydrogenase (variant B: D94A-Q154L-D158G-T173I-R199M-H249N) from *Ureibacillus thermosphaericus*	LB	30
YiaE (wild type) from *E. coli*	LB	20
D-amino acid dehydrogenase (variant: H227V) from *Symbiobacterium thermophilum*	LB	
L-2-hydroxyisocaproic acid dehydrogenase (wild type) from *Lactobacillus confuses*	LB	25
D-2-hydroxyisocaproic acid dehydrogenase (wild type) from *Lactobacillus paracasei*	LB	25
L-amino acid deaminase from *Proteus myxofaciens*	LB	30
membrane bound, dye-linked D-amino acid deaminase “dadA” (wild type) from *Pseudomonas aeruginosa*	LB	30
D-amino acid oxidase (wild type) from *Rhodotorula gracilis*	LB	30
L-lactate dehydrogenase (variant: I37K-D38S-F16Q-C81S-N85R) from *Bacillus stearothermophilus*	TB	20
D-2-hydroxy acid dehydrogenase (wild type) from *Haloferax mediterranei*	TB	20
soluble and dye-linked D-amino acid deaminase “dauA” from *Pseudomonas aeruginosa* PAO1	TB	20
D-amino acid oxidase (variant: M213G) from *Rhodotorula gracilis*	TB	20
D-amino acid oxidase from *Trigonopsis variabilis*	TB	20

To harvest the cells, the culture was centrifuged (4000 rpm, 20 min, 4 °C), the cell pellet was resuspended in wash buffer (1 g cells per 10 mL phosphate buffer, pH 7) and then centrifuged again under the same conditions. After analysis on SDS-page according to the general procedure, the washed cell pellet was resuspended in a small amount of the wash buffer (phosphate buffer, pH 7), shock frozen in a bath of liquid nitrogen and lyophilized.

4.5 Synthesis

4.5.1 Synthesis of 3-acetylphenyl ethyl(methyl)carbamate (**6a**)

Sodium hydride (60% in mineral oil, 405 mg, 10.1 mmol, 5.9 eq.) was added to a dry and inert 250 mL round bottom flask and washed with pentane (abs., 2 × 20 mL). THF (abs., 80 mL) and 3-hydroxyacetophenone (232 mg, 1.71 mmol) in THF (abs., 20 mL) were added to the solution. A solution of *N*-ethyl-*N*-methylcarbamoyl chloride (297 mg, 2.44 mmol, 1.4 eq.) in THF (abs., 20 mL) was added to the mixture over 10 min. After 1.25 h of stirring at room temperature (21 °C), TLC indicated full conversion. A solution of sodium hydroxide (20 mL, 1 M) was added. The organic layer was separated off and the aqueous layer was extracted with ethyl acetate (3 × 20 mL). The combined organic layers were washed with a solution of sodium hydroxide (20 mL, 1 M) and dried over sodium sulfate (anhydrous). The solvent was removed under reduced pressure to give 3-acetylphenyl ethyl(methyl)carbamate (**6a**) as yellow oil (359 mg, 1.64 mmol, 96%): ^{1}H-NMR ($CDCl_3$): 7.83 - 7.80 (m, 1 H), 7.65 (bs, 1 H), 7.54 (t, 1 H, J = 7.90 Hz), 7.42 - 7.38 (m, 1 H), 3.44 (q, 1 H, J = 7.03 Hz, 1 rotamer), 3.36 - 3.29 (m, 1.5 H, 1 rotamer), 3.04 (s, 1.5 H, 1 rotamer), 2.91 (s, 1.5 H, 1 rotamer), 2.58 (s, 3 H), 1.20 (t, 1.7 H, 1 rotamer), 1.11 ppm (t, 1.6 H, 1 rotamer); ^{13}C-NMR ($CDCl_3$): 197.2, 153.4 (1 rotamer), 153.3 (1 rotamer), 151.5, 138.0, 129.6, 126.8 (1 rotamer), 125.0 (1 rotamer), 121.3, 43.5, 35.0, 33.9 (1 rotamer), 33.6 (1 rotamer), 26.9, 13.1 (1 rotamer), 12.3 ppm (1 rotamer).

4.6 Biotransformations

All reactions were carried out as triplicates.

4.6.1 General procedure for the enzymatic amination of **6a** with transaminases according to literature method[138]

The transaminase from *Paracoccus denitrificans* or *Vibrio fluvialis* (lyophilized whole cells, 20 mg) was rehydrated with phosphate buffer (1 mL, pH 7.04, 100 mM) containing pyridoxal-5'-phosphate (1 mM) in a 2.0 L Eppendorf tube (20 min, 30 °C, 120 rpm). Subsequently PRM (30 mg) containing D-glucose, glucose dehydrogenase, and lactate dehydrogenase, L-alanine (21 mg, 0.25 M, 5 eq) and 3-acetylphenyl ethyl(methyl)carbamate (**6a**, 12 mg, 50 mM) were added and the reaction mixture was shaken for 24 h (30 °C, 120 rpm). After incubation, saturated, aqueous K_2CO_3 was added (200 µL) and the mixture was extracted with ethyl acetate (2 × 500 µL). Denaturated enzyme was removed by centrifugation. The combined organic layers were dried over Na_2SO_4 and subjected to GC–MS-analysis.

4.6.2 Adaption of the literature procedure[138] for the enzymatic amination of **6a** with transaminases

The general procedure[138] was applied with 3-acetylphenyl ethyl(methyl)carbamate (**6a**) as substrate with the following alterations (five reactions in total).

- General procedure with the transaminase from *Paracoccus denitrificans*
- General procedure with the transaminase from *Vibrio fluvialis*
- General procedure with twice the amount of the transaminase from *Paracoccus denitrificans* (40 mg)
- General procedure with the transaminase from *Paracoccus denitrificans* and twice the amount of PRM (60 mg)
- General procedure without transaminase

4.6.3 Enzymatic amination of **7a**-**11a with** transaminases

The general procedure was applied for five different substrates and the two enzymes *V.f.* TA or *P.d.* TA: acetophenone (**7a**), *m*-methoxyacetophenone (**8a**), *m*-hydroxyacetophenone (**9a**) with *V.f.* TA or *P.d.* TA, *m*-chloroacetophenone (**10a**), *p*-

nitroacetophenone (**11a**). A reaction with *P.d.* TA and 3-acetylphenyl ethyl(methyl)carbamate (**6a**) was added as positive blank.

4.6.4 Photometric plate reader activity measurements of amino acid dehydrogenases

A suitable amount of lyophilized cells [7.2 mg of L-leucine dehydrogenase (variant: D203A-I204R-D210R) from *Thermoactinomyces intermedius*, 6.5 mg of variant F11 L-Glutamate dehydrogenase from *E. coli*, 7.7 mg of L-glutamate dehydrogenase (variant F18: K92A-A166G-V377A) from *E. coli*, 55.5 mg of variant meso-diaminopimelate dehydrogenase (wild type) from *Corynebacterium glutamonicum*, 29.4 mg of D-amino acid dehydrogenase (variant: Q154L-D158G-T173I-R199M-H249N) from *Ureibacillus thermosphaericus*, 31.3 mg of D-amino acid dehydrogenase (variant: D94A-Q154L-D158G-T173I-R199M-H249N) from *Ureibacillus thermosphaericus*, or 30.1 mg of D-amino acid dehydrogenase (variant: H227V) from *Symbiobacterium thermophilum*] was rehydrated in ammonium chloride buffer (1.0 mL, pH 8.93, 300 mM) for 30 min at 30 °C and 120 rpm. The suspension was either directly applied as catalyst for the biotransformation (susp., suspended, lyophilized whole cells), or digested by ultrasonication (amplitude 30%, 0.1 sec on, 0.5 sec off, 2 × 15 sec, intermediate cooling on ice), separated from the insoluble fraction by centrifugation (2 × 5 min, 14800 rpm) with intermediate cooling on ice (5 min) and applied as lysate (lys., lysate of lyophilized, digested whole cells).

The enzyme solution (5 µL, susp. or lys.) and substrate (**2b** or **4b**, 4 mM in ammonium chloride buffer 300 mM, pH 8.93, 50 µL) were mixed in a 96 well plate. The reaction was initiated by the addition of the cofactor-solution (4 mM NADH or NADPH in ammonium chloride buffer 300 mM, pH 8.93, 50 µL). After 6 sec of initial shaking for mixing, the decrease in absorption of NAD(P)H (maximum at 340 nm) was followed for 30 min at 30 °C (21 sec or 16 sec intervals for YiaE from *E. coli* K12). For each enzyme a blank reaction without added substrate (instead ammonium chloride buffer, 300 mM, pH 8.93, 50 µL) was run to determine the cell background activity. Values below the average of the cell background activity plus three times its standard deviation were defined as inactive (below limit of detection). For the final value the corresponding average cell background activity was subtracted.

4.6.5 Photometric plate reader activity measurements of α-hydroxy acid dehydrogenases

The method described in 4.6.4 was applied on α-hydroxy acid dehydrogenases.

A suitable amount of lyophilized cells [2.0 mg of L-α-keto acid dehydrogenase from *Lactobacillus confuses* DSM 20196, 5.9 mg of L-lactate dehydrogenase (variant: I37K-D38S-F16Q-C81S-N85R) from *Bacillus stearothermophilus*, 2.8 mg of D-α-keto acid dehydrogenase from *Lactobacillus paracasei*, 7.6 mg of D-2-hydroxy acid dehydrogenase (wild type) from *Haloferax mediterranei*, 2.1 mg of YiaE (wild type) from *E. coli* K12 or variant D-lactate dehydrogenase (variant: D176S-I177R-F178T) from *Lactobacillus bulgaricus*] was rehydrated in potassium phosphate buffer (1.5 mL for L-α-keto acid dehydrogenase from *Lactobacillus confuses* DSM 20196 and D-α-keto acid dehydrogenase from *Lactobacillus paracasei* or 10 mL for YiaE from *E. coli* or 1,0 mL for all other preparations, pH 7.04, 100 mM) instead of ammonium chloride buffer. All reagents were prepared and applied according to 4.6.4, but potassium phosphate buffer (pH 7.04, 100 mM) was used instead of ammonium chloride buffer.

Intervals of 21 sec or 16 sec (for L-α-keto acid dehydrogenase from Lactobacillus confuses DSM 20196 and D-α-keto acid dehydrogenase from Lactobacillus paracasei) were defined between individual photometric readings.

4.6.6 HPLC based activity measurements of amino acid oxidases and amino acid deaminases

Lyophilized whole cells (L-amino acid deaminase from *Proteus myxofaciens*, membrane bound, dye-linked D-amino acid deaminase “dadA” (wild type) from *Pseudomonas aeruginosa* the D-amino acid oxidase (wild type) from *Rhodotorula gracilis*, soluble and dye-linked D-amino acid deaminase “dauA” from *Pseudomonas aeruginosa* PAO1, D-amino acid oxidase (variant: M213G) from *Rhodotorula gracilis*, the D-amino acid oxidase from *Trigonopsis variabilis*, and the commercial (Sigma) D-amino acid oxidase from porcine kidney), were rehydrated in potassium phosphate buffer (2 mL, pH 7.00, 100 mM) for 30 min at 30 °C and 120 rpm. Racemic leucine (*rac*-**2a**) or racemic phenylalanine (*rac*-**4a**) were dissolved in potassium phosphate buffer (15 mL, pH 7.00, 100 mM) and bubbled with oxygen for 10 min at rt to saturate the buffer with oxygen. The oxidation reaction was performed in open 2 mL Eppendorf vials at 30 °C, 300 rpm in a benchtop shaker. To start the reaction, the oxygenated

solution of racemic leucine or racemic phenylalanine (*rac*-**2a** or *rac*-**4a** 900 µL, 11.1 mM) was added to the cell suspension (100 µL). To quench the reaction, aqueous HCl (100 µL, 2 M) was added after 5, 30, 60, 90 or 180 sec. All reactions were performed as triplicates. The quenched reaction mixtures were saturated with sodium chloride and extracted with isopropanol (2 × 400 µL, 250 + 400 µL collected as organic phase). Part of the isopropanol phase (100 µL) was added to heptane (900 µL, 0.1% trifluoracetic acid), dried with sodium sulphate (anhydrous) and analysed on HPLC/UV.

4.6.7 Conversion after four hours with amino acid oxidases and amino acid deaminases

A suitable amount of lyophilized cells (142.7 mg soluble, dye-linked D-amino acid deaminase “dauA” (wild type) from *Pseudomonas aeruginosa* PAO1, 137.1 mg membrane bound, dye-linked D-amino acid deaminase “dadA” (wild type) from *Pseudomonas aeruginosa*, 91.1 mg D-amino acid oxidase (wild type) from *Rhodotorula gracilis*, 137.9 mg D-amino acid oxidase (wild type) from *Trigonopsis variabilis*, 112.4 mg L-amino acid deaminase from *Proteus myxofaciens*, 6.1 mg D-amino acid oxidase from porcine kidney or 140.9 mg empty *E. coli* BL21 DE3) was rehydrated in potassium phosphate buffer (3.5 mL, pH 7.00, 100 mM). A solution of racemic phenylalanine (*rac*-**4a,** 49.2 mg, 15 mL, 19.9 mM) and FAD (5.3 mg, 0.4 mM) in potassium phosphate buffer (pH 7.00, 100 mM) was bubbled with oxygen for 10 min at 30 °C. A solution of racemic leucine (*rac*-**2a**, 40.0 mg, 15 mL, 20.3 mM) and FAD (4.9 mg, 0.4 mM) in potassium phosphate buffer (pH 7.00, 100 mM) was bubbled with oxygen for 10 min at 30 °C. The reaction was performed in open 2 mL Eppendorf vials at 30 °C, 120 rpm. To start the reaction, the solution of the appropriate substrate (500 µL) was added to the cell suspension (500 µL). After 4 h 30 min incubation in the open vials, evaporation was compensated by filling up the reaction mixture to 1 mL with dest. water. Part of the reaction mixture (100 µL) was added to the eluent (900 µL, 50% acetonitrile, 50% water, 0.1% formic acid), centrifuged (1400 rpm, 10 min) and applied to HPLC/MS. The remaining part (900 µL) was quenched with aqueous HCl (100 µL, 2 M). The acidified reaction mixtures were saturated with sodium chloride and extracted with isopropanol (2 × 400 µL, 250 + 400 µL collected as organic phase). Part of the isopropanol phase (100 µL) was added to heptane (900 µL, 0.1% trifluoracetic acid) and dried with sodium sulphate (anhydrous). The sample was analysed on HPLC/UV.

4.6.8 Conversion after four hours with amino acid dehydrogenases

The method described in 4.6.7 was applied on amino acid dehydrogenases.

A suitable amount of lyophilized cells [20.8 mg L-leucine dehydrogenase (variant D203A-I204R-D210R) from *Thermoactinomyces intermedius*, 120.0 mg L-glutamate dehydrogenase (variant F18: K92A-A166G-V377A) from *E. coli*, 139.5 mg *meso*-D-aminopimelate dehydrogenase (variant A: Q154LD158G- T173I-R199M-H249N) from *Ureibacillus thermosphaericus*, 139.0 mg *meso*-D-aminopimelate dehydrogenase (variant B: D94AQ-154L-D158G-T173I-R199M-H249N) from *Ureibacillus thermosphaericus*] was rehydrated in ammonium chloride buffer (3.5 mL, pH 8.50, 300 mM). A solution of racemic leucine or racemic pheylpyruvic acid (**4b** 49.2 mg, 15 mL, 19.9 mM) and NADPH (141.3 mg, 24.2 mM, 1.2 eq.) in ammonium chloride buffer (pH 8.50, 300 mM) was prepared. A solution of 2-oxoisocaproic acid (**2b**, 19.2 mg, 7 mL, 21.1 mM) and NADPH (141.2 mg, 24.2 mM, 1.1 eq.) in ammonium chloride buffer (pH 8.50, 300 mM) was prepared.

Reaction, workup and analytics were performed as described in 4.6.7 except the vials were closed, thus no evaporation had to be compensated. The reaction was run for four hours.

4.6.9 Conversion after four hours with α-hydroxy acid dehydrogenases

The method described in 4.6.7 was applied on amino acid dehydrogenases.

A suitable amount of lyophilized cells (13.5 mg L-2-hydroxyisocaproic acid dehydrogenase from *Lactobacillus confuses* DSM 20196, 21.7 mg D-2-hydroxyisocaproic acid dehydrogenase from *Lactobacillus paracasei* DSM 20008, 141.0 mg YiaE from *E. coli* K12) was rehydrated in potassium phosphate buffer (3.5 mL, pH 7.00, 100 mM). A solution of phenylpyruvate (**4b**, 17.0 mg, 5 mL, 20.7 mM) and NADPH (99.7 mg, 23.9 mM, 1.2 eq.) in potassium phosphate buffer (pH 7.00, 100 mM) was prepared. A solution of 2-oxoisocaproic acid (**2b**, 13.3 mg, 5 mL, 20.4 mM) and NADPH (100.6 mg, 24.1 mM, 1.2 eq.) in potassium phosphate buffer (pH 7.00, 100 mM) was prepared.

Reaction, workup and analytics were performed as described in 4.6.7 except the vials were closed, thus no evaporation had to be compensated. The reaction was run for four hours.

4.6.10 Transformation of racemic leucine (*rac*-**2a**) to L-leucine (L-**2a**) in an enzymatic cascade

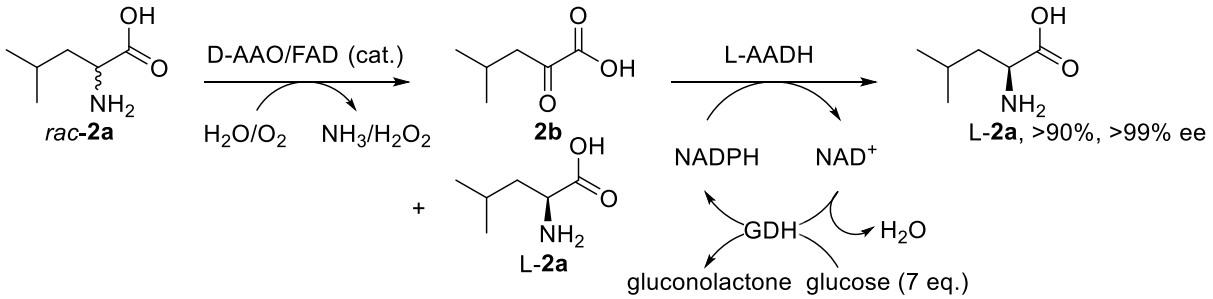

Figure 50: Cascade a[leu]: conversion of *rac*-**2a** to L-**2a**. Reaction conditions: substrate 10 mM, $NADP^+$ 0.5 mM, FAD 0.2 mM, 0.2 atm O_2, 2 U reductive enzyme, 1 U oxidative enzyme; enzymes applied as suspended whole lyophilized cells; 30 °C, 120 rpm, 48 h reaction time, glucose dehydrogenase 15 U, glucose >5 eq, catalase >5000 U, ammonium chloride buffer (100 mM, pH 8.5).

Lyophilized cells [20.5 mg, 8.0 U D-amino acid oxidase from *Rhodotorula gracilis* in *E. coli* BL21 (DE3); 10.8 mg, 18.4 U triple variant L-amino acid dehydrogenase D203A-I204R-D210R from *Thermoactinomyces intermedius* in *E. coli* BL21 (DE3) and 9.2 mg, 110 U GDH001], catalase (80 µL, >5000 U), flavin adenine dinucleotide disodium salt hydrate, (2.3 mg, 2.8 µmol) and β-nicotinamide adenine dinucleotide phosphate sodium salt hydrate (2.9 mg, 3.8 µmol) were rehydrated in ammonium chloride buffer (4.0 mL, pH 8.50, 300 mM) for 30 min at 30 °C and 120 rpm (cell-mix). *rac*-Leucine (*rac*-**2a**, 5.3 mg, 40 µmol) was dissolved in ammonium chloride buffer (2.0 mL, pH 8.50, 300 mM, substrate solution, blank). *rac*-Leucine, (4.9 mg, 18.7 mM) and D-glucose (47.5 mg, 264 µmol, 7.1 eq) were dissolved in ammonium chloride buffer (2.0 mL, pH 8.50, 300 mM, substrate solution).

The reactions were performed in 2 mL open Eppendorf vials at 30 °C, 120 rpm. The cascade was started by pipetting the cell-mix (500 µL) and the substrate mix (500 µL) into an Eppendorf vial. Blank reactions were started by pipetting the cell-mix (500 µL) and the substrate solution (500 µL) into an Eppendorf vial. After 22 h 40 min, evaporation was compensated by filling up the reaction mixture with dest. water (350 µL). After another 21 h 10 min evaporation was compensated by filling up the reaction mixture with dest. water (350 µL).

After 48 h total reaction time, the reaction mixture was filled up to 1 mL with dest. water. Part of the reaction mixture (100 µL) was added the eluent (900 µL, of 50% acetonitrile, 50% water, 0.1% formic acid), centrifuged (1400 rpm, 10 min) and applied to HPLC/MS.

4.6.11 Transformation of L-leucine (L-**2a**) to D-leucine (D-**2a**) in an enzymatic cascade

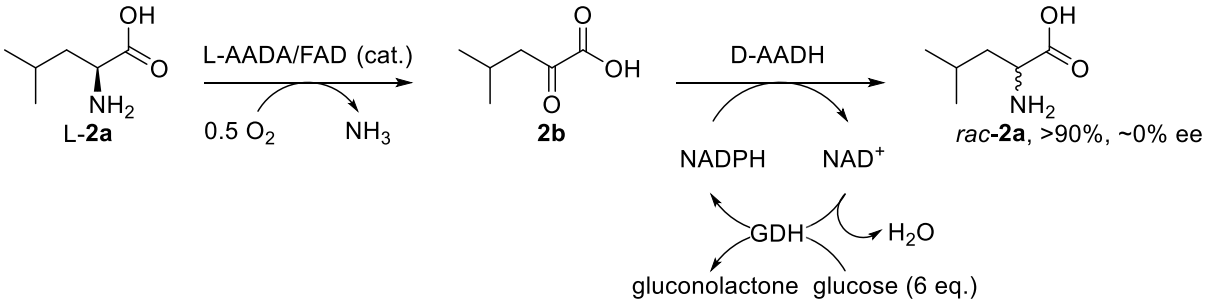

Figure 51: Cascade b[leu]: conversion of L-**2a** to D-2a. Reaction conditions: substrate 10 mM, $NADP^+$ 0.5 mM, FAD 0.2 mM, 0.2 atm O_2, 2 U reductive enzyme, 1 U oxidative enzyme; enzymes applied as suspended whole lyophilized cells; 30 °C, 120 rpm, 48 h reaction time, glucose dehydrogenase 15 U, glucose >5 eq, ammonium chloride buffer (100 mM, pH 8.5).

Lyophilized cells [22.0 mg, 6.8 U L-amino acid deaminase from *Proteus myxofaciens* in *E. coli* BL21 (DE3), 515 mg, 14.4 U D-amino acid dehydrogenase PEG207 in *E. coli* BL21 (DE3), 4.4 mg, 53 U GDH001], flavin adenine dinucleotide disodium salt hydrate (1.2 mg, 1.4 µmol) and β-nicotinamide adenine dinucleotide phosphate sodium salt hydrate (3.4 mg, 4.4 µmol) were rehydrated in ammonium chloride buffer (4.0 mL, pH 8.50, 300 mM) for 30 min at 30 °C and 120 rpm (cell-mix). L-Leucine (L-**2a**, 4.9 mg, 37 µmol) was dissolved in ammonium chloride buffer (2.0 mL, pH 8.50, 300 mM, substrate solution, blank). L-Leucine, (L-**2a**, 5.6 mg, 43 µmol) and D-glucose (44.9 mg, 249 µmol, 5.8 eq.) were dissolved in ammonium chloride buffer (2.0 mL, pH 8.50, 300 mM, substrate solution).

The reactions were performed as described in 4.6.10 and run for 48 h.

After 22 h 40 min, evaporation was compensated by filling up the reaction mixture with dest. water (350 µL). After another 21 h 10 min evaporation was compensated by filling up the reaction mixture with dest. water (350 µL).

Workup and analytics were performed as described in 4.6.10.

4.6.12 Transformation of racemic leucine (*rac*-**2a**) to L-2-hydroxy-4-methylpentanoic acid (L-**2c**) in an enzymatic cascade.

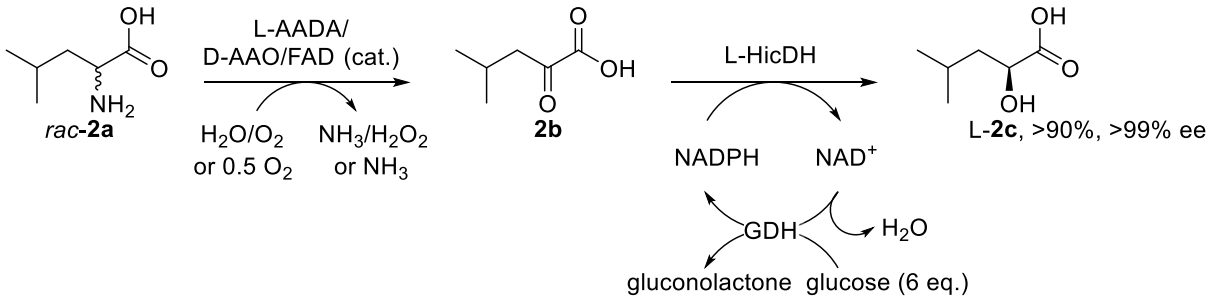

Figure 52: Cascade c[leu]: conversion of *rac*-**2a** to L-**2c**. Reaction conditions: substrate 10 mM, $NADP^+$ 0.5 mM, FAD 0.2 mM, 0.2 atm O_2, 2 U reductive enzyme, 1 U oxidative enzyme; enzymes applied as suspended whole lyophilized cells; 30 °C, 120 rpm, 48 h reaction time, glucose dehydrogenase 15 U, glucose >5 eq, catalase >5000 U, potassium phosphate buffer (100 mM, pH 7.0).

Lyophilized cells [25.8 mg, 8.0 U L-amino acid deaminase from *Proteus myxofaciens* in *E. coli* BL21 (DE3), 21.4 mg, 8.35 U D-amino acid oxidase from *Rhodotorula gracilis* in *E. coli* BL21 (DE3), 7.4 mg, 19 U L-hydroxy acid dehydrogenase from *Lactobacillus paracasei* in *E. coli* BL21 (DE3), 5.2 mg, and 62 U GDH001], catalase (80 µL, >5000 U), flavin adenine dinucleotide disodium salt hydrate, (1.9 mg, 2.3 µmol) and β-nicotinamide adenine dinucleotide phosphate sodium salt hydrate (5.0 mg, 6.5 µmol) were rehydrated in potassium phosphate buffer (4.0 mL, pH 7.00, 100 mM) for 30 min at 30 °C and 120 rpm (cell-mix). *rac*-Leucine (*rac*-**2a**, 5.2 mg, 40 µmol) was dissolved in potassium phosphate buffer (2.0 mL, pH 7.00, 100 mM, substrate solution, blank). *rac*-Leucine (*rac*-**2a**, 5.3 mg, 40 µmol) and D-glucose (43.2 mg, 240 µmol, 5.9 eq.) were dissolved in potassium phosphate buffer (2.0 mL, pH 7.00, 100 mM, substrate-mix).

The reactions were performed as described in 4.6.10 and run for 48 h.

After 22 h 40 min, evaporation was compensated by filling up the reaction mixture with dest. water (350 µL). After another 21 h 10 min evaporation was compensated by filling up the reaction mixture with dest. water (350 µL).

Workup and analytics were performed as described in 4.6.10, but the remaining reaction mixture (900 µL) was quenched with aqueous HCl (100 µL, 2 M), saturated with sodium sulphate and extracted with ethyl acetate (400 + 250 µL, 2 × 250 µL collected as organic phase). The organic phase was reduced to dryness and the

soluble portion of the residue was dissolved in dry ethyl acetate (100 µL). Methanol (10 µL) and (trimethylsilyl)diazomethane were added to the dissolved residue and then it was subjected to GC/FID.

4.6.13 Transformation of L-leucine (L-**2a**) to D-2-hydroxy-4-methylpentanoic acid (D-**2c**) in an enzymatic cascade

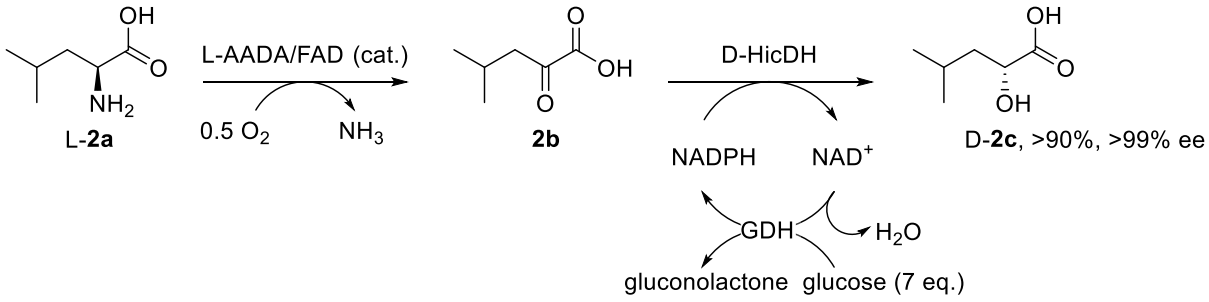

Figure 53: Cascade d[leu]: conversion of L-**2a** to D-**2c**.Reaction conditions: substrate 10 mM, $NADP^+$ 0.5 mM, FAD 0.2 mM, 0.2 atm O_2, 2 U reductive enzyme, 1 U oxidative enzyme; enzymes applied as suspended whole lyophilized cells; 30 °C, 120 rpm, 48 h reaction time, glucose dehydrogenase 15 U, glucose >5 eq, potassium phosphate buffer (100 mM, pH 7.0).

Lyophilized cells [26.2 mg, 8.1 U L-amino acid deaminase from *Proteus myxofaciens* in *E. coli* BL21 (DE3), 9.0 mg, 16 U D-hydroxy acid dehydrogenase from *Lactobacillus confuses* in *E. coli* BL21 (DE3), 9.9 mg, 119 U GDH001], flavin adenine dinucleotide disodium salt hydrate, (1.5 mg, 1.8 µmol) and β-nicotinamide adenine dinucleotide phosphate sodium salt hydrate (3.5 mg, 4.6 µmol) were rehydrated in potassium phosphate buffer (4.0 mL, pH 7.00, 100 mM) for 30 min at 30 °C and 120 rpm (cell-mix). L-Leucine (L-**2a**, 5.2 mg, 40 µmol) was dissolved in potassium phosphate buffer (2.0 mL, pH 7.00, 100 mM, substrate solution, blank). L-Leucine (L-**2a**, 5.3 mg, 40 µmol) and D-glucose (52.2 mg, 290 µmol, 7.2 eq.) were dissolved in potassium phosphate buffer (2.0 mL, pH 7.00, 100 mM, substrate-solution).

The reactions were performed as described in 4.6.10 and run for 48 h.

After 22 h 40 min, evaporation was compensated by filling up the reaction mixture with dest. water (350 µL). After another 21 h 10 min evaporation was compensated by filling up the reaction mixture with dest. water (350 µL).

Workup and analytics were performed as described in 4.6.12.

4.6.14 Transformation of racemic phenylalanine (*rac*-**4a**) to L-phenylalanine (L-**4a**) in an enzymatic cascade

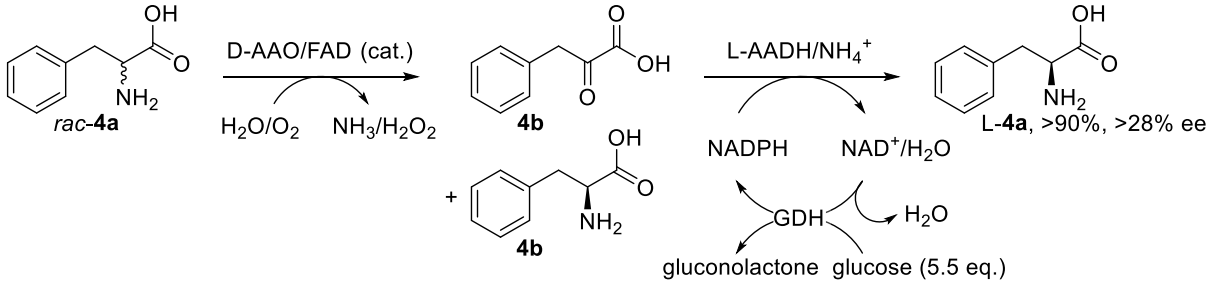

Figure 54: Cascade a[phe]: conversion of *rac*-**4a** to L-**4a**. Reaction conditions: substrate 10 mM, $NADP^+$ 0.5 mM, FAD 0.2 mM, 0.2 atm O_2, 2 U reductive enzyme, 1 U oxidative enzyme; enzymes applied as suspended whole lyophilized cells; 30 °C, 120 rpm, 48 h reaction time, glucose dehydrogenase 15 U, glucose >5 eq, catalase >5000 U, ammonium chloride buffer (100 mM, pH 8.5).

Lyophilized cells [17.0 mg, 8.8 U D-amino acid oxidase from *Rhodotorula gracilis* in *E. coli* BL21 (DE3), 10.0 mg, 16 U L-glutamate dehydrogenase variant F18 K92A-A166GV377A from *E. coli* in *E. coli* BL21 (DE3), and 4.1 mg, 49 U GDH001], catalase (80 µL, >5000 U), flavin adenine dinucleotide disodium salt hydrate, (1.2 mg, 1.4 µmol) and β-nicotinamide adenine dinucleotide phosphate sodium salt hydrate (3.5 mg, 4.6 µmol) were rehydrated in ammonium chloride buffer (4.0 mL, pH 8.50, 300 mM) for 30 min at 30 °C and 120 rpm (cell-mix). *rac*-Phenylalanine (*rac*-**4a**, 7.3 mg, 44 µmol) was dissolved in ammonium chloride buffer (2.0 mL, pH 8.50, 300 mM, substrate solution, blank). *rac*-Phenylalanine (*rac*-**4a**, 7.4 mg, 45 µmol) and D-glucose (44.7 mg, 248 µmol, 5.5 eq.) were dissolved in ammonium chloride buffer (2.0 mL, pH 8.50, 300 mM, substrate-solution).

The reactions were performed as described in 4.6.10 and run for 48 h.

After 18 h 20 min, evaporation was compensated by filling up the reaction mixture with dest. water (350 µL). After another 23 h 20 min evaporation was compensated by filling up the reaction mixture with dest. water (350 µL).

Workup and analytics were performed as described in 4.6.10, but the remaining reaction mixture (900 µL) was quenched with aqueous HCl (100 µL, 2 M), saturated with sodium sulphate and extracted with isopropanol (2 × 400 µL, 250 + 400 µL collected as organic phase). Part of the isopropanol phase (100 µL) was added to heptane (900 µL, 0.1% trifluoracetic acid) and dried with sodium sulphate (anhydrous). The sample was analysed on HPLC/UV.

4.6.15 Transformation of L-phenylalanine (L-**4a**) to D-phenylalanine (D-**4a**) in an enzymatic cascade

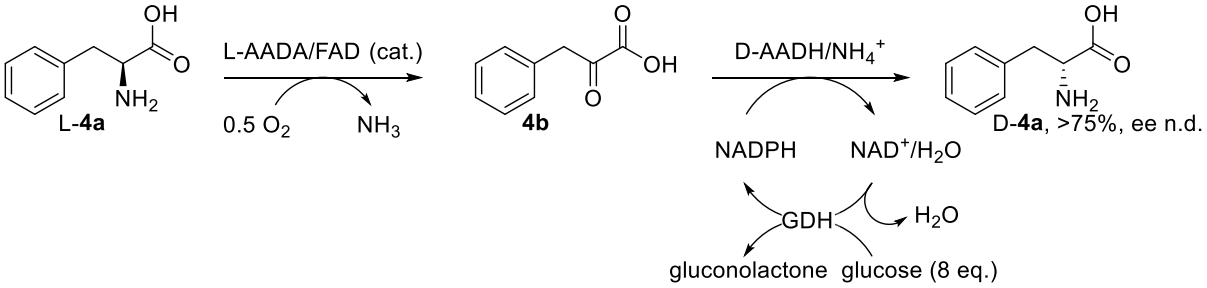

Figure 55: Cascade b[phe]: conversion of L-**4a** to D-**4a**. Reaction conditions: substrate 10 mM, $NADP^+$ 0.5 mM, FAD 0.2 mM, 0.2 atm O_2, 2 U reductive enzyme, 0.5 U oxidative enzyme; enzymes applied as suspended whole lyophilized cells; 30 °C, 120 rpm, 48 h reaction time, glucose dehydrogenase 15 U, glucose >5 eq, ammonium chloride buffer (100 mM, pH 8.5).

Lyophilized cells [104 mg, 4.3 U L-amino acid deaminase from *Proteus myxofaciens* in *E. coli* BL21 (DE3), 207 mg, 8.3 U D-amino acid dehydrogenase variant D94A-Q154L-D158GT173I-R199M-H249N from *Ureibacillus thermosphaericus* in *E. coli* BL21 (DE3), 3.0 mg, 36 U GDH001], flavin adenine dinucleotide disodium salt hydrate, (1.7 mg, 2.0 µmol) and β-nicotinamide adenine dinucleotide phosphate sodium salt hydrate (1.8 mg, 2.4 µmol) were rehydrated in ammonium chloride buffer (4.0 mL, pH 8.50, 300 mM) for 30 min at 30 °C and 120 rpm (cell-mix). L-Phenylalanine (L-**4a**, 6.8 mg, 41 µmol) was dissolved in ammonium chloride buffer (2.0 mL, pH 8.50, 300 mM, substrate solution, blank). L-Phenylalanine (L-**4a**, 7.1 mg, 43 µmol) and D-glucose (63.2 mg, 351 µmol, 8.2 eq.) were dissolved in ammonium chloride buffer (2.0 mL, pH 8.50, 300 mM, substrate solution).

The reactions were performed as described in 4.6.10 and run for 48 h.

After 18 h 20 min, evaporation was compensated by filling up the reaction mixture with dest. water (350 µL). After another 23 h 20 min evaporation was compensated by filling up the reaction mixture with dest. water (350 µL).

Workup and analytics were performed as described in 4.6.14.

4.6.16 Transformation of racemic phenylalanine (*rac*-**4a**) to L-2-hydroxy-3-phenylpropionic acid (L-**4c**)

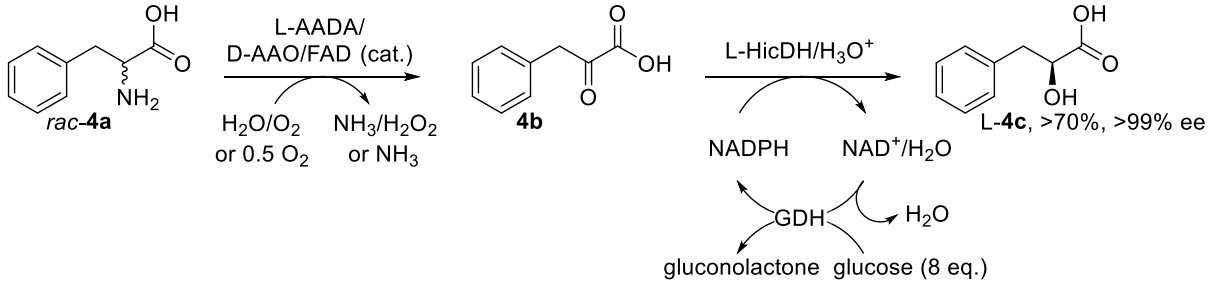

Figure 56: Cascade c[phe]: conversion of *rac*-**4a** to L-**4c**. Reaction conditions: substrate 10 mM, $NADP^+$ 0.5 mM, FAD 0.2 mM, 0.2 atm O_2, 2 U reductive enzyme, 1 U oxidative enzyme; enzymes applied as suspended whole lyophilized cells; 30 °C, 120 rpm, 48 h reaction time, glucose dehydrogenase 15 U, glucose >5 eq, catalase >5000 U, potassium phosphate buffer (100 mM, pH 7.0).

Lyophilized cells [204 mg, 8.3 U L-amino acid deaminase from *Proteus myxofaciens* in *E. coli* BL21 (DE3), 18.4 mg, 9.6 U D-amino acid oxidase from *Rhodotorula gracilis* in *E. coli* BL21 (DE3), 4.1 mg, 19 U L-hydroxy acid dehydrogenase from *Lactobacillus paracasei* in *E. coli* BL21 (DE3), 2.7 mg, 32 U GDH001], catalase (80 µL, >5000 U), flavin adenine dinucleotide disodium salt hydrate, (1.1 mg, 1.3 µmol) and β-nicotinamide adenine dinucleotide phosphate sodium salt hydrate (3.5 mg, 4.6 µmol) were rehydrated in potassium phosphate buffer (4.0 mL, pH 7.00, 100 mM) for 30 min at 30 °C and 120 rpm (cell-mix). *rac*-Phenylalanine (*rac*-**4a**, 6.9 mg, 42 µmol) was dissolved in potassium phosphate buffer (2.0 mL, pH 7.00, 100 mM, substrate solution, blank). *rac*-Phenylalanine (*rac*-**4a**, 6.1 mg, 37 µmol) and D-glucose (51.9 mg, 288 µmol, 7.8 eq.) were dissolved in potassium phosphate buffer (2.0 mL, pH 7.00, 100 mM, substrate solution).

The reactions were performed as described in 4.6.10 and run for 48 h.

After 18 h 20 min, evaporation was compensated by filling up the reaction mixture with dest. water (350 µL). After another 23 h 20 min evaporation was compensated by filling up the reaction mixture with dest. water (350 µL).

Workup and analytics were performed as described in 4.6.14.

4.6.17 Transformation of L-phenylalanine (L-**4a**) to D-2-hydroxy-3-phenylpropionic acid (D-**4c**) in an enzymatic cascade

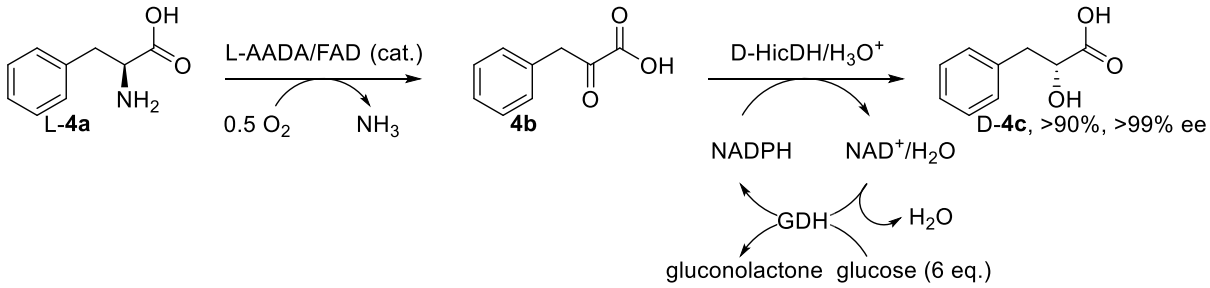

Figure 57: Cascade d[phe]: conversion of L-**4a** to D-**4c**. Reaction conditions: substrate 10 mM, $NADP^+$ 0.5 mM, FAD 0.2 mM, 0.2 atm O_2, 2 U reductive enzyme, 1 U oxidative enzyme; enzymes applied as suspended whole lyophilized cells; 30 °C, 120 rpm, 48 h reaction time, glucose dehydrogenase 15 U, glucose >5 eq, potassium phosphate buffer (100 mM, pH 7.0).

Lyophilized cells [201 mg, 8.2 U L-amino acid deaminase from *Proteus myxofaciens* in *E. coli* BL21 (DE3), 2.6 mg, 33 U D-hydroxy acid dehydrogenase from *Lactobacillus confuses* in *E. coli* BL21 (DE3), 3.2 mg, 38 U GDH001], flavin adenine dinucleotide disodium salt hydrate, (1.1 mg, 1.3 µmol) and β-nicotinamide adenine dinucleotide phosphate sodium salt hydrate (3.2 mg, 4.2 µmol) were rehydrated in potassium phosphate buffer (4.0 mL, pH 7.00, 100 mM) for 30 min at 30 °C and 120 rpm (cell-mix). L-Phenylalanine (L-**4a**, 7.0 mg, 42 µmol) was dissolved in potassium phosphate buffer (2.0 mL, pH 7.00, 100 mM, substrate solution, blank). L-Phenylalanine (L-**4a**, 7.1 mg, 43 µmol) and D-glucose (48.0 mg, 266 µmol, 6.2 eq.) were dissolved in potassium phosphate buffer (2.0 mL, pH 7.00, 100 mM, substrate solution).

The reactions were performed as described in 4.6.10 and run for 48 h.

After 18 h 20 min, evaporation was compensated by filling up the reaction mixture with dest. water (350 µL). After another 23 h 20 min evaporation was compensated by filling up the reaction mixture with dest. water (350 µL).

Workup and analytics were performed as described in 4.6.14.

4.7 Analytics

4.7.1 Concentrations and conversions

4.7.1.1 HPLC/MS measurement of leucine (**2a**), 4-methyl-2-oxopentanoic acid (**2b**), 2-hydroxy-4-methylpentanoic acid (**2c**), phenylalanine (**4a**) and phenyllactic acid (**4c**) concentrations

HPLC/MS (EI, Agilent 1260 Infinity, Agilent Q6120 quadrupole MS, Phenomenex Kinetex C18 column 50 × 4.6 mm, particle size 2.6 µm, pore size 100 nm, method: starting from 100% water with 0.1% formic acid, going to 55% water with 0.1% formic acid and 45% acetonitrile with 0.1% formic acid over six minutes, going to 100% acetonitrile with 0.1% formic acid over one minute, going back to 100% water with 0.1% acetonitrile over one minute, holding at water with 0.1% acetonitrile for two minutes, 30°C, 1 mL flow, 10 min t_{ret}(leucine, **2a**) = 1.30 min, t_{ret}(4-methyl-2-oxopentanoic acid, **2b**) = 3.29 min, t_{ret}(2-hydroxy-4-methylpentanoic acid, **2c**) = 3.49 min, t_{ret}(phenylalanine, **4a**) = 2.29 min, t_{ret}(phenyllactic acid, **4c**) = 4.21 min.

Detection at M^+ = 132 u (leucine, **2a**), M^- = 129 u (4-methyl-2-oxopentanoic acid, **2b**), M^- = 131 u (2-hydroxy-4-methylpentanoic acid, **2c**), M^+ = 166 u (phenylalanine, **4a**), M^- = 165 u (phenyllactic acid, **4c**).

4.7.1.2 HPLC/UV measurement of phenylpyruvic acid (**4b**) concentration

HPLC/UV [Shimadzu system (DGU-20A5 degasser, LC-20AD liquid chromatograph, SIL-20AC autosampler, CBM-20A communication module, SPD-M20A diode array detector, and CTO-20AC column oven, Chiralpak IA-column (amylose tris(3,5-dimethylphenylcarbamate), immobilized on 3 µm silica-gel, 250 × 4.6 mm), method: 90% n-heptane, 10% *iso*-propanol, 0.1% formic acid, 15 min, 30°C, 1 mL flow]: t_{ret}(phenylpyruvic acid, **4b**) = 5.02 min.

Detection at 290 nm.

4.7.1.3 GC/MS measurement of 1-phenylethane-1-amine derivates (**6b**-**11b**) conversions

GC-MS (EI, Agilent J&W GC HP5-MS column, 30 m, i.d. 0.250 mm, film 0.25 µm, in-house method ACHIRAL-MSD: 100 °C for 0.5 min to 300 °C, 10 °C min^{-1}): t_{ret}(3-acetylphenyl ethyl(methyl)carbamate, **6a**) = 12.12 min, t_{ret}(3-(1-aminoethyl)phenyl ethyl(methyl)carbamate, **6b**) = 11.99 min, t_{ret}(acetophenone, **7a**) = 3.74 min, t_{ret}(1-amino-1-phenylethane, **7b**) = 3.55 min, t_{ret}(*m*-methoxyacetophenone, **8a**) = 6.25 min,

t_{ret}(1-amino-1-(1-(3-methoxyphenyl)ethan-1-amine, **8b**) = 6.11 min, t_{ret}(*m*-hydroxyacetophenone, **9a**) = 7.25 min, t_{ret}(3-(1-aminoethyl)phenol, **9b**) = 6.77 min, t_{ret}(*m*-chloroacetophenone) = 5.44 min, t_{ret}(1-(3-chlorophenyl)ethan-1-amine) = 5.56 min, t_{ret}(*p*-nitroacetophenone) = 8.03 min, t_{ret}(1-(4-nitrophenyl)ethan-1-amine) = 8.87 min, t_{ret}(3-acetylphenyl ethyl(methyl)carbamate) = 12.12 min, t_{ret}(3-(1-aminoethyl)phenyl ethyl(methyl)carbamate) = 11.99 min.

4.7.2 Enantiomeric excess

4.7.2.1 Determination of the enantiomeric excess of leucine (**2a**) and phenylalanine (**4a**) on HPLC/MS

HPLC/MS (EI, Agilent 1260 Infinity, Agilent Q6120 quadrupole MS, Astec Chirobiotic T column, 150 × 4.6 mm, particle size 5 µm, method: isocratic, 20% water, 80% acetonitrile, 0.1% formic acid, 1mL × min^{-1}, 10 min, 30 °C): t_{ret}(L-leucine, L-**2a**) = 5.38 min, t_{ret}(D-leucine, D-**2a**) = 5.66 min, t_{ret}(L-phenylalanine, L-**4a**) = 5.36 min, t_{ret}(D-phenylalanine, D-**4a**) = 5.66 min.

Detection at M^+ = 132 u (leucine, **2a**) and M^+ = 166 u (phenylalanine, **4a**).

4.7.2.2 Determination of the enantiomeric excess of 2-hydroxy-4-methylpentanoic acid (**4c**) on HPLC/UV

HPLC/UV [Shimadzu system (DGU-20A5 degasser, LC-20AD liquid chromatograph, SIL-20AC autosampler, CBM-20A communication module, SPD-M20A diode array detector, and CTO-20AC column oven, Chiralpak IA-column (amylose tris(3,5-dimethylphenylcarbamate), immobilized on 3 µm silica-gel, 250 × 4.6 mm), method: 90% n-heptane, 10% *iso*-propanol, 0.1% formic acid, 15 min, 30°C, 1 mL flow]: t_{ret}(phenylpyruvic acid, L-**4c**) = 5.02 min, t_{ret}(phenylpyruvic acid, L-**4c**) = 5.02 min.

4.7.2.3 Determination of the enantiomeric excess of 2-hydroxy-4-methylpentanoic acid (**2c**) on GC/FID

GC/FID (Agilent 7890A GC-FID System, 7693 Autosampler, Agilent J&W CPChirasil DexCB column (25 m × 0,32 mm × 0,25 µm), method: 60 °C for 2.0 min to 110 °C, 3 °C min^{-1} to 200 °C, 10 °C min^{-1}): t_{ret}(S-2-hydroxy-4-methylpentanoic acid, S-**2c**) = 12.81 min min, t_{ret}(R-2-hydroxy-4-methylpentanoic acid, R-**2c**) = 12.21 min.

5 Appendix

5.1 References

[1] Köninger, K.; Gómez Baraibar, Á.; Mügge, C.; Paul, C. E.; Hollmann, F.; Nowaczyk, M. M.; Kourist, R., *Angew. Chem. Int. Ed.* **2016**, *55*, 5582–5585.

[2] Kroutil, W.; Rueping, M., *ACS Catal.* **2014**, *4*, 2086–2087.

[3] Oger, N.; Dhalluin, M.; Le Grognec, E.; Felpin, F. X., *Org. Process Res. Dev.* **2014**, *18*, 1786–1801.

[4] Schrittwieser, J. H.; Velikogne, S.; Hall, M.; Kroutil, W., *Chem. Rev.* **2018**, *118*, 270–348.

[5] Schrittwieser, J. H.; Sattler, J.; Resch, V.; Mutti, F. G.; Kroutil, W., *Curr. Opin. Chem. Biol.* **2011**, *15*, 249–256.

[6] Sperl, J. M.; Sieber, V., *ACS Catal.* **2018**, *8*, 2385–2396.

[7] Gore, M. G., *Int. J. Biochem.* **1981**, *13*, 879–886.

[8] Stillman, T. J.; Baker, P. J.; Britton, K. L.; Rice, D. W., *J. Mol. Biol* **1993**, *234*, 1131–1139.

[9] Prakash, P.; Punekar, N. S.; Bhaumik, P., *J. Biol. Chem.* **2018**, *293*, 6241–6258.

[10] Li, H.; Liao, J. C., *ACS Synth. Biol.* **2014**, *3*, 13–20.

[11] Plaitakis, A.; Zaganas, I., *J. Neurosci. Res.* **2001**, *66*, 899–908.

[12] Rossmann, M. G.; Moras, D.; Olsen, K. W., *Nature* **1974**, *250*, 194–199.

[13] Yu, L.; Golden, E.; Chen, N.; Zhao, Y.; Vrielink, A.; Karton, A., *Sci. Rep.* **2017**, *7*, 1–13.

[14] Baker, P. J.; Turnbull, A. P.; Sedelnikova, S. E.; Stillman, T. J.; Rice, D. W., *Structure* **1995**, *3*, 693–705.

[15] Ross, N. T.; Katt, W. P.; Hamilton, A. D., *Philos. T. R. Soc. A* **2010**, *368*, 989–1008.

[16] Zhang, J.; Pierick, A. Ten; Van Rossum, H. M.; Maleki Seifar, R.; Ras, C.; Daran, J. M.; Heijnen, J. J.; Aljoscha Wahl, S., *Sci. Rep.* **2015**, *5*, 1–12.

[17] Zhou, Y.; Wang, L.; Yang, F.; Lin, X.; Zhang, S.; Zhao, Z. K., *Appl. Environ. Microb.* **2011**, *77*, 6133–6140.

[18] Ohshima, T.; Soda, K., *Adv. Biochem. Eng. Biotechnol.* **1990**, *42*, 187–209.

[19] Ohshima, T.; Nishida, N.; Bakthavatsalam, S.; Kataoka, K.; Takada, H.; Yoshimura, T.; Soda, K.; Esaki, N., *Eur. J. Biochem.* **1994**, *222*, 305–312.

[20] Turnbull, A. P.; Ashford, S. R.; Baker, P. J.; Rice, D. W.; Rodgers, F. H.; Stillman, T. J., *J. Mol. Biol.* **1994**, *236*, 663–665.

[21] Cui, Q.; Elstner, M.; Karplus, M., *J. Phys. Chem. B* **2002**, *106*, 2721–2740.

[22] Wang, X.; Britton, K. L.; Stillman, T. J.; Rice, D. W.; Engel, P. C., *Eur. J. Biochem.* **2001**, *268*, 5791–5799.

[23] Feeney, R.; Clarke, A. R.; Holbrook, J. J., *Biochem. Biophys. Res. Commun.* **1990**, *166*, 667–672.

[24] Galkin, A.; Kulakova, L.; Ohshima, T.; Esaki, N.; Soda, K., *Protein Eng.* **1997**, *10*, 687–690.

[25] Misono, H.; Ogasawara, M.; Nagasaki, S., *Agr. Biol. Chem. Tokyo* **1986**, *50*, 2729–2734.

[26] Gao, X.; Zhang, Z.; Zhang, Y.; Li, Y.; Zhu, H.; Wang, S.; Li, C., *Appl. Environ. Microb.* **2017**, *83*, e00476-17.

[27] Vedha-Peters, K.; Gunawardana, M.; Rozzell, J. D.; Novick, S. J., *J. Am. Chem. Soc.* **2006**, *128*, 10923–10929.

[28] Akita, H.; Doi, K.; Kawarabayasi, Y.; Ohshima, T., *Biotechnol. Lett.* **2012**, *34*, 1693–1699.

[29] Hayashi, J.; Seto, T.; Akita, H.; Watanabe, M.; Tamotsu, H.; Yoneda, K.; Ohshima, T.; Sakuraba, H., *Appl. Environ. Microb.* **2017**, *83*, :e00491-17.

[30] Gao, X.; Huang, F.; Feng, J.; Chen, X.; Zhang, H.; Wang, Z.; Wu, Q.; Zhu, D., *Appl. Environ. Microb.* **2013**, *79*, 5078–5081.

[31] Liu, W.; Li, Z.; Huang, C. H.; Guo, R. T.; Zhao, L.; Zhang, D.; Chen, X.; Wu, Q.; Zhu, D., *ChemBioChem* **2014**, *15*, 217–222.

[32] Akita, H.; Seto, T.; Ohshima, T.; Sakuraba, H., *Acta Crystallogr. Sect. D Biol. Crystallogr.* **2015**, *D71*, 1136–1146.

[33] Parmeggiani, F.; Ahmed, S. T.; Thompson, M. P.; Weise, N. J.; Galman, J. L.; Gahloth, D.; Dunstan, M. S.; Leys, D.; Turner, N. J., *Adv. Synth. Catal.* **2016**, *358*, 3298–3306.

[34] Scapin, G.; Reddy, S. G.; Blanchard, J. S.; Biol, J. M., *Biochemistry* **1996**, *35*, 13540–13551.

[35] Wang, H.; Kellogg, G. E.; Xu, P.; Zhang, Y., *J. Mol. Graph. Model.* **2018**, *83*, 100–111.

[36] Scapin, G.; Cirilli, M.; Reddy, S. G.; Gao, Y.; Vederas, J. C.; Blanchard, J. S., *Biochemistry* **1998**, *37*, 3278–3285.

[37] Bur, D.; Luyten, M. A.; Wynn, H.; Provencher, L. R.; Jones, J. B.; Gold, M.; Friesen, J. D.; Clarke, A. R.; Holbrook, J. J., *Can. J. Chem.* **1989**, *67*, 1065–1070.

[38] Piontek, K.; Chakrabarti, P.; Schär, H. P.; Rossmann, M. G.; Zuber, H., *Proteins* **1990**, *7*, 74–92.

[39] Grau, U. M.; Trommer, W. E.; Rossmann, M. G., *J. Mol. Biol.* **1981**, *151*, 289–307.

[40] Wigley, D. B.; Gamblin, S. J.; Turkenburg, J. P.; Dodson, E. J.; Piontek, K.; Muirhead, H.; Holbrook, J. J., *J. Mol. Biol.* **1992**, *223*, 317–335.

[41] Flores, H.; Ellington, A. D., *Protein Eng. Des. Sel.* **2005**, *18*, 369–377.

[42] Clarke, A. R.; Waldman, A. D. B.; Munro, I.; Holbrook, J. J., *Biochim. Biophys. Acta - Protein Struct. Mol.* **1985**, *828*, 375–379.

[43] Clarke, A. R.; Atkinson, T.; Campbell, J. W.; John Holbrook, J., *Biochim. Biophys. Acta - Protein Struct. Mol.* **1985**, *829*, 387–396.

[44] Hart, K. W.; Clarke, A. R.; Wigley, D. B.; Waldman, A. D. B.; Chia, W. N.; Barstow, D. A.; Atkinson, T.; Jones, J. B.; Holbrook, J. J., *Biochim. Biophys. Acta - Protein Struct. Mol.* **1987**, *914*, 294–298.

[45] Clarke, A. R.; Wilks, H. M.; Barstow, D. A.; Atkinson, T.; Chia, W. N.; Holbrook, J. J., *Biochemistry* **1988**, *27*, 1617–1622.

[46] Clarke, A. R.; Wigley, D. B.; Chia, W. N.; Barstow, D.; Atkinson, T.; Holbrook, J. J., *Nature* **1986**, *324*, 699–702.

[47] Martinez, C. R.; Iverson, B. L., *Chem. Sci.* **2012**, *3*, 2191–2201.

[48] Clarke, A. R.; Wigley, D. B.; Barstow, D. A.; Chia, W. N.; Atkinson, T.; Holbrook, J. J., *Biochim. Biophys. Acta - Protein Struct. Mol.* **1987**, *913*, 72–80.

[49] Dib, I.; Stanzer, D.; Nidetzky, B., *Appl. Environ. Microb.* **2007**, *73*, 331–333.

[50] Wilkinson, J. H., In *Isoenzymes*; Springer US: Boston, MA, 1970; pp 134–203.

[51] *Pyridine Nucleotide-Dependent Dehydrogenases*; Sund, H., Ed.; Springer-Verlag: Heidelberg, 1970.

[52] Wilks, H. M.; Halsall, D. J.; Atkinson, T.; Chia, W. N.; Clarke, A. R.; Holbrook, J. J., *Biochemistry* **1990**, *29*, 8587–8591.

[53] Holmberg, N.; Ryde, U.; Bülow, L., *Protein Eng. Des. Sel.* **1999**, *12*, 851–856.

[54] Hensel, R.; Mayr, U.; Yang, C., *Eur. J. Biochem.* **1983**, *134*, 503–511.

[55] Taylor, S. S., *J. Biol. Chem.* **1977**, *252*, 1799–1806.

[56] Schütte, H.; Hummel, W.; Kula, M. R., *Appl. Microbiol. Biotechnol.* **1984**, *19*, 167–176.

[57] Busto, E.; Richter, N.; Grischek, B.; Kroutil, W., *Chem. - A Eur. J.* **2014**, *20*, 11225–11228.

[58] Gourinchas, G.; Busto, E.; Killinger, M.; Richter, N.; Wiltschi, B.; Kroutil, W., *Chem. Commun.* **2015**, *51*, 2828–2831.

[59] Niefind, K.; Hecht, H. J.; Schomburg, D., *J. Mol. Biol.* **1995**, *251*, 256–281.

[60] Gerstein, M.; Chothia, C., *J. Mol. Biol.* **1991**, *220*, 133–149.

[61] Dunn, C. R.; Wilks, H. M.; Halsall, D. J.; Atkinson, T.; Clarke, A. R.; Muirhead, H.; Holbrook, J. J., *Philos. T. R. Soc. Lond. B* **1991**, *332*, 177–184.

[62] Feil, I. K.; Lerch, H. P.; Schomburg, D., *Eur. J. Biochem.* **1994**, *223*, 857–863.

[63] Grant, G. A., *Biochem. Biophys. Res. Commun.* **1989**, *165*, 1371–1374.

[64] Taguchi, H.; Ohta, T., *J. Biol. Chem.* **1991**, *266*, 12588–12594.

[65] Lamzin, V. S.; Dauter, Z.; Popov, V. O.; Harutyunyan, E. H.; Wilson, K. S., *J. Mol. Biol.* **1994**, *236*, 759–785.

[66] Dengler, U.; Niefind, K.; Kieß, M.; Schomburg, D., *J. Mol. Biol.* **1997**, *267*, 640–660.

[67] Hummel, W.; Schütte, H.; Kula, M. R., *Appl. Microbiol. Biotechnol.* **1985**, *21*, 7–15.

[68] Lerch, H. P.; Blöcker, H.; Kallwass, H.; Hoppe, J.; Tsai, H.; Collins, J., *Gene* **1989**, *78*, 47–

57.

[69] Domenech, J.; Ferrer, J., *Biochim. Biophys. Acta - Gen. Subj.* **2006**, *1760*, 1667–1674.

[70] Kallwass, H.; Tsai, H.; Schütte, H., *FEMS Microbiol. Lett.* **1987**, *43*, 263–267.

[71] Domenech, J.; Nieto, J. M.; Ferrer, J., *J. Mol. Catal. B Enzym.* **2009**, *61*, 168–173.

[72] Casadaban, M. J., *J. Mol. Biol.* **1976**, *104*, 541–555.

[73] Nuñez, M. F.; Pellicer, M. T.; Badia, J.; Aguilar, J.; Baldoma, L., *Biochem. J.* **2001**, *354*, 707–715.

[74] Yun, H.; Choi, H.-L.; Fadnavis, N. W.; Kim, B.-G., *Biotechnol. Prog.* **2005**, *21*, 366–371.

[75] Yum, D.; Lee, B.; Hahm, D.; Pan, J.-G., *J. Bacteriol.* **1998**, *180*, 5984–5988.

[76] Meng, H.; Liu, P.; Sun, H.; Cai, Z.; Zhou, J.; Lin, J.; Li, Y., *Sci. Rep.* **2016**, *6*, 24887.

[77] Razeto, A.; Kochhar, S.; Hottinger, H.; Dauter, M.; Wilson, K. S.; Lamzin, V. S., *J. Mol. Biol.* **2002**, *318*, 109–119.

[78] Vinals, C.; De Bolle, X.; Depiereux, E.; Feytmans, E., *Proteins* **1995**, *21*, 307–318.

[79] Kochhar, S.; Hunziker, P. E.; Leong-Morgenthaler, P.; Hottinger, H., *J. Biol. Chem.* **1992**, *267*, 8499–8513.

[80] Holton, S. J.; Anandhakrishnan, M.; Geerlof, A.; Wilmanns, M., *J. Struct. Biol.* **2013**, *181*, 179–184.

[81] Ptitsyn, O. B., *FEBS Lett.* **1978**, *93*, 1–4.

[82] Li, C.; Tao, F.; Ni, J.; Wang, Y.; Yao, F.; Xu, P., *Sci. Rep.* **2015**, *5*, 09777.

[83] Taguchi, H.; Ohta, T.; Matsuzawa, H., *J. Biochem.* **1997**, *122*, 802–809.

[84] Taguchi, H.; Ohta, T., *J. Biochem.* **1994**, *115*, 930–936.

[85] Dey, S.; Hu, Z.; Xiao, L. X.; Sacchettini, J. C.; Grant, G. A., *J. Biol. Chem.* **2007**, *282*, 18418–18426.

[86] Krebs, H. A., *Hoppe-Seyler´s Zeitschrift für Physiol. Chemie* **1933**, *217*, 191–227.

[87] Krebs, H. A., *Biochem. J.* **1935**, *29*, 1620–1644.

[88] Warburg, O.; Christian, W., *Biochem. Z.* **1938**, *217*, 191.

[89] Mazzeo, B. P.; Romeo, A., *J. Chem. Soc. Perkin Trans. 1* **1972**, *20*, 2532.

[90] Bianchi, D.; Bortolo, R.; Golini, P.; Cesti, P., *Appl. Biochem. Biotechnol. - Part A Enzym. Eng. Biotechnol.* **1998**, *73*, 257–268.

[91] Conlon, H. D.; Baqai, J.; Baker, K.; Shen, Y. Q.; Wong, B. L.; Noiles, R.; Rausch, C. W., *Biotechnol. Bioeng.* **1995**, *46*, 510–513.

[92] Inaba, Y.; Mizukami, K.; Hamada-Sato, N.; Kobayashi, T.; Imada, C.; Watanabe, E., *Biosens. Bioelectron.* **2003**, *19*, 423–431.

[93] Patel, R. N., *Adv. Appl. Microbiol.* **2000**, *47*, 33–78.

[94] Pilone, M. S., *Cell. Mol. Life Sci.* **2000**, *57*, 1732–1747.

[95] LaRue, T.; Spencer, J., *Can. J. Microbiol.* **1967**, *13*, 777–788.

[96] Lin, L. L.; Chien, H. R.; Wang, W. C.; Hwang, T. S.; Fu, H. M.; Hsu, W. H., *Enzyme Microb. Technol.* **2000**, *27*, 482–491.

[97] Chien, L. J.; Wu, J. M.; Kuan, I. C.; Lee, C. K., *Biotechnol. Prog.* **2004**, *20*, 1359–1365.

[98] Makrides, S., *Microbiol. Rev.* **1996**, *60*, 512–538.

[99] Blackwell, J. R.; Horgan, R., *FEBS* **1991**, *295*, 10–12.

[100] Mizutani, H.; Miyahara, I.; Hirotsu, K.; Nishina, Y.; Shiga, K.; Setoyama, C.; Miura, R., *J. Biochem.* **1996**, *120*, 14–17.

[101] Tishkov, V. I.; Khoronenkova, S. V., *Biochem.* **2005**, *70*, 40–54.

[102] Piubelli, L.; Molla, G.; Caldinelli, L.; Pilone, M. S.; Pollegioni, L., *Protein Eng.* **2003**, *16*, 1063–1069.

[103] Pollegioni, L.; Iametti, S.; Fessas, D.; Caldinelli, L.; Piubelli, L.; Barbiroli, A.; Pilone, M. S.; Bonomi, F., *Protein Sci.* **2003**, *12*, 1018–1029.

[104] Mattevi, A.; Vanoni, M.; Todone, F.; Rizzi, M.; Teplyakov, A.; Coda, A.; Bolognesi, M.; Curti, B., *Proc. Natl. Acad. Sci USA* **1996**, *93*, 7496–7501.

[105] Mattevi, A., *Trends Biochem. Sci.* **2006**, *31*, 276–283.

[106] Saam, J.; Rosini, E.; Molla, G.; Schulten, K.; Pollegioni, L.; Ghisla, S., *J. Biol. Chem.* **2010**, *285*, 24439–24446.

[107] Molla, G.; Melis, R.; Pollegioni, L., *Biotechnol. Adv.* **2017**, *35* (6), 657–668.

[108] Pawelek, P. D., *EMBO J.* **2000**, *19*, 4204–4215.

[109] Umhau, S.; Pollegioni, L.; Molla, G.; Diederichs, K.; Welte, W.; Pilone, M. S.; Ghisla, S., *Proc. Natl. Acad. Sci.* **2000**, *97*, 12463–12468.

[110] Miyano, M.; Fukui, K.; Watanabe, F.; Takahashi, S.; Tada, M.; Kanashiro, M.; Miyake, Y., *J. Biochem.* **1991**, *109*, 171–177.

[111] Pollegioni, L.; Langkau, B.; Tischer, W.; Ghisla, S.; Pilone, M. S., *J. Biol. Chem.* **1993**, *268*, 13850–13857.

[112] Pollegioni, L.; Fukui, K.; Massey, V., *J. Biol. Chem.* **1994**, *269*, 31666–31673.

[113] Marcotte, P.; Walsh, C., *Biochemistry* **1978**, *17*, 2864–2868.

[114] Rudie, N. G.; Porter, D. J.; Bright, H. J., *J. Biol. Chem.* **1980**, *255*, 498–508.

[115] Ronchi, S.; Galliano, M.; Curti, B.; Rudie, N. G.; Porter, D. J. T.; Brightj, H. J., *J. Biol. Chem.* **1980**, *255*, 6044–6046.

[116] Curti, B.; Ronchi, S.; Pilone Simonetta, M., In *Chemistry and Biochemistry of Flavoenzymes Vol. 3*; F., M., Ed.; CRC Press: Boca Raton, 1992; pp 69–94.

[117] Todone, F.; Vanoni, M. A.; Mozzarelli, A.; Bolognesi, M.; Coda, A.; Curti, B.; Mattevi, A.,

Biochemistry **1997**, *36*, 5853–5860.

[118] Caligiuri, A.; D'Arrigo, P.; Rosini, E.; Tessaro, D.; Molla, G.; Servi, S.; Pollegioni, L., *Adv. Synth. Catal.* **2006**, *348*, 2183–2190.

[119] Molla, G.; Porrini, D.; Job, V.; Motteran, L.; Vegezzi, C.; Campaner, S.; Pilone, M. S.; Pollegioni, L., *J. Biol. Chem.* **2000**, *275*, 24715–24721.

[120] Smith, S. M.; Uslaner, J. M.; Hutson, P. H., *Open Med. Chem. J.* **2010**, *4*, 3–9.

[121] Zeller, E. A.; Maritz., A., *Helv. Chim. Acta* **1944**, *27*, 1888–1902.

[122] Motta, P.; Molla, G.; Pollegioni, L.; Nardini, M., *J. Biol. Chem.* **2016**, *291*, 10457–10475.

[123] Takahashi, E.; Furui, M.; Seko, H.; Shibatani, T., *Appl. Microbiol. Biotechnol.* **1997**, *47*, 173–179.

[124] Ju, Y.; Tong, S.; Gao, Y.; Zhao, W.; Liu, Q.; Gu, Q.; Xu, J.; Niu, L.; Teng, M.; Zhou, H., *J. Struct. Biol.* **2016**, *195*, 306–315.

[125] Busto, E.; Simon, R. C.; Richter, N.; Kroutil, W., *ACS Catal.* **2016**, *6*, 2393–2397.

[126] Hanson, R. L.; Bembenek, K. S.; Patel, R. N.; Szarka, L. J., *Appl. Microbiol. Biotechnol.* **1992**, *37*, 599–603.

[127] Baek, J. O.; Seo, J. W.; Kwon, O.; Seong, S. Il; Kim, I. H.; Kim, C. H., *J. Basic Microbiol.* **2011**, *51*, 129–135.

[128] Pantaleone, D. P.; Geller, A. M.; Taylor, P. P., *J. Mol. Catal. - B Enzym.* **2001**, *11*, 795–803.

[129] Shabbiri, K.; Ahmad, W.; Syed, Q.; Adnan, A., *Brazilian J. Microbiol.* **2010**, *41*, 796–804.

[130] Volbeda, A.; Darnault, C.; Parkin, A.; Sargent, F.; Armstrong, F. A.; Fontecilla-Camps, J. C., *Structure* **2013**, *21*, 184–190.

[131] Rausch, C.; Lerchner, A.; Schiefner, A.; Skerra, A., *Proteins* **2013**, *81*, 774–787.

[132] Midelfort, K. S.; Kumar, R.; Han, S.; Karmilowicz, M. J.; McConnell, K.; Gehlhaar, D. K.; Mistry, A.; Chang, J. S.; Anderson, M.; Villalobos, A.; et al., *Protein Eng. Des. Sel.* **2013**, *26*, 25–33.

[133] Shin, J. S.; Kim, B. G., *J. Org. Chem.* **2002**, *67*, 2848–2853.

[134] Genz, M.; Vickers, C.; van den Bergh, T.; Joosten, H. J.; Dörr, M.; Höhne, M.; Bornscheuer, U. T., *Int. J. Mol. Sci.* **2015**, *16*, 26953–26963.

[135] Okamoto, A.; Ishii, S.; Hirotsu, K.; Kagamiyama, H., *Biochemistry* **1999**, *38*, 1176–1184.

[136] Seo, Y. M.; Mathew, S.; Bea, H. S.; Khang, Y. H.; Lee, S. H.; Kim, B. G.; Yun, H., *Org. Biomol. Chem.* **2012**, *10*, 2482–2485.

[137] Fuchs, M.; Koszelewski, D.; Tauber, K.; Kroutil, W.; Faber, K., *Chem. Commun.* **2010**, *46*, 5500–5502.

[138] Fuchs, M.; Koszelewski, D.; Tauber, K.; Sattler, J.; Banko, W.; Holzer, A. K.; Pickl, M.; Kroutil, W.; Faber, K., *Tetrahedron* **2012**, *68*, 7691–7694.

[139] Shorter, J., *Chem. Unserer Zeit* **1985**, *19*, 197–208.

[140] Pollard, C. B.; Young, D. C., *J. Org. Chem.* **1951**, *16*, 661–672.

[141] Wei, Y.; Wang, C.; Jiang, X.; Xue, D.; Liu, Z. T.; Xiao, J., *Green Chem.* **2014**, *16*, 1093–1096.

[142] Li, C.; Lu, C. D., *Proc. Natl. Acad. Sci. U. S. A.* **2009**, *106*, 906–911.

[143] He, W.; Li, C.; Lu, C. D., *J. Bacteriol.* **2011**, *193*, 2107–2115.

[144] Caligiuri, A.; D'Arrigo, P.; Gefflaut, T.; Molla, G.; Pollegioni, L.; Rosini, E.; Rossi, C.; Servi, S., *Biocatal. Biotransformation* **2006**, *24*, 409–413.

[145] Parmeggiani, F.; Lovelock, S. L.; Weise, N. J.; Ahmed, S. T.; Turner, N. J., *Angew. Chem. Int. Ed.* **2015**, *54*, 4608–4611.

[146] Cirilli, M.; Scapin, G.; Sutherland, A.; Vederas, J. C.; Blanchard, J. S., *Protein Sci. A Publ. Protein Soc.* **2000**, *9*, 2034–2037.

[147] Page Ruler, Thermofisher scientific https://assets.thermofisher.com/TFS-Assets/LSG/figures/26616-ladder-002.jpg-650.jpg.

[148] Hanai, K.; Kuwae, A.; Kawai, S.; Ono, Y., *J. Phys. Chem.* **1989**, *93*, 6013–6016.

[149] Hanai, K.; Kawai, S.; Kuwae, A., *J. Mol. Struct.* **1991**, *245*, 21–27.

[150] Gourinchas, G.; Busto, E.; Killinger, M.; Richter, N.; Wiltschi, B.; Kroutil, W., *Chem. Commun.* **2015**, *51*, 2828–2831.

[151] Bernát, G.; Waschewski, N.; Rögner, M., *Photosynth. Res.* **2009**, *99*, 205–216.

[152] Manufacturer of LEDs http://www.nichia.co.jp.

[153] User:Degre., Picture of Solar Spectrum wikipedia.de.

[154] Bermeyer, H. U., *Methoden Der Enzymatischen Analyse*, Vol. 1.; Verl. Chemie: Weinheim, 1974.

[155] Karlsson, J.-O.; Ostwald, K.; Kabjörn, C.; Andersson, M., *Anal. Biochem.* **1994**, *219*, 144–146.

5.2 NMR

5.2.1 ^{1}H-NMR of 3-acetylphenyl ethyl(methyl)carbamate (**6a**)

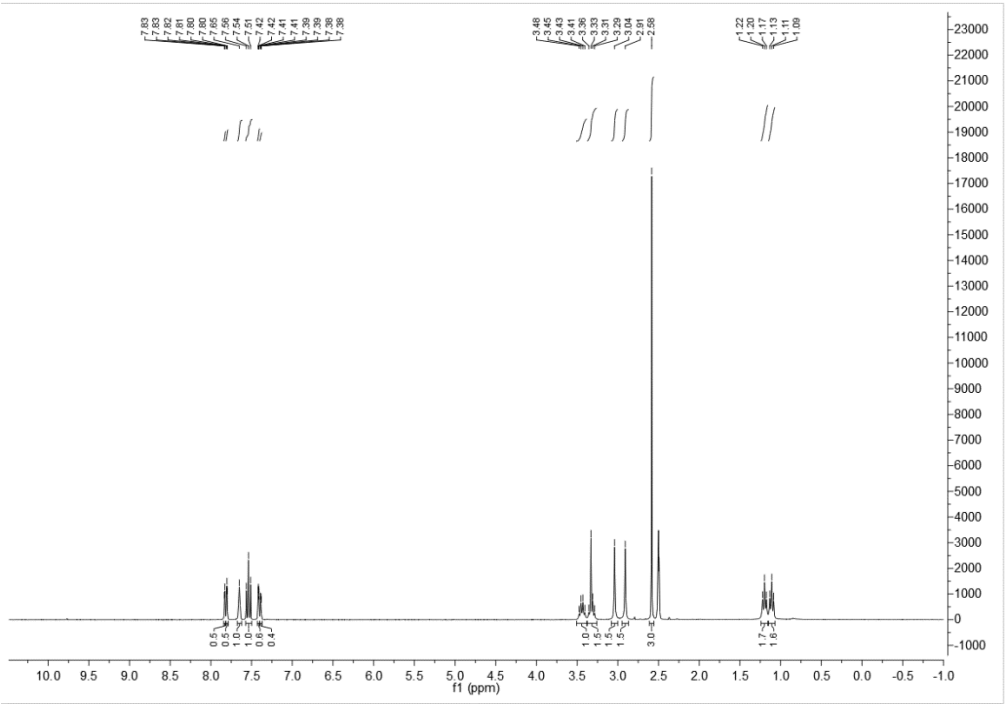

Figure 58: ^{1}H-NMR of 3-acetylphenyl ethyl(methyl)carbamate (**6a**).

5.2.2 ^{13}C-NMR of 3-acetylphenyl ethyl(methyl)carbamate (**6a**)

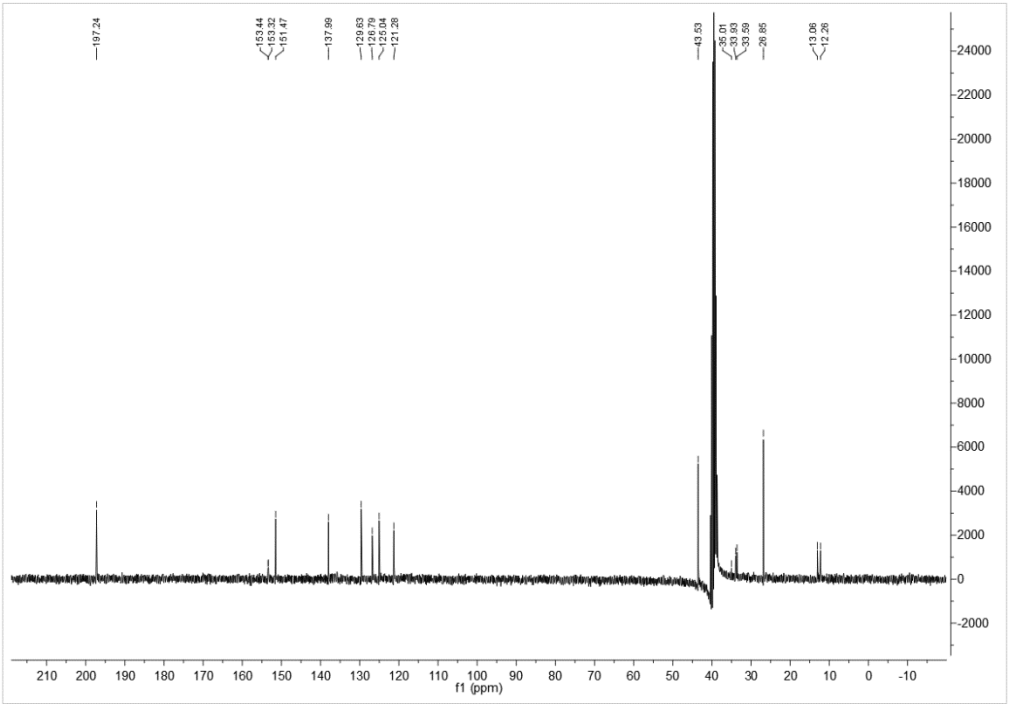

Figure 59: ^{13}C-NMR of 3-acetylphenyl ethyl(methyl)carbamate (**6a**).